QUANTIZATION INDEX MODULATION BASED WATERMARKING USING
DIGITAL HOLOGRAPHY

A THESIS SUBMITTED TO
THE GRADUATE SCHOOL OF NATURAL AND APPLIED SCIENCES
OF
MIDDLE EAST TECHNICAL UNIVERSITY

BY

OSMAN ERMAN OKMAN

IN PARTIAL FULFILLMENT OF THE REQUIREMENTS
FOR
THE DEGREE OF MASTER OF SCIENCE
IN
ELECTRICAL AND ELECTRONICS ENGINEERING

SEPTEMBER 2006

Approval of the Graduate School of Natural and Applied Sciences

                                                     _____

                                                         Prof. Dr. Canan Özgen
                                                               Director

I certify that this thesis satisfies all the requirements as a thesis for the degree of Master of Science.

                                                     _____

                                                           Prof. Dr. İsmet Erkmen
                                                         Head of Department

This is to certify that we have read this thesis and that in our opinion it is fully adequate, in scope and quality, as a thesis for the degree of Master of Science.

                                                   _____

                                             Assoc. Prof. Dr. Gözde Bozdağı Akar
                                                                 Supervisor

Examining Committee Members

| | | |
|---|---|---|
| Assoc. Prof. Dr. A. Aydın Alatan | (METU, EE) | —————————— |
| Assoc. Prof. Dr. Gözde Bozdağı Akar | (METU, EE) | —————————— |
| Prof. Dr. Mete Severcan | (METU, EE) | —————————— |
| Assist. Prof. Dr. Çağatay Candan | (METU, EE) | —————————— |
| Ersin Esen | (TUBITAK, UZAY) | —————————— |

I hereby declare that all information in this document has been obtained and presented in accordance with academic rules and ethical conduct. I also declare that, as required by these rules and conduct, I have fully cited and referenced all material and results that are not original to this work.

Name, Last Name: Osman Erman Okman

Signature            :

# ABSTRACT

## QUANTIZATION INDEX MODULATION BASED IMAGE WATERMARKING USING DIGITAL HOLOGRAPHY

Okman, Osman Erman

M.S., Department of Electrical and Electronics Engineering
Supervisor: Assoc. Prof. Dr. Gözde Bozdağı Akar

September 2006,   111 pages

The multimedia watermarking techniques are evolved very quickly in the last years with the increase in the use of internet. The evolution of the internet makes the copyright issues very important and many different approaches are appeared to protect the digital content. On the other hand, holography is the method to store the 3-D information of an object but it is very applicable to use as a watermark because of the nature of the holographic data. The 3-D object can be reconstructed from the hologram even if the hologram is cropped or occluded. However, watermarking of an image with a hologram is a very novel approach and there are only a few works in the literature which are not very robust against the attacks like filtering or compression. In this thesis, we propose to embed the phase of the hologram to an image using quantization index modulation (QIM). QIM is utilized to make the watermarking scheme blind and degrade the host image as low as possible. The robustness of the proposed technique is also tested against several attacks such as filtering, compression, etc. The evaluated performance of this system is compared with the existing methods in the literature which uses either holograms or logos as

the secret mark. Furthermore, the characteristics of the holograms are investigated and the findings about the hologram compression are reported in this work.

Keywords: Watermarking, phase shifting digital holography, quantization index modulation (QIM), digital wavelet transform

# ÖZ

## HOLOGRAM KULLANARAK NİCEMLEME DİZİN MODULASYONU TABANLI İMGE DAMGALAMA

Okman, Osman Erman

Yüksek Lisans, Elektrik Elektronik Mühendisliği Bölümü
Tez Yöneticisi: Doç. Dr. Gözde Bozdağı Akar

Eylül 2006,   111 sayfa

Son seneler içinde, internet kullanımın artması sebebiyle çokluortam damgalama teknikleri çok hızlı bir şekilde gelişmiştir. Bunun sebebi, internet teknolojisinin çok gelişmesinin telif hakkı konularına çok önem verilmesine neden olmasıdır. Bu konuyla ilgili çok değişik yaklaşımlar da ortaya çıkmıştır. Öte yandan, holografi bir nesnenin 3 boyut bilgisini saklamak için kullanılan bir yöntemdir. Ancak hologramların kendilerine has özellikleri, onları damga olarak kullanılabilir kılmaktadır. Örneğin, hologramın kırpılması ya da örtülmesi durumlarında dahi, bilgisini sakladığı 3 boyutlu nesne geri çatılabilmektedir. Buna karşın hologram kullanarak imge damgalama şu an için oldukça yeni bir yöntemdir ve bu konuyla ilgili, literatürde sadece birkaç çalışma bulunmaktadır. Bu çalışmalarda sunulan yaklaşımlar da sıkıştırma ya da süzme gibi ataklara karşı dayanıklı değildir. Bu tezde, hologramı damga olarak kullanan ve damgayı imgenin içerisine nicemleme dizin modulasyonu tekniği ile saklayan bir yöntem sunulmaktadır. Bu sayede, sunulan metotun alındısız olması ve imge üzerindeki bozulmaların olabildiğince az olması sağlanmaktadır. Sunulan metotun süzme ve sıkıştırma gibi saldırılara karşı

gürbüzlüğü de test edilmiş ve elde edilen sonuçlar literatürdeki diğer yöntemlerin sonuçlarıyla kıyaslnamıştır. Bu yöntemler damga olarak hologram ya da logo kullananlar olmak üzere ikiye ayrılmaktadır. Bunun yanında, hologramların özellikler araştırlmış ve de hologramların sıkıştırılması için çeşitli deneyler yapılıp, sonuçları sunulmuştur.

Anahtar Kelimeler: Damgalama, faz kaydırmalı sayısal holografi, nicemleme dizin modulasyonu, sayısal dalgacık dönüşümü

*To my parents and*

*to who provides all the support and help whenever I need*

# ACKNOWLEDGEMENTS

# TABLE OF CONTENTS

# LIST OF TABLES

# LIST OF FIGURES

xiv

xviii

# LIST OF ABBREVIATIONS

QIM          Quantization Index Modulation

DCT          Discrete Cosine Transform

DFT          Digital Fourier Transform

DWT          Digital Wavelet Transform

IDWT         Inverse Digital Wavelet Transform

PSNR         Peak Signal to Noise Ratio

HVS          Human Visual System

CC           Correlation Coefficient

BCR          Bit Correct Ratio

MSE          Mean Square Error

JPEG         Joint Photographic Experts Group

# CHAPTER 1

# INTRODUCTION

## 1.1  Overview

In the past years, there has been an extensive growth in many different kinds of digital imaging technologies with their applications. On the other hand, these digital contents are vulnerable against duplication and processing. Moreover, with the rapid development of the internet technologies it is very easy for anyone to obtain them. Hence, the copyright and authentication issues become as one of the most important issues, in order to protect these multimedia contents from illegal duplication or identifying the source of the multimedia data.

Authenticating any multimedia information by adding an amount of information, which is called watermarking, is one of the most widely used approaches to protect the content of the multimedia data. However, in order the watermarking to be effective the embedded information should be accessible in anytime for the content owner and remain in the host data after different kinds of manipulations, [1].

The watermarking is not used only for copyright protection or owner identification but also for different applications like broadcast monitoring, authentication, fingerprinting, etc. However, the requirements of a watermarking process like robustness, fidelity, computational cost, and etc. vary from an application to another one.

## 1.2    Aim and Scope of Thesis

The main objective of this thesis is to propose a new watermarking approach which embeds visually meaningful patterns as the watermark. This objective is achieved by embedding the hologram of that watermark into the image. Upon investigating the methods for embedding the hologram, we also conducted researches and performed experiments on hologram especially for data compression.

Since one of the main motivations of this work is to create an effective watermarking scheme applicable to many different approaches, some experiments are also performed to evaluate its performance. One of the criteria about the success of the watermarking is its fidelity which is in fact the invisibility of the hidden information in the host data. Robustness is another major concern for most of the watermark algorithms. A robust watermark must resist to possible processing and remains detectable. These processing get a common name, *attack*. There are many kinds of attacks and it is probably impossible for a watermark to resist all kind of attacks, however, it is unnecessary and excessive. Hence, the experiments are mainly focused on the robustness of the proposed scheme.

## 1.3    Outline of Dissertation

The structure of this thesis closely follows the order in which the work was undertaken in response to the aims as they were initially conceived. It consists of eight further chapters.

Chapter 2 briefly summarizes the history and general idea behind the watermarking. The main characteristics of a watermarking scheme will be given with its possible application areas.

Third chapter focuses on the holography. The mathematical background of the wave theory will also be explained in order to explain the recording and

reconstruction of the holograms. This is also beneficial to understand the properties of the holograms.

Chapter 4 explains the recording and reconstruction process of the phase shifting digital holography since these types of holograms will be used in this work. Besides, the characteristics of the holograms are investigated and the results for hologram data compression are given.

Fifth chapter summarizes the existing watermarking approaches which hide perceptually meaningful patterns as the watermark.

Chapter 6 summarizes design and implementation details of the proposed watermarking approach.

Chapter 7 illustrates the results of the experiments done to evaluate the performance of the proposed method. The comparisons between the existing approaches are also given in this chapter.

Finally, Chapter 8 summarizes the work done within the scope of this thesis and discusses the conclusions drawn from the work carried out. It also addresses the further recommendations for the similar works that are intended to be done.

# CHAPTER 2

# WATERMARKING

## 2.1 Information Hiding

There is an interest for the methods that allow transmission of some hidden information or embedded data into another data. These techniques are used for many different applications like broadcast monitoring, copyright protection or authentication [2, 3]. The information hiding techniques are mainly divided into two groups as cryptography and steganography [4].

Cryptography is composed of Greek words and means "secret writing". This method is used for protecting the information during the transmission. The digital content is encrypted before transmission and decrypted after the receiver obtains this content with the help of a key. Therefore the content of the transmitted data can only be used by the person who has the key. On the other hand, after decryption the digital content is not protected anymore.

Steganography, on the other hand, is used to hide or embed the secret data into another, possibly an unsuspected, data [1]. It is also coined from two Greek words "steganos" and "graphia" which end up with meaning "covered writing" [5]. Steganographic techniques are used if the covert communication is unknown therefore; the hidden message is undetectable if the cover data is corrupted.

Watermarking, as opposed to the steganography, concerns the robustness criteria. The robustness is not a clear term since depending on the application but generally it defines as the ability to detect the watermark after attacks to destroy or disrupt the hidden mark [2].

## 2.2    Watermarking Framework

Watermarking is defined in [6] as the insertion of a signal, watermark, into a multimedia content such that watermark can be detected or extracted later to make an assertion about the content. In a watermarking system, there are three main parts which are considered in design procedure. These parts can be given as follows:

- watermark signal,
- encoder to embed the watermark into the host data,
- decoder to extract watermark from the watermarked data

In Figure 2.1, the general watermark embedding procedure is given. According to this system, let I be the multimedia content to be watermarked, W be the watermark and I' be the resultant marked content. If the embedding function is E(), then the watermarking procedure is expressed with the following equation:

$$E(I,W) = I' \qquad\qquad (2.1)$$
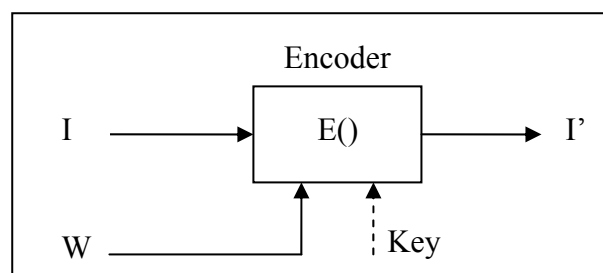


*Figure 2.1 Watermark embedding*

The most common watermarking technique is the spread spectrum watermarking, [7], which will be explained in details in the following sections. This technique can be seen as analogous of the spread spectrum communication. A pseudo-random noise like signal with small amplitude is added to the host data as the watermark. The watermark embedding can be performed either in spatial domain or transform domain.

The last part of the system, the decoder, encounters with the contents which can be unwatermarked or watermarked and possibly corrupted because of the transmission channel or the attacks of the hackers. It is used to determine whether this content is watermarked or not and extract the watermark to determine the owner of the content. The decoder may need or may not need the original unwatermarked content depending on the embedding algorithm, which is designed depending on application. If the detector does not need the original data, the watermarking method is defined as blind (public) watermarking, where if it requires the original copy the method is defined as non-blind watermarking. Therefore, if the decoding function is D, the incoming content is J and the recovered watermark is W', the following equation holds in the process of watermark extraction:

$$W' = \begin{cases} D(J), \text{if the decoder is blind} \\ D(J, I), \text{if the detector is non - blind} \end{cases} \qquad (2.2)$$

The presence of the watermark is usually proved by a correlation method. In this method, the correlation (or difference) between the original watermark, W, and the extracted one, W', is calculated with a specified metric. Then the evaluated value is compared with a threshold and decided if the multimedia content is watermarked or not. In Figure 2.2, this process is illustrated.
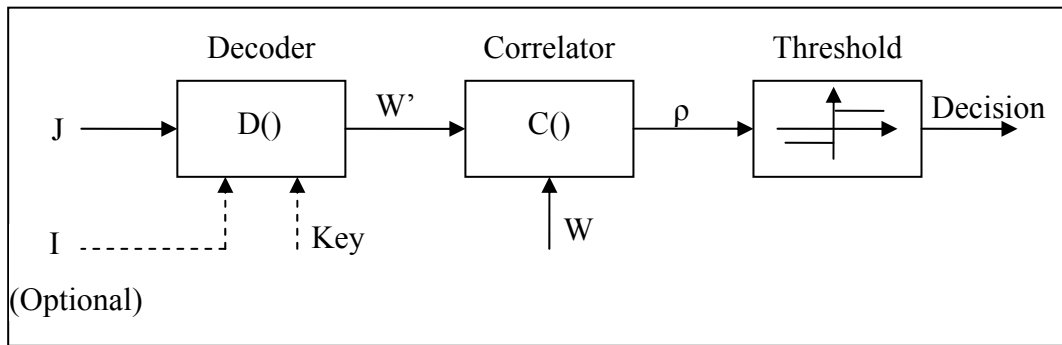
*Figure 2.2 Watermark extraction and decision making*

## 2.3 History of Watermarking

The very first paper watermarks appeared in 1292, after more than 300 years later than the invention of the paper [2]. The origin of them was an Italian town Fabriano where the papermaking industry was localized. At that time there were about 40 paper markets producing paper with different quality, format and price. There were a high competition between the paper mills and the artisans who smoothed the paper to make it writable and it was very difficult to identify the format or the quality of the paper [5]. The watermarks were started to be used in this area in order to indicate paper brand or the paper mill and then spread all over Europe as the indicator of paper format, quality and strength.

By the eighteenth century, watermarks began to be used against counterfeiting measures on money and other documents [2]. At end of the eighteenth century, it was first called as watermark. The name is probably given because the marks resemble the effects of water on paper. At the same time the counterfeiters began to develop some methods to forge the watermarks on the paper money. Therefore, some new approaches were appeared to improve watermarking technologies. In 1821, William Congreve invented a colored watermarking technique which insets dyed material into the middle of the paper during papermaking process. It was very difficult to forge them but it was also very difficult to make them so Bank of

England declined to use this technique. A more practical technique is invented in 1848 by William Henry Smith. By this technique a kind of shallow relief sculpture is pressed into the paper mold. Therefore, resulting variations on the surface created beautiful watermarks with varying shades of gray and these kinds of watermarks are called as light and shade watermark.

The digital watermarks are inspired by these paper watermarks in bank notes or stamps [1, 5]. There is not an exact date about the first discussion of the digital watermark. In 1979, Szepanski described a machine-detectable pattern to be placed on the documents and in 1988 Holt et al. suggested a method to hide an identification code into the audio signals [2]. However, it was Komatsu and Tominaga who have first used the term digital watermarking, in 1988, [2]. Digital image watermarking arose in 1990 by a work of Tanaka et al. [8]. It was after 1995 when the watermarking took great attention and since then; there have been many different works have been going on about this issue.

## 2.4    Applications of Watermarking

As described before, there is not a common definition of the robustness since it depends on the application. The robustness criteria may differ depending on the aim of the watermarking scheme. This causes existence of different kinds of watermarking methods. In this part, these proposed watermarking applications will be explained.

Copyright protection is probably the most well-known application of the watermarking [5]. The traditional way of copyrighting is to add a visual text as "© date owner" however, it is no more enough to protect the owner identification since it is easy to destroy this mark anymore. Thus by watermarking it is very practical for the copyright owner to claim the copyright on the data if the watermarking method provides high level of robustness.

Another application of watermarking is broadcast monitoring. This application is important for the owners whose contents are being broadcasted through television or radio. Different types of organizations and individuals are interested in this application of watermarking. For instance, the advertisers want to see if their advertisements are broadcasting for the time they purchase where the copyright owners guarantee the illegal broadcasting of their property [6].

The watermarks can also be used for authentication [6, 9]. Authentication is based on detection of whether the original content is changed or not, therefore, the watermarks should be corrupted if the original content is altered. In this kind of applications, "fragile watermarks" are used in order to achieve this goal. Moreover, some semi-fragile watermarks are also used to make the technique robust against some attacks, i.e. lossy compression of images, and sensitive to other possible modifications [10].

Fingerprinting is another application of watermarking. In this technique, each copy of the content is marked using a unique watermark. Therefore, the source of an illegal copy can be identified. This technique can prevent illegal duplication of the digital contents indirectly. Another method of copy protection is to add a watermark indicating the copy status of the data [5]. The DVD system is a very good example of this application since the copy information is embedded to the data as a watermark.

Watermarking is also used for some non-security applications like indexing of videos [9] or detecting and concealment of transmission errors [11, 12].

## 2.5    Requirements of Watermarking

There are many different requirements that a watermarking system should satisfy like robustness, fidelity, low computational cost, security, high capacity, etc. [2]. However, to satisfy all these properties is not practically possible. Thus, the

properties of a watermarking scheme is determined depend on the desired application. In this section, these requirements are explained.

Imperceptibility or fidelity is one of the most important requirements of a watermarking scheme [1] since a watermarking system is of no use to anyone if the host data is distorted so much that the resultant image becomes useless or highly distracting. There are some works that measures the fidelity of the system by subjective tests [13], however, in most of the works in the literature PSNR values given in equation (2.3) are used to compare the original and the watermarked data.

$$PSNR = 20 \cdot \log \left( \frac{255 \cdot M \cdot N}{\sum_{i=1}^{M} \sum_{j=1}^{N} [x(i,j) - x'(i,j)]^2} \right) \qquad (2.3)$$

where $x$ is original and $x'$ is the watermarked MxN images.

Robustness is another major requirement of a watermarking method. It refers to the ability to detect the watermark after some common signal processing operations. These operations are so called "attacks" in the literature since they are seen as the possible operation a person can do who wants the watermark to be undetectable but does not know the watermarking scheme the content owner used. The very common attacks include lossy compression, filtering, noise addition, geometric distortion, etc. However, the attacks against which a system should be robust differ from an application to another [2]. For example, in TV broadcast monitoring the watermark should survive for only transmission process where in digital video monitoring the watermarking scheme should provide robustness against many compression or filtering operations. In many of the applications robustness is the major concern with fidelity but in some applications like fragile watermarking, robustness is undesirable.

As the number of bits embedded into a host increases the probability of error in verifying and distinguishing the embedded watermark. Thus, capacity of a watermarking system is very important if there are differently watermarked versions of data [14]. Moreover, it is obvious that increasing the capacity of a system increases the robustness.

## 2.6  Spread Spectrum Watermarking

As explained before, one of the most common watermarking techniques in the literature is spread spectrum watermarking, especially for images. The idea of spread spectrum watermarking aroused because of the resultant trade-off in the watermarking process. If the watermark is embedded only in high frequency components of an image, the system is not robust against watermark removal attacks. On the other hand, embedding the watermark into the low frequency components creates fidelity problems. As a result, the problem is then, defined as inserting the watermark into low frequency components of an image while preserving the high fidelity [2, 7].

In order to solve this problem an analogy between the watermarking and the spread spectrum communication is established. In spread spectrum communication, the message to be sent (possibly a narrowband signal) is modulated by a broadband carrier which spreads the narrowband signal. Thus, the energy of the message signal in any frequency is undetectable. Therefore, it is possible to get the message if the location of the message signal is known.

In spread spectrum watermarking, the frequency spectrum of the host image is seen as a communication channel and the watermark is seen as a message to be sent through this channel. The watermark signal is well placed into the frequency components of the frequency components of the host image. The energy of the watermark signal in each frequency component of the host image is tuned and the watermark becomes imperceptible if this energy is low enough in each component. In the presence of the host data, it is very easy to extract the watermark if the

location of the watermark signal is known as spread spectrum watermarking. There are lots of different spread spectrum watermarking algorithms which embed watermarks into the host image in different transform domains.

### 2.6.1.  DCT Domain Approaches

In Figure 2.3, a very simple example of this method is presented. In this method, first of all, the frequency components of a host image, ($c_i$), is obtained by taking DCT, and the largest 1000 of these DCT coefficients are taken. Then, these coefficients are marked by the randomly generated and Gaussian distributed watermark sequence, W, as given in the following equation:

$$c_i' = c_i + \alpha.w_i, \mathrm{i} = 1,2,...,1000 \tag{2.4}$$

where α is a constant. The watermarked image is obtained by taking the IDCT of the modified coefficients.

Using this watermarking scheme it is also possible to illustrate the trade-off in the watermarking process. As explained before, it is possible to make the watermark imperceptible by selecting an appropriate α value given in Equation (2.4). However, the choice of this value also determines the robustness of the system. In Figure 2.3 (c) and (d), the watermarked Lena images can be seen with α value 0.3 and 0.5, respectively.

As it can be easily understood from Figure 2.3 *(b)-(d),* increase in α value causes the watermark to become perceptible. On the other hand, this increase makes the system more robust against various attacks since the energy of the watermark in the host signal increases. This trade-off is the major one which can be seen many watermarking schemes in the literature[1, 7, 15-17]. As a result, the best solution for this problem is defining the optimum fidelity-robustness criteria depending on the application.

*Figure 2.3  (a) Original, (b) watermarked Lena images when α=0.1 (PSNR=35.88 dB), (c)  α=0.3(PSNR=26.37 dB) and (d) α=0.5 (PSNR=20.07 dB)*

In [18] a better approach is proposed in terms of the watermark invisibility. In this method, first of all the DCT coefficients are zig-zag scanned to form a vector $\{c_1, c_2, \ldots, c_N\}$ where N is the multiplication of the image width and height. The watermark, $W=\{w_1, w_2, \ldots, w_M\}$, consists of M randomly generated real numbers; each of them is a Gaussian random variable having zero mean and unity variance. Then these watermark sequence is added to the DCT coefficients as given in equation (2.5).

$$c'_{L+i} = c_{L+i} + \alpha \cdot |c_{L+i}| \cdot w_{L+i} \qquad (2.5)$$

After reordering the modified DCT coefficients, the watermarked image is obtained by taking the IDCT of these coefficients. Since the watermark is embedded into the first M coefficients after the first L coefficients, the watermark becomes less noticeable for human eye. In Figure 2.4, the watermarked Lena image obtained with this method is illustrated.



*Figure 2.4 (a)Original Lena image  and (b) its watermarked version with Barni et. al.'s method while L=M=16000 and α=0.3(PSNR=43.03 dB)*

### 2.6.2.  DFT Domain Approaches

Another transform domain popular in watermarking approaches is DFT domain. The main advantage of this transform domain is to provide systems more robust against geometrical attacks.

One of the DFT domain approaches is proposed by Ruanaidh and Pun [19]. In this method the watermark is added to the host signal in a rotation, scaling and transformation (RST) invariant domain. First of all, the DFT of the host image is

followed by Fourier-Mellin transform, which is in fact another DFT following log-polar mapping (LPM), in order to obtain the RST invariant coefficients to be marked. Despite there is not any data loss in continuous case, the log-polar mapping operation causes huge amount of data loss because of the many of the rounding operations in trigonometric and logarithmic operation [4]. Hence the watermarked image quality is very low.

Pitas and Solachidis [20] proposed to embed a 2-D circularly symmetric sequence composed of 1's and -1's with zero mean as the watermark in DFT domain. However, the watermark should be located the optimum place in order the watermark to be invisible and the system to be robust against attacks like compression or LP-filtering. In other words, if the zero frequency term is in the middle of the transform domain, the watermark should be a ring covering these frequency components.

In order to explain the method better, define $V_M(k,l)$ as the magnitude and $V_P(k,l)$ as the phase of DFT of an NxN original image. Let also $W(k,l)$ be the watermark. The watermark is created that locates in the middle frequency components hence:

$$W(r,\theta) = \begin{cases} 0, \text{if } r < R_1 \text{ or } r > R_2 \\ 1 \text{ or } -1, \text{if } R_1 < r < R_2 \end{cases} \tag{2.6}$$

where $r = \sqrt{k^2 + l^2}$ and $\theta = \arctan\dfrac{l}{k}$. After that, the watermark $W$ is added to the magnitude of DFT of the host image, $V_M$, with after scaling by a factor $\alpha$ as given below:

$$V'_M(k,l) = V_M(k,l) + \alpha \cdot W(k,l) \tag{2.7}$$

The watermarked image is obtained by taking the IDFT of the modified frequency components. Note that, the watermark should be created to have the symmetry

property given in equation (2.8) since the DFT of a real data is symmetric and in order to obtain a real image after IDFT the modified DFT coefficients should be symmetric:

$$W(k,l) = W(N-k, N-l), \quad \forall \mathrm{k}, \mathrm{l} \in [1, N] \tag{2.8}$$

This method is much simpler than Ruanaidh and Pun's method since Fourier-Mellin transform is an operation with high computational cost. Furthermore, if the parameters $R_1$, $R_2$ and $\alpha$ are selected effectively a high quality watermarked image is obtained that robust against many kinds of attacks especially geometrical ones. In Figure 2.5, the watermarked Lena image is given obtained by Solachidis and Pitas' method.



*Figure 2.5 (a) Original Lena image and (b) its watermarked version with Solachidis and Pitas' method when $R_1$=60, $R_2$=150 and $\alpha$=2000 (PSNR=42.6 dB)*

### 2.6.3. DWT Domain Approaches

DWT domain is mostly used for multi-resolution analysis of the images. Hence in this domain, the regions of the host image to be watermarked can be determined in

terms of HVS characteristics. Hence an image adaptive watermarking scheme can be proposed.

One of the primary watermarking methods in DWT domain is proposed by Dugad et. al. [21]. This is very similar to Barni et. al.'s method but adapted to DWT domain. In this method, the watermark is embedded to all DWT coefficients larger than a specified threshold rather than predefined number of coefficients.

The watermark in this method is a Gaussian distributed pseudo-random real number sequence with the same length of selected coefficients. These coefficients are obtained by 3-level DWT with Daubechies 8-tap filter. The lowest-frequency band is picked out and the watermark is added as equation (2.9) to remaining ones which are above a threshold T.

$$c_i^{'} = c_i + \alpha \cdot |c_i| \cdot w_i \qquad (2.9)$$

where $i$ runs over all the selected DWT coefficients, $c_i$ represent the DWT coefficients, $w_i$ represents the watermark and $c'_i$ is the modified DWT coefficient. The watermarked image is obtained by taking IDWT of the modified coefficients. In Figure 2.6, the watermarked Lena image can be seen. In this image, the number of watermarked coefficients is low since it is a smooth image and the 3 high sub-band coefficients are small. However, for the images with high frequency characteristics (i.e. Baboon image) much more coefficients are chosen to be watermarked.

*Figure 2.6 (a) (a)Original Lena image  and (b) its watermarked version with Dugad et. al.'s'  method when T=40 and α=0.3 (PSNR=37.19 dB)*

# CHAPTER 3

# HOLOGRAPHY AND WAVE THEORY

## 3.1 What is Holography

Holography is one of the three dimensional (3-D) techniques. Unlike the other existing methods, like stereoscopy, holography is the only one that provides all depth cues[22]. These depth cues are given as accommodation, binocular disparity, motion parallax and occlusion. Stereoscopic techniques, on the other hand, use the psychology of perception in order to create 3-D views and uses mainly binocular disparity. However, the lack of motion parallax and occlusion therefore, these techniques provide worse quality 3-D scenes for one viewing angle only. Accommodation is a weak depth cue about focusing which is effective for short viewing distances. Binocular disparity provides different views for both eyes where motion parallax causes the scene change when the viewer moves around the object. Occlusion is caused by the overlapping of two objects.

Holographic recording technique is related to the wave theory of the light but very similar to the conventional photography. In photography, only the amplitude of the light reflected from the objects (object wave) is stored. However, in holography the phase of the waves is recorded by use of a "coherent background", [23] which enables to store phase information with respect to this background. As the described background a reference wave is used and the diffraction pattern of the reflected wave and a reference wave is stored on the film. Another difference

between the holography and the photography is the used light sources since holograms can be created with only coherent light sources, i.e. laser. As a result, both photographs and holograms are 2-D images but the holograms create a duplication of the object wave, therefore a 3-D scene, where the photographs contain only 2-D information.

By understanding the wave diffraction theory and the mathematics of the interference it is very easy to understand the theory behind the holography. On the other hand there are some practical problems during the hologram creation. Any movement of the film to be stored or the object during exposure time may spoil the recorded hologram. However, many of these problems are overcame by use of digital holographic techniques, [24], [25].

## 3.2   History of Holography

The theoretical principles underlying holography were worked out as early as 1816 when Auguste Fresnel calculated the diffraction patterns of different objects,[22]. He used Thomas Young's diffraction theory (1802) and Christian Huygen's wave model (1678) to build his mathematical model. At the same time the first experiments of the photography were carried out by Thomas Wedgwood (1802) and Nicephore Niepce (1816). However, the development of the holographic theory rose after more than a century. Holography was invented by an English (native Hungarian) scientist Denis Gabor in 1948, [26-28]. He primarily aimed to improve the resolution of electron microscopy by this technique, [29]. First of all Gabor called this technique as wavefront reconstruction but soon he created the term hologram by combining the Greek words "holos" meaning whole and "gramma" meaning message.

The Gabor's idea was adapted to optical field by some scientists like Rogers, El-Sum, Kirkpatrick and Lohmann, [24], but the interest to this technique declined because of poor quality of the holographic images obtained. However, in 1960 N. Bassov, A. Prokhorov and C. Townes invented the laser which is a coherent light

source ideal for hologram creation,[22]. In 1962, Emmett Leith and Juris Upatnieks introduced the off-axis holographic technique, [30], and they obtained one of the earliest laser transmission holograms seen in Figure 3.1.



*Figure 3.1 Reconstruction of the off-axis hologram recorded by Leith and Upatnikes in early 1960's.*

In the same year a Soviet scientist, Y. N. Denisyuk, produced the first hologram which can be viewed by using white light. In 1965, a model of computer generated hologram(CGH) was presented by B. R. Brown and A. W. Lohmann [22]. These achievements are led to the discovery of holographic interferometry in 1965 by Stetson and Powell [24]. Another major advance in holography occurred when Stephen A. Benton invented white-light transmission holography. This type of holograms can be viewed by using white lights and created a rainbow image. Because of his invention, Denis Gabor is awarded the Nobel Prize in Physics in 1971. In 1989, a holographic video system is designed by MIT Media Laboratory Spatial Group, [31], [32]. This system could work in real time but the information content was reduced by elimination of vertical parallax, reduction of hologram size and resolution.

## 3.3   Light Waves

The primary phenomena that build the holography are interference and diffraction, which come from the wave nature of the light. As a result, it is required to know the basics of the wave theory of the light in order to understand the recording and reconstruction stages of the holography. The wave equation of the light, which is followed from the Maxell equations, is as given:

$$\nabla^2 \vec{E} - \frac{1}{c^2} \frac{\partial^2 \vec{E}}{\partial t^2} = 0 \tag{3.1}$$

where $\vec{E}$ is the electric field strength, c is the speed of light ($\sim 3.10^8$ m/s) and $\nabla^2$ is the Laplace operator:

$$\nabla^2 = \frac{\partial^2}{\partial x^2} + \frac{\partial^2}{\partial y^2} + \frac{\partial^2}{\partial z^2} \tag{3.2}$$

The wave equation is set by vector notation since it may vibrate in any direction however, for most applications the wave is assumed to vibrate in a single plane. This kind of wave is so called plane polarized and the scalar wave equation is given as:

$$\frac{\partial^2 E}{\partial z^2} + \frac{1}{c^2} \frac{\partial^2 E}{\partial t^2} = 0 \tag{3.3}$$

The most important solution for this equation is the harmonic wave which is:

$$E(z,t) = E_0 \cos(kz - wt + \varphi) \tag{3.4}$$

where $E_0$ is the real amplitude, w is the angular frequency, φ is the relative phase and k is the wave number, defining as

$$k = \frac{2\pi}{\lambda} \qquad (3.5)$$

By using the Euler formula the harmonic wave can be described as follows:

$$E(z,t) = \frac{1}{2}E_0 e^{j(kz-wt-\varphi)} + \frac{1}{2}E_0 e^{-j(kz-wt-\varphi)} \qquad (3.6)$$

In equation (3.6), the second term is the complex conjugate of the first term and can be omitted since only the real part of E(z,t) represents the physical wave. Thus the harmonic wave in complex notation is:

$$E(z,t) = \frac{1}{2}E_0 e^{j(kz-wt-\varphi)} \qquad (3.7)$$

A wavefront is the locus of points having the same phase. In other words, it refers to the spatial distribution of the maxima of the wave, or other surfaces of constant phase, as these surfaces propagate, [24]. The wavefronts are normal to the direction of propagation. If a wave has constant phase in all planes orthogonal to the propagation direction for a given time t, this wave is called plane wave. Then,

$$\vec{k} \cdot \vec{r} = const. \qquad (3.8)$$

where, $\vec{k}$ is the wave vector, $(k_x, k_y, k_z)$ and the r is the spatial vector, (x, y, z). Thus a plane harmonic wave is described as follows:

$$E(\overrightarrow{r,t}) = E_0 e^{j(\vec{k} \cdot \vec{r} - wt + \varphi)} \qquad (3.9)$$

Another waveform that is widely used is the spherical wave whose phase is constant on each spherical surface. The importance of this kind of waves comes from Huygen's principle, [24]. According to Huygen's principle, every point on a

propagating wavefront serves as the source of spherical secondary wavelets, such that the wavefront at some later time is the envelope of these wavelets. In other words, if the propagating wave has a frequency, f, and is transmitted through the medium at a speed, v, then the secondary wavelets will have the same frequency and speed.

In order to describe the spherical harmonic wave, it is better to transform the Cartesian coordinates, (x, y, z), to the polar coordinates, (r, θ, ψ), using the equations:

$$x = r \sin \theta \cos \psi \tag{3.10}$$

$$y = r \sin \theta \sin \psi \tag{3.11}$$

$$z = r \cos \theta \tag{3.12}$$

The scalar wave equation in the polar coordinates becomes:

$$\frac{1}{r} \frac{\partial^2 (rE)}{\partial r^2} - \frac{1}{c^2} \frac{\partial^2 E}{\partial t^2} \tag{3.13}$$

Then, the solution of the spherical harmonic wave is:

$$E(r,t) = \frac{E_0}{r} e^{j(kr - wt + \varphi)} \tag{3.14}$$

## 3.4   Diffraction Theory

Since the holography strictly builds upon the wave nature of the light, it is required to be familiar with the diffraction effects. Diffraction is a phenomenon by which wavefronts of propagating waves bend in the neighborhood of obstacles.

Let's consider the problem of diffraction by an aperture Λ in an infinite opaque screen. The geometry of the aperture can be seen in Figure 3.2.
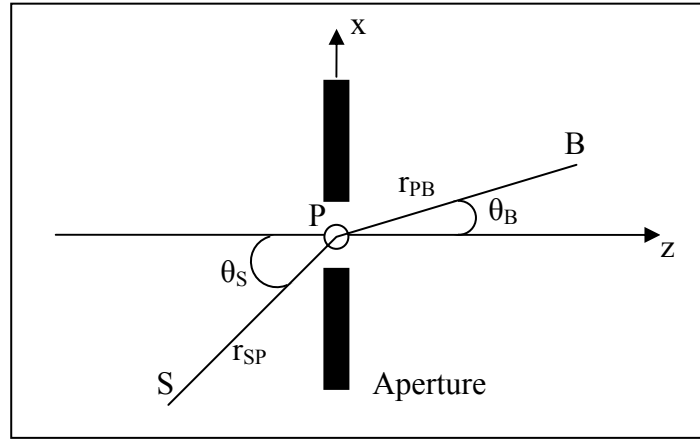
*Figure 3.2 Geometry for Fresnel-Kirchoff diffraction formula*

In this configuration, the aperture is in the z=0 plane of a Cartesian coordinate system. It is illuminated by a spherical wave $E(r) = \dfrac{E_0}{r} e^{jkr}$ emitted from point S and observed from point B. The distance from S to an arbitrary point in the aperture P is $r_{SP}$, and the distance from P to B is $r_{PB}$. The angles between z axis and the vectors $\overrightarrow{SP}$ and $\overrightarrow{PB}$ are $\theta_S$ and $\theta_B$, respectively. Then the field at the observation point, B, is evaluated by the Fresnel-Kirchoff integral given by:

$$E(B) = \frac{jE_0}{\lambda} \iint_\Lambda \frac{e^{-jk(r_{SP}+r_{PB})}}{r_{SP}r_{PB}} \left( \frac{\cos\theta_B - \cos\theta_S}{2} \right) dxdy \qquad (3.15)$$

Note that, in order to hold this equation, k must be much greater than $\dfrac{1}{r_{PB}}$, meaning that the observation point must be many optical wavelengths apart from the aperture.

Another case for the diffraction is illumination of an amplitude transmittance, $\tau(x,y)$ which can be placed in the z=0 axis as seen in Figure 3.3. Let this transmittance is illuminated by a plane wave $E_i(x,y) = E_0 e^{j\vec{k}\cdot\vec{r}}$, propagating parallel to the z-axis.

25
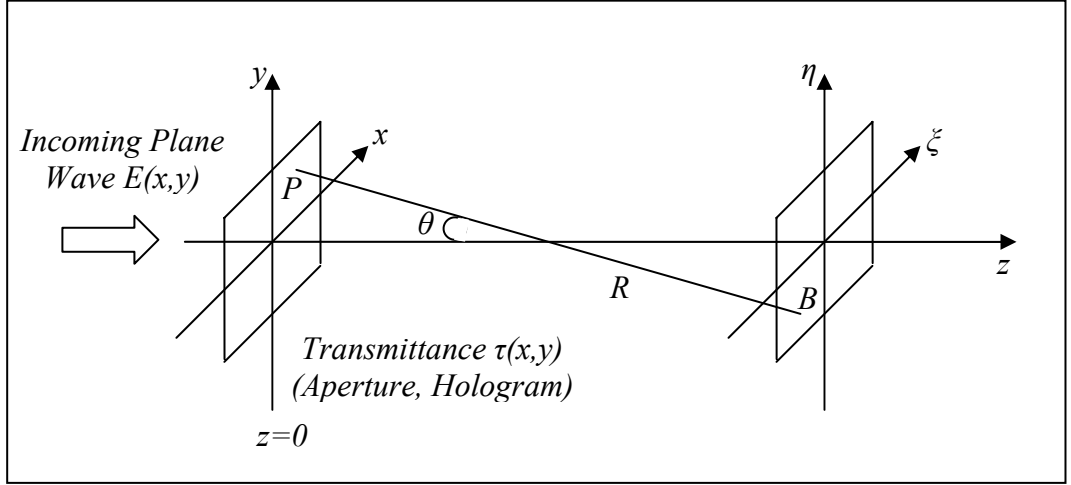
*Figure 3.3 Plane wave illumination of a transmittance*

This setup illustrated above can be seen as a hologram illuminated by a plane reference wave. In this case, the transmittance just after the transmittance (z=0), the field is:

$$E(x, y) = \tau(x, y)E_i(x, y) \tag{3.16}$$

As a result, the field at points far from the z=0 plane is evaluated by the integration of all spherical waves emitted from the (x,y,0) as shown below:

$$E(\xi, \eta, z) = \frac{E_0}{j\lambda} \int_{-\infty}^{\infty}\int_{-\infty}^{\infty} \tau(x, y) \frac{e^{jkR}}{R}(\frac{1}{2} + \frac{1}{2}\cos\theta)dxdy \tag{3.17}$$

The integral shown in (3.17) is so called Fresnel-Kirchoff integral.

In order the equation (3.17) to hold, all x, y, $\xi$ and $\eta$ values should be much less than the z value. As a result, the angle $\theta$ is also small and $\cos\theta \approx 1$. Moreover, the R value, which is equal to $\sqrt{(\xi - x)^2 + (\eta - y)^2 + z^2}$, can be approximated to z and R can be expressed by the first terms of the Taylor series expansion as:

$$R = z\sqrt{1 + \frac{(\xi - x)^2}{z^2} + \frac{(\eta - y)^2}{z^2}} \tag{3.18}$$

$$\Rightarrow R \approx z + \frac{(\xi - x)^2}{2z} + \frac{(\eta - y)^2}{2z} \tag{3.19}$$

These manipulations yield to the Fresnel approximation of the Fresnel-Kirchoff integral which is:

$$E(\xi,\eta,z) = \frac{E_0 e^{jkz}}{j\lambda z} \int\limits_{-\infty}^{\infty}\int\limits_{-\infty}^{\infty} \tau(x,y) e^{\frac{jk}{2z}\left[(\xi-x)^2+(\eta-y)^2\right]} dxdy \tag{3.20}$$

The factor $e^{jkz}$ factor can be omitted in equation (3.20) since it only affects the overall phase independently of $\xi$ and $\eta$. Moreover after multiplying the terms in the argument of the exponential under the integrals, the equation becomes:

$$E(\xi,\eta,z) = \frac{E_0}{j\lambda z} e^{\frac{j\pi}{\lambda z}(\xi^2+\eta^2)} \int\limits_{-\infty}^{\infty}\int\limits_{-\infty}^{\infty} \tau(x,y) e^{\frac{j\pi}{\lambda z}(x^2+y^2)} e^{-\frac{j2\pi}{\lambda z}(\xi x+\eta y)} dxdy \tag{3.21}$$

From the equation above, it is easily seen that the Fresnel approximation, up to a spherical phase factor, is the inverse Fourier Transform of the transmittance $\tau(x,y)$ multiplied with a varying phase factor. Then, the equation (3.21) is equal to

$$E(\xi,\eta,z) = \frac{E_0}{j\lambda z} e^{\frac{j\pi}{\lambda z}(\xi^2+\eta^2)} \Im\left\{ \tau(x,y) e^{-\frac{j\pi}{\lambda z}(x^2+y^2)} \right\} \tag{3.22}$$

where $\Im$ represents the Fourier Transform.

The Fresnel approximation can be used for distances greater than about ten wavelengths, [24]. For very large distances of the observation plane from the diffraction plane, the varying phase factor multiplied by the transmittance is very

close to 1 then the resulting field becomes the Fourier Transform of the transmittance multiplied with the spherical phase factor.

## 3.5   Types of Holograms

There are very different types of holograms, [22], and usually they are classified according to the way they are produced and they can incorporate and store the information for playback. There are two main categories of the holograms called as transmission and reflection holograms. In transmission holography, the reference and object beams interfere on the holography recording material from the same side i.e. the light passes through the holographic plate. During the 3-D object reconstruction process the hologram should be illuminated by the same reference wave in the recording process located at the same position but the back of the hologram.

On the other hand, the reflection holograms are made by the object and reference beams incident from opposite sides of the recording material. In the reconstruction process the reference wave is located at the same side with the viewer unlike the transmission holography and these types of holograms are visible without laser light used in recording.

Another classification of the holograms is defined in terms of the location of the reference light source with respect to the 3-D object. These types of holography are in-line and off-axis holography. In-line holography is the recording scheme proposed by Gabor [26], in 1948. In this setup, a light source is located behind the object to be recorded and the light passing unaffected from the particles is used as the reference wave where the scattered light is the object wave, [24]. As a result, this type of holography is more appropriate to record transparent objects. Since there is no beam splitting into reference and object waves, this type of holography is also called as single beam holography. In the reconstruction process the hologram is illuminated by the light source in the recording process which creates the virtual image in the original position of the 3-D object as well as the real image

on the opposite side of the hologram. The main disadvantages of this recording setup are the distributed reconstruction due to the bright reference wave and the twin image problem. The twin image problem is caused of laying the virtual and real images on the same line of sight. So, while focusing on one of the images, this image is affected by out of focus image of the other one. These disadvantages are avoided by the off-axis arrangement, [22, 24]. In this arrangement the light emitted from the source is spitted into two pieces as object and reference waves, which makes the method to be called as split beam or two beam holography. If the angle between the object and reference wave is large enough, then the real and imaginary images do not overlap.

The requirement of a coherent light source in both recording and reconstruction processes makes the holography impractical. If a typical hologram is illuminated with white light, each component in different frequency is diffracted to different directions and reconstruction becomes impossible since these wave fields are superimposed. Another type of the holography, white light holography, presents a partial solution to this problem. Despite recording the hologram using a laser source, this type of holography eliminates the need of a coherent light source in the reconstruction process by using thickness of the photographic emulsion.

In this setup reference wave is the light coming directly from the laser and the object wave is the light passing through the recording media and reflected from the 3-D object. Note that, in order to get good results with this setup, it is required to use a strongly reflecting object and the hologram plate should be close to the object. In the reconstruction, the object is seen in the color of the laser if the hologram is illuminated by the light with the angle in recording and with a specific viewing angle determined by the wavelength of the laser light and the angle of the reference wave.

Rainbow holography is another type of holography and by exchanging the variation of the vertical parallax against a variation of a wavelength. The first task in this

method is to record a usual hologram of a 3-D object which is called master hologram. Then a real pseudoscopic image is reconstructed by reversing the hologram or the direction of the reference wave. In front of the hologram a slit aperture is placed and the hologram of the wave field passing through this slit is recorded.

This process makes the vertical parallax lost but it is not recognized immediately, as long as the eyes of the observer are horizontally arranged, [24]. Another effect of this process is that the object is reconstructed in different colors converging to different reconstructed slits, i.e. if ones look from different vertical locations; the reconstruction of the object is seen in different color. Since by this way the object can be seen in the colors of the rainbow, this kind of holography is called as rainbow holography [22].

Another type of the holography is holographic interferometry, which is based on the comparison of the wave fields, [24]. This interferometric comparison is between the holographically reconstructed wave fields and either another holographically reconstructed wave field or a wave field directly scattered by the object. In this technique, better results are obtained with the increasing the number of the wave fields to be compared. There are various types of interferometry techniques and phase shifting digital interferometry (holography) will be explained in details since this type of holograms are used in this work.

## 3.6    Phase Shifting Digital Holography

The practical applications of conventional holography were so limited since the developing the holograms took long time and high cost. Hence, the idea of reconstruction of a hologram by a computer was firstly proposed by Goodman and Laurance, [33], in 1967. This process reduces the recording time substantially and makes it possible to process the holograms digitally to facilitate many different kinds of applications [34].

In early times, this method lacks of adequate imaging devices and powerful computers. Today these handicaps have been overcome and it is possible to record holograms with an inexpensive CCD camera and the reconstruction can be performed with a personal computer. However, it is still one of the most problematic issues of the digital holography that the resolution of the CCD cameras used for hologram recording is lower than the photographic films used in conventional holography. Another issue that should be taken into account in digital holography is suppression of the zero order term and the conjugate image [34]. As a result, some techniques have been proposed in order to eliminate these terms and increase the reconstructed image quality.

Up to now, various kinds of digital holography techniques have been proposed [33, 35, 36]. These techniques used off-axis recording setup to suppress the DC term and conjugate image easily. However, this method increases the spatial resolution requirements of the system and causes to low resolution resultant holograms. In [25, 37], the resolution problem is solved using an in-line setup and measuring the complex amplitude of the object wave at the CCD plane by phase shifting interferometry. The phase of the reference waves is changed stepwise and the resulting interference fringes are processed by a computer to obtain the distribution of the complex amplitude of the wave. This process is called phase shifting digital interferometry. In this thesis, phase shifted digital holograms will be used, therefore, in this section; this type of hologram recording and reconstruction processes will be explained in detail.

### 3.6.1. *Hologram Recording*

One approach used for recording a hologram by phase shifting digital holography technique is given in Figure 3.4. This setup is called Mach-Zehnder interferometry.
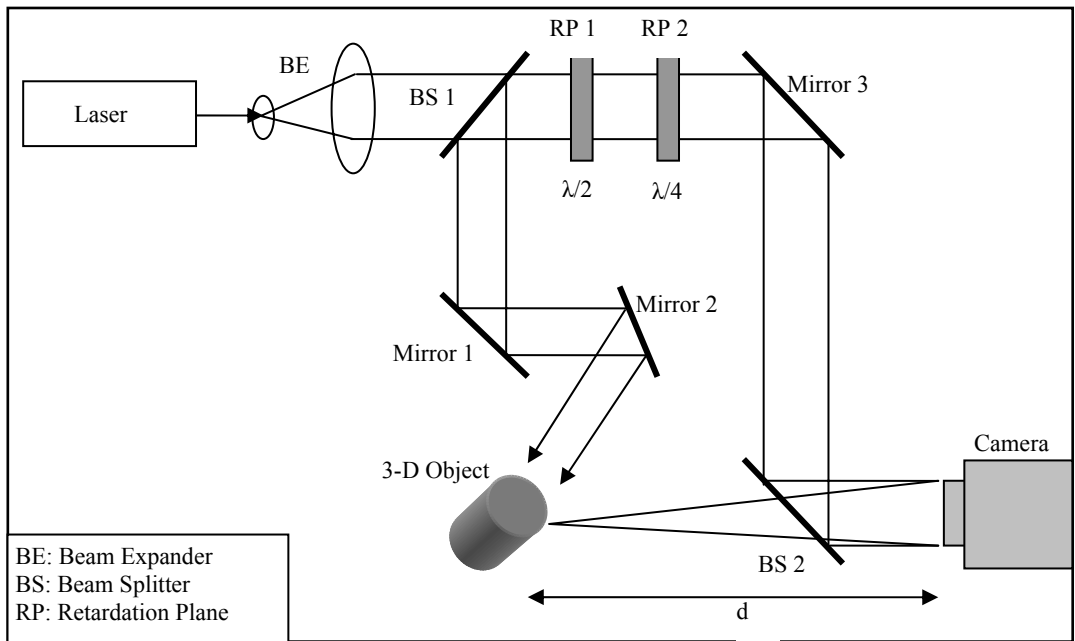
*Figure 3.4 Arrangement for phase shifting digital holography*

In this setup, the laser beam is firstly divided into object and reference waves which are both filtered and expanded. In order to describe the mechanism in this arrangement and analyze the numerical construction and reconstruction of the hologram the coordinate system shown in Figure 3.5 is used.
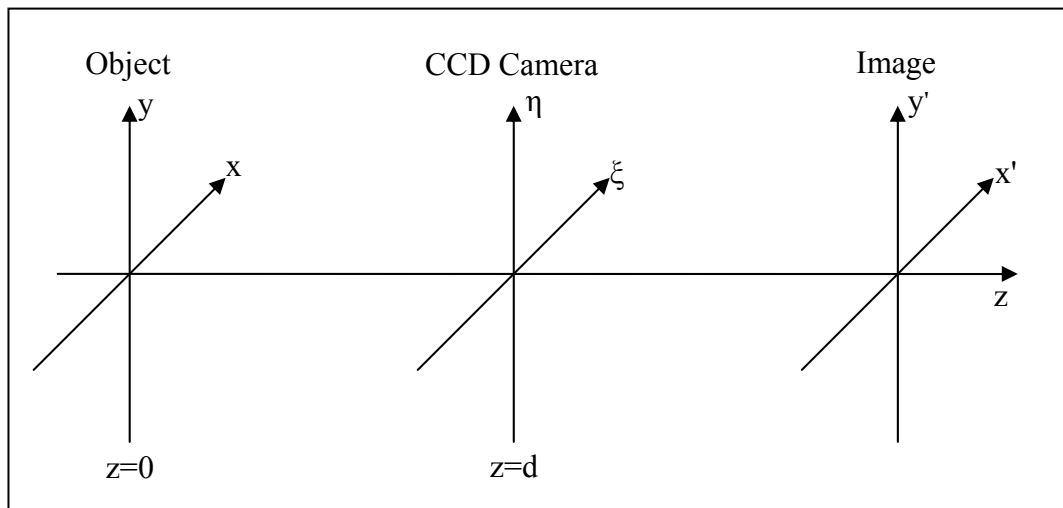


*Figure 3.5 Coordinate system adopted for numerical analysis of hologram recording and reconstruction processes*

32

The first beam illuminates the 3-D object located in distance of d from the CCD camera. Then the object wave at the camera plane can be described as in Equation (3.23) using the free space propagation and the Fresnel approximation given in equation (3.20):

$$U(\xi,\eta) = \frac{e^{jkd}}{j\lambda d} \int\limits_{-\infty}^{\infty}\int\limits_{-\infty}^{\infty} U_0(x,y)e^{\frac{jk}{2d}\left[(\xi-x)^2+(\eta-y)^2\right]}dxdy \qquad (3.23)$$

where $U_0(x,y)$ describes object wave just after reflecting from the 3-D object.

The second beam, forming the reference wave, passes through two retardation planes and interferes with the object wave at the camera plane. The first of the retardation plates, $RP_1$, is the half-wave plate where the second one, $RP_2$, is the quarter-wave plate. Therefore, by rotating these plates, the linearly polarized reference wave can be phase modulated and four phase shifts of 0, $\pi/2$, $\pi$, $3\pi/2$ can be achieved in this arrangement. For each of the shifted reference wave, one interferogram is recorded by the CCD camera which can be expressed as follows:

$$I(\xi,\eta;\theta) = \left|U_R(\xi,\eta)e^{j\theta} + U(\xi,\eta)\right|^2 \qquad (3.24)$$

$$\Rightarrow I(\xi,\eta;\theta) = \left|U_R(\xi,\eta)\right|^2 + \left|U(\xi,\eta)\right|^2 + 2\operatorname{Re}\left\{U_R(\xi,\eta)U^*(\xi,\eta)e^{j\theta}\right\} \qquad (3.25)$$

where $I(\xi, \eta; \theta)$ represents the recorded interference pattern for $\theta$ radians of phase shift, $U_R(\xi, \eta)$ is the reference wave on the CCD plane and $^*$ denotes the complex conjugate.

Figure 3.6 shows examples of recorded interferograms[1] using phase shifting interferometry. In the recording process, a 532nm laser beam and a 512x512 pixels CCD camera with 9μm pixel pitch are used. The distance between the object and

---

[1] Recorded by Bremer Institut für angewandte Strahltechnik (BIAS) and given for use for EU 3D-TV project.

the camera set to 36cm.



*(a)* *(b)*



*(c)* *(d)*
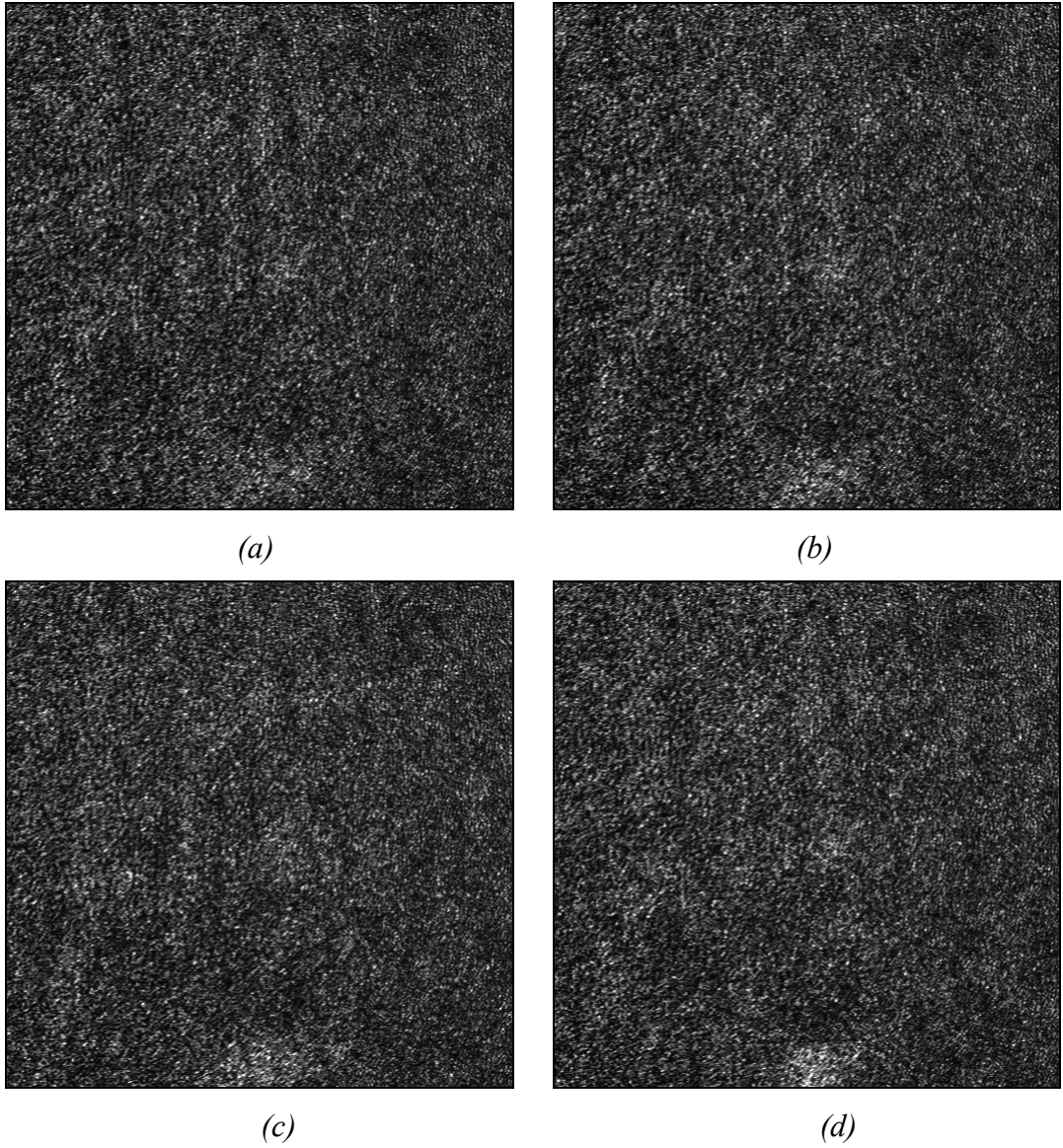
*Figure 3.6 Recorded interference patterns for phase shifts (a) 0, (b) π/2, (c) π, (d)*
*3π/2 radians*

Then, using these interferograms the following equations can be obtained:

$$I_1 = I(\xi,\eta;0) - I(\xi,\eta;\pi) = 4\text{Re}\{U_R U^*\} \tag{3.26}$$

$$I_2 = I(\xi,\eta;\pi/2) - I(\xi,\eta;3\pi/2) = 4\,\mathrm{Re}\{jU_R U^*\} \tag{3.27}$$

Using equations (4.4) and (4.5):

$$I_1 + jI_2 = 4\mathrm{Re}\{U_R U^*\} - j4\mathrm{Im}\{U_R U^*\} \tag{3.28}$$

$$\Rightarrow I_1 + jI_2 = 4(U_R U^*)^* = 4U_R{}^* U \tag{3.29}$$

Finally, the complex amplitude of the object wave, which is basically the hologram of the 3-D object, is derived by:

$$h(\xi,\eta) = U(\xi,\eta) = \frac{I(\xi,\eta;0) - I(\xi,\eta;\pi) + j[I(\xi,\eta;\pi/2) - I(\xi,\eta;3\pi/2)]}{4U_R{}^*} \tag{3.30}$$

As a result, it is possible to record the hologram of a 3-D object by taking four interferograms for four different phase shifts of the reference wave. Note that, because of the approximations done in the Fresnel Transformation (see Chapter 3.5) the obtained result, h(ξ,η), is an approximation of the real hologram. The hologram obtained by equation (3.30) from the interferograms in Figure 3.6 can be seen in Figure 3.7. This hologram will be called "Chess Knight Hologram" rest of the thesis since it is the hologram of a chess knight.

### 3.6.2. Hologram Reconstruction

The reconstruction of a hologram is achieved by illuminating the hologram by the reference wave which was used in the recording process. In digital holography, the hologram can be reconstructed by illuminating the hologram and evaluating the Fresnel Transformation of this complex amplitude as follows:

$$U_0{}'(x',y') = \frac{e^{jkz}}{j\lambda z} \int\limits_{-\infty}^{\infty}\int\limits_{-\infty}^{\infty} h(\xi,\eta)R(\xi,\eta)e^{\frac{jk}{2z}[(x'-\xi)^2 + (y'-\eta)^2]} d\xi d\eta \tag{3.31}$$

*(a)*                      *(b)*
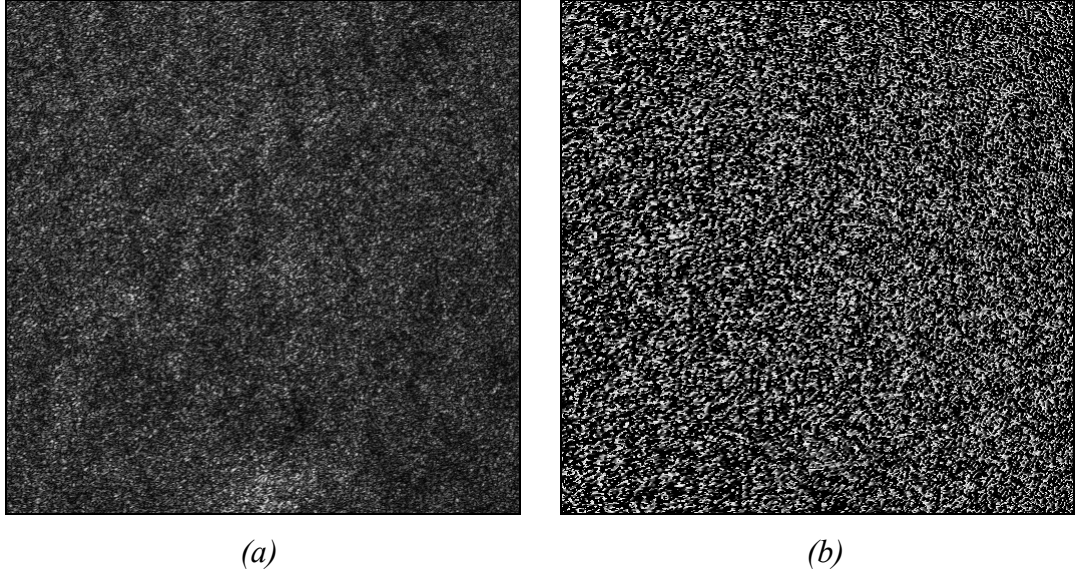
*Figure 3.7 The (a) magnitude, (b) phase of the hologram obtained by phase shifting holography*

Put U($\xi$,$\eta$) in (3.23) instead of h($\xi$,$\eta$) in the equation above:

$$U_0'(x',y',z) = \frac{e^{jkz}}{j\lambda z} \int_{-\infty}^{\infty}\int_{-\infty}^{\infty} \left( \frac{e^{jkd}}{j\lambda d} \int_{-\infty}^{\infty}\int_{-\infty}^{\infty} U_0(x,y) e^{\frac{jk}{2d}\left[(\xi-x)^2+(\eta-y)^2\right]} dxdy \right) R(\xi,\eta) e^{\frac{jk}{2z}\left[(x'-\xi)^2+(y'-\eta)^2\right]} d\xi d\eta$$

$$(3.32)$$

$$U_0'(x',y',z) = \frac{e^{jkz}}{j\lambda z} \frac{e^{jkd}}{j\lambda d} \int_{-\infty}^{\infty}\int_{-\infty}^{\infty}\int_{-\infty}^{\infty}\int_{-\infty}^{\infty} U_0(x,y) R(\xi,\eta) e^{\frac{jk}{2d}\left[(\xi-x)^2+(\eta-y)^2\right]} e^{\frac{jk}{2z}\left[(x'-\xi)^2+(y'-\eta)^2\right]} d\xi d\eta dxdy$$

$$(3.33)$$

$$U_0'(x',y',z) = -\frac{e^{jk\left(z+d+\frac{x'^2+y'^2}{2z}\right)}}{\lambda^2 zd} \int_{-\infty}^{\infty}\int_{-\infty}^{\infty}\int_{-\infty}^{\infty}\int_{-\infty}^{\infty} U_0(x,y) R(\xi,\eta) e^{jk\left\{\frac{\xi^2+\eta^2}{2}\left(\frac{1}{d+z}\right)+\frac{x^2+y^2}{2d}\right\}} e^{-jk\left\{\xi\left(\frac{x}{d}+\frac{x'}{z}\right)+\eta\left(\frac{y}{d}+\frac{y'}{z}\right)\right\}} d\xi d\eta dxdy$$

$$(3.34)$$

The image plane is determined from the condition that the quadratic term of x and y vanishes in the exponent vanishes, [37], i.e. z=-d. Therefore,

$$U_0{}'(x',y',-d) = U_0(x',y')$$ (3.35)

As a result, the reconstruction of the hologram is achieved by taking the Fresnel Transform of h(ξ,η) multiplied with R(ξ,η) at the distance -d as expressed below:

$$U_0{}'(x',y') = \frac{j}{\lambda d} e^{-jkd} \int\limits_{-\infty}^{\infty}\int\limits_{-\infty}^{\infty} h(\xi,\eta) R(\xi,\eta) e^{\frac{-jk}{2d}\left[(x'-\xi)^2+(y'-\eta)^2\right]} d\xi d\eta$$ (3.36)

Note that equation (3.36) is also equal to the inverse Fresnel Transform of h(ξ,η) multiplied with R(ξ,η) at the distance d. Moreover, R(ξ,η) is a real valued multiplicative term and can be neglected for most of the applications, [34]. Finally, after carrying the similar manipulations in equations (3.20) to (3.22) the inverse Fresnel Transform can be expressed with the inverse Fourier Transform as follows:

$$U_0{}'(x',y') = \frac{j}{\lambda d} e^{\frac{jk}{2d}(x'^2+y'^2)} \Im^{-1}\left\{ h(\xi,\eta) e^{-j\frac{\pi}{\lambda d}(\xi^2+\eta^2)} \right\}$$ (3.37)



*Figure 3.8 The reconstruction of the Chess Knight hologram*

In Figure 3.8, the reconstruction of the hologram given in Figure 3.7 can be seen. The reconstruction process is performed by evaluating equation (3.37) with FFT algorithm and taking its magnitude as the reconstructed image of the hologram.

### 3.6.3. Computer Generated Holograms

The hologram generation technique described in the previous section can also be simulated numerically. This process can be achieved by discritization of equation (3.23) and using an image as the object but it is multiplied by a random phase to simulate the object wave, $U_0(x,y)$. Then the equation becomes as in (3.38).

$$h(k,l) = \frac{1}{j\lambda d} e^{j\frac{2\pi}{\lambda}d} \sum_{m=\frac{-M}{2}}^{\frac{M}{2}} \sum_{n=\frac{-N}{2}}^{\frac{N}{2}} U_0(m,n) e^{\frac{j\pi}{\lambda d}\left[(k.\Delta\xi - m.\Delta x)^2 + (l.\Delta\eta - n.\Delta y)^2\right]} \qquad (3.38)$$

where k=-M/2,…,0,1,…M/2 and l=-N/2,…,0,1,…N/2. Here $\Delta\xi$ and $\Delta\eta$ are the vertical and horizontal distances between the neighboring points in the hologram, which are in fact the pixel sizes in the CCD plane where $\Delta x$ and $\Delta y$ are the distance between the pixels of the image. In [35, 36], the relation between $\Delta\xi$, $\Delta\eta$ and $\Delta x$, $\Delta y$ is given as follows:

$$\Delta x = \frac{\lambda d}{M.\Delta\xi}, \qquad \Delta y = \frac{\lambda d}{N.\Delta\eta} \qquad (3.39)$$

Using (3.38) and (3.39) the hologram can be expressed as follows which is the Fourier Transform of the image multiplied by a spherical phase factor:

$$h(k,l) = \frac{1}{j\lambda d} e^{j\frac{2\pi}{\lambda}d} e^{\frac{j\pi}{\lambda d}\left(k^2.\Delta\xi^2 + l^2.\Delta\eta^2\right)} \sum_{m=\frac{-M}{2}}^{\frac{M}{2}} \sum_{n=\frac{-N}{2}}^{\frac{N}{2}} U_0(m,n) e^{\frac{j\pi}{\lambda d}\left(m^2.\Delta x^2 + n^2.\Delta y^2\right)} e^{-j2\pi\left(\frac{km}{M} + \frac{ln}{N}\right)} \qquad (3.40)$$

In Figure 3.9, a 64x64 emblem of the METU can be seen. It is used to generate a hologram using the formula above and the results are presented in Figure 3.10. This hologram is evaluated by the keeping the same parameters in Chapter 3.6.1 for λ, d and the CCD pitch.



Figure 3.9 METU emblem, used to generate hologram



*(a)*                       *(b)*
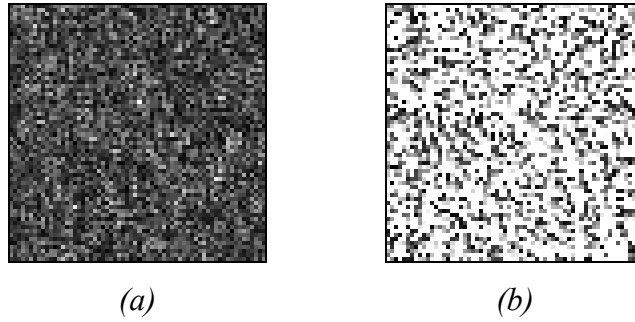
Figure 3.10 (a) Magnitude, (b) phase of the hologram of the METU emblem

The reconstruction process is also performed by evaluating the equation (3.36) numerically. Thus, the reconstruction of the hologram is obtained by the formula:

$$U_0'(m,n) = \frac{j}{\lambda d} e^{-j\frac{2\pi}{\lambda}d} \sum_{k=\frac{-M}{2}}^{\frac{M}{2}} \sum_{l=\frac{-N}{2}}^{\frac{N}{2}} h(k,l) e^{\frac{-j\pi}{\lambda d}\left[(m.\Delta x - k.\Delta \xi)^2 + (n.\Delta y - l.\Delta \eta)^2\right]} \tag{3.41}$$

Since equation (3.39) is also valid for this case the reconstruction formula is expressed by equation (3.42).

$$U_0(m,n) = \frac{1}{j\lambda d} e^{-j\frac{2\pi}{\lambda}d} e^{-\frac{j\pi}{\lambda d}\left(m^2.\Delta x^2 + n^2.\Delta y^2\right)} \sum_{k=\frac{-M}{2}}^{\frac{M}{2}} \sum_{l=\frac{-N}{2}}^{\frac{N}{2}} h(k,l) e^{\frac{-j\pi}{\lambda d}\left(k^2.\Delta\xi^2 + l^2.\Delta\eta^2\right)} e^{j2\pi\left(\frac{km}{M} + \frac{ln}{N}\right)} \quad (3.42)$$

In Figure 3.11, the reconstruction of the hologram given in Figure 3.10 can be seen.
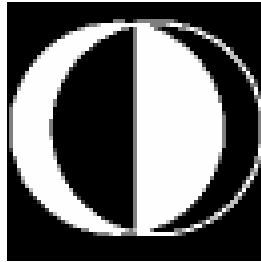


*Figure 3.11 Reconstruction from the generated hologram given in Figure 3.10*

To sum up, equations (3.40) and (3.42) shows that the hologram generation and reconstruction processes can be performed very fast with fast FT algorithms.

# CHAPTER 4

# CHARACTERISTICS OF PHASE SHIFTING DIGITAL HOLOGRAMS

## 4.1    Introduction

As explained in the previous chapters, we propose a method that hides a hologram into a digital image as the watermark. A hologram is chosen for this purpose because of some of its unique characteristics. In this chapter, these properties of the holograms that enable them to use as a watermark will be explained and investigated by the experiments performed.

## 4.2    Properties of Holograms

As explained in the previous chapter, hologram is a signal that stores the 3-D information of an object. Moreover, this signal has impressive characteristics which can be appropriate for many applications.

One of the most impressive properties of holograms is the correlation between the parts of the data. As a result of this characteristic of them, a hologram can be reconstructed from either a piece of the data or a mostly occluded version of it, [38]. To illustrate this property, the reconstructions of different parts of the hologram given in Figure 3.7 are given in Figure 4.1. Furthermore, 90% of this hologram is

occluded (see Figure 4.2 (a)) and the obtained reconstruction from this data is presented in Figure 4.2 (b).



(a)                                      (b)                    (c)
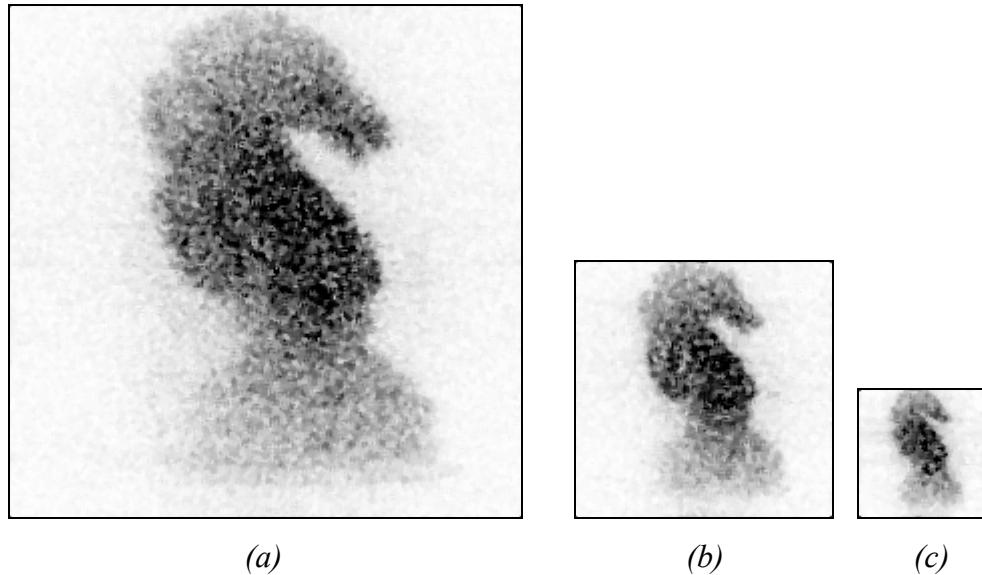
*Figure 4.1 Reconstruction of (a)256x256, (b)128x128, (c)64x64 parts of the Chess Knight hologram*



(a)                                              (b)
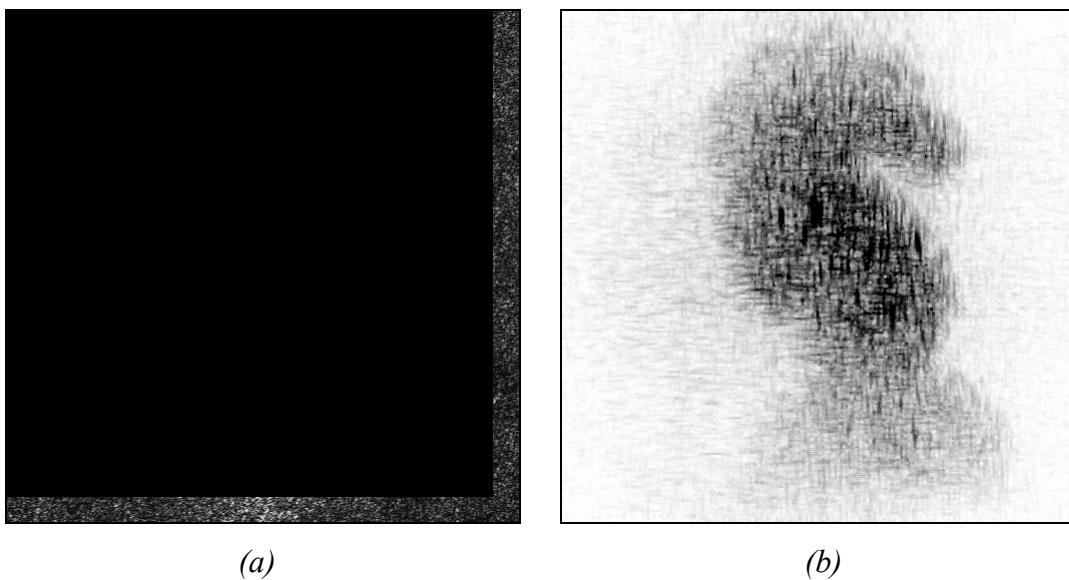
*Figure 4.2 (a) 90% occluded Chess Knight hologram and (b) its reconstruction*

The experiments also show that the holograms can be reconstructed even if one has its real, imaginary or phase parts. This is illustrated in Figure 4.3. As seen from this figure, the quality of the reconstructed image reduces much when only one of the real or imaginary parts of the hologram is used. On the other hand, using only the phase information provides much better reconstructed images. Note that, the object cannot be reconstructed with only the magnitude of the hologram (see Figure 4.3 (d)).



*(a)*                                            *(b)*

*(c)*                                            *(d)*
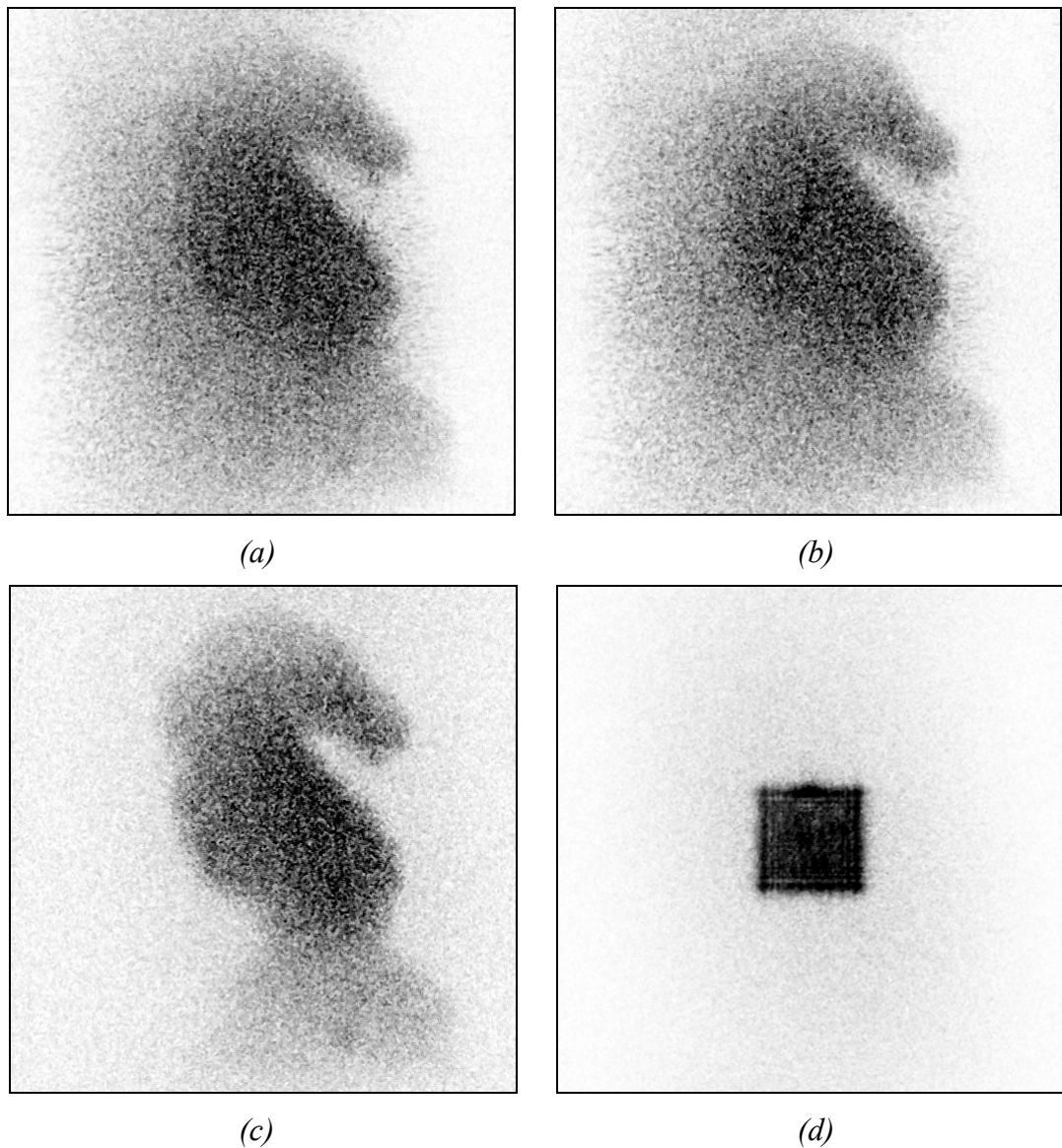
*Figure 4.3 Reconstructed images from (a) real, (b) imaginary, (c) phase and (d) magnitude part of the Chess Knight hologram*

## 4.3    Compression of Holograms

As previously explained, the hologram is a complex signal i.e. it has real and imaginary parts which yields up with a huge sized content. Thus, for storage and transmission of enormous frames of this complex amplitude, this information is required to be compressed in several applications[39-42]. In [40] and [41], the hologram is separated into its real and imaginary parts and the some lossless (Lempel-Ziv, Huffman, Burrows-Wheeler) and lossy (subsampling, quantization) techniques are applied to those parts separately. In [42], the success of these techniques is investigate for the encrypted hologram and similar results are presented. From those results, it is shown that applying the lossless schemes directly to the hologram achieves a compression rate about 1.05. This result is quite predictable since in [43] it is stated that the hologram is of the form of a complex Gaussian noise since its magnitude has a Rayleigh distribution and its phase is uniformly distributed in $[0, 2\pi)$. However, lossless coding is effective when it combines with the quantization, [42], since the size of alphabet of the becomes much smaller.

Based upon these works, the effect of quantization of the hologram is investigated in this thesis. The PSNR values for the reconstructed images for the quantized hologram given in Figure 3.7 are evaluated for the technique described above. These values can be seen in the table below.

The first row in Table 4.1 indicates the number of bits to quantize the real part where the first column indicates the number of bits used in imaginary part quantization. In the quantization process, the real and the imaginary parts are quantized separately using a uniform quantizer. Therefore, first of all the maximum and minimum values of them is found and the intervals between these values are divided into $2^b$ equal parts if b bits is used.

*Table 4.1 PSNR values in dB between the reconstructed images from the original hologram and quantized Chess Knight hologram for different bit depths*

| Real Imag. | 0 | 1 | 2 | 3 | 4 | 5 | 6 | 7 | 8 |
|---|---|---|---|---|---|---|---|---|---|
| **0** | 17.596 | 22.796 | 22.764 | 25.009 | 26.225 | 26.513 | 26.580 | 26.634 | 26.637 |
| **1** | 24.039 | 27.251 | 26.132 | 25.346 | 25.371 | 25.399 | 25.401 | 25.394 | 25.410 |
| **2** | 24.323 | 25.783 | 27.492 | 27.488 | 27.695 | 27.880 | 27.911 | 27.939 | 27.959 |
| **3** | 26.053 | 25.477 | 28.693 | 32.084 | 34.413 | 35.089 | 35.180 | 35.228 | 35.285 |
| **4** | 26.589 | 25.594 | 29.358 | 34.551 | 38.966 | 40.724 | 41.329 | 41.479 | 41.478 |
| **5** | 26.703 | 25.568 | 29.472 | 35.171 | 40.935 | 44.400 | 45.908 | 46.387 | 46.531 |
| **6** | 26.871 | 25.611 | 29.529 | 35.380 | 41.541 | 46.141 | 48.875 | 50.187 | 50.648 |
| **7** | 26.810 | 25.585 | 29.530 | 35.433 | 41.703 | 46.652 | 50.312 | 52.530 | 53.610 |
| **8** | 26.840 | 25.594 | 29.539 | 35.483 | 41.730 | 46.810 | 50.689 | 53.454 | 55.414 |

As seen from Table 4.1, the optimum solution for a desired bit rate and the quality is obtained when the number of bits used to quantize real and imaginary parts is equal. To illustrate this fact, Figure 4.4 is given. The qualities of the first three images are similar while the last one is significantly better than those ones.

In this thesis, the explained quantization scheme is extended for the magnitude and phase quantization of the hologram. Table 4.2 shows the effect of the number of bits used to quantize the magnitude and phase of the hologram on the reconstructed image. For this case, it can be easily seen that the phase information is more important than the magnitude information. For instance, if one uses 4 bits/pixel for phase and 3 bits/pixel for magnitude quantization, the reconstructed image is better than the one obtained by using 3 bits/pixel for phase and 4 bits/pixel for magnitude quantization.
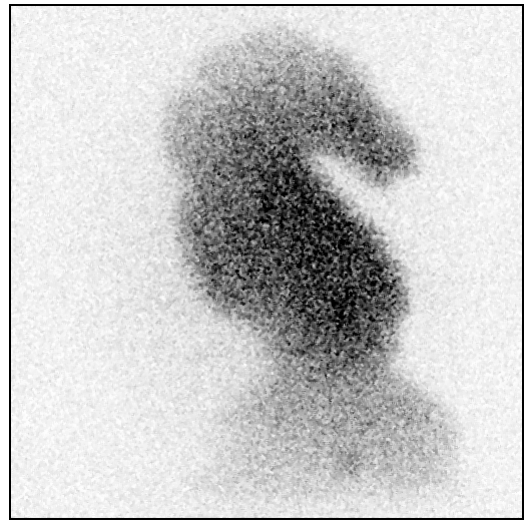
*(a)*                      *(b)*
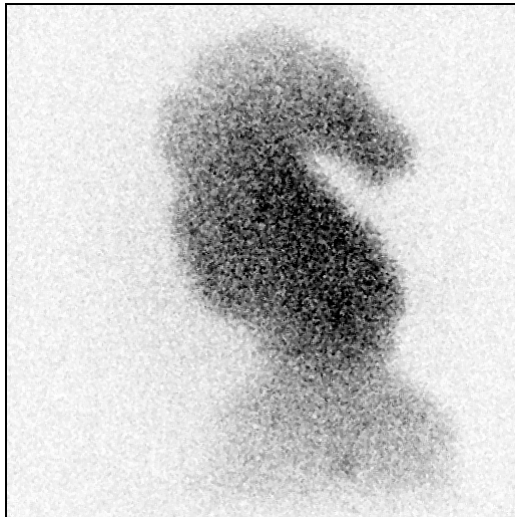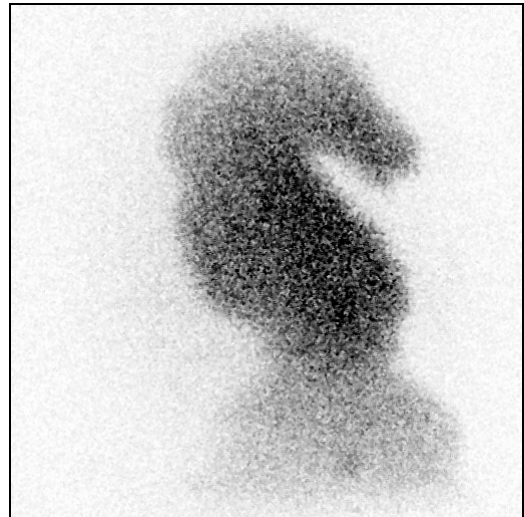
*(c)*                      *(d)*

*Figure 4.4 Reconstructed images for the quantized Chess Knight hologram using (a) 3 bits for real, 3 bits for imaginary, (b) 3 bits for real, 4 bits for imaginary, (c) 4 bits for real, 3 bits for imaginary, (d) 4 bits for real, 4 bits for imaginary parts*

*Table 4.2 PSNR values in dB for the reconstructed images from the quantized magnitude and phase information of the Chess Knight hologram for different bit depths*

| Phs.<br>Amp. | 0 | 1 | 2 | 3 | 4 | 5 | 6 | 7 | 8 |
|---|---|---|---|---|---|---|---|---|---|
| **0** | 17.596 | 24.343 | 27.009 | 29.516 | 30.391 | 30.620 | 30.654 | 30.661 | 30.673 |
| **1** | 22.397 | 19.251 | 19.251 | 19.032 | 19.420 | 19.314 | 19.470 | 19.433 | 19.407 |
| **2** | 22.266 | 23.879 | 26.953 | 30.325 | 31.459 | 31.713 | 31.760 | 31.787 | 31.810 |
| **3** | 21.740 | 25.924 | 29.903 | 34.786 | 37.901 | 39.009 | 39.335 | 39.408 | 39.439 |
| **4** | 21.559 | 25.893 | 30.035 | 36.031 | 41.178 | 43.802 | 44.845 | 45.147 | 45.226 |
| **5** | 21.595 | 25.940 | 30.321 | 36.236 | 42.072 | 45.753 | 48.366 | 49.249 | 49.518 |
| **6** | 21.601 | 26.053 | 30.289 | 36.376 | 42.433 | 46.832 | 50.413 | 52.256 | 52.972 |
| **7** | 21.583 | 26.025 | 30.307 | 36.321 | 42.551 | 47.135 | 51.068 | 53.668 | 55.163 |
| **8** | 21.588 | 26.041 | 30.311 | 36.373 | 42.568 | 47.170 | 51.271 | 54.170 | 56.438 |

It has already been demonstrated in Figure 4.3 (c) that a hologram can be reconstructed using only the phase information. This fact makes using phase only information popular, especially for real time applications [39, 44]. The experiments performed in these works also show that using 4 bit uniform quantizers is enough for phase only coding of the hologram. This is because the quality of the reconstructed image is almost same with the one obtained from the original phase information. The reconstructed image from 4-bit quantized hologram is given in Figure 4.5 and its PSNR value is 30.391 dB where this value is 30.670 dB for the reconstruction from original phase data.
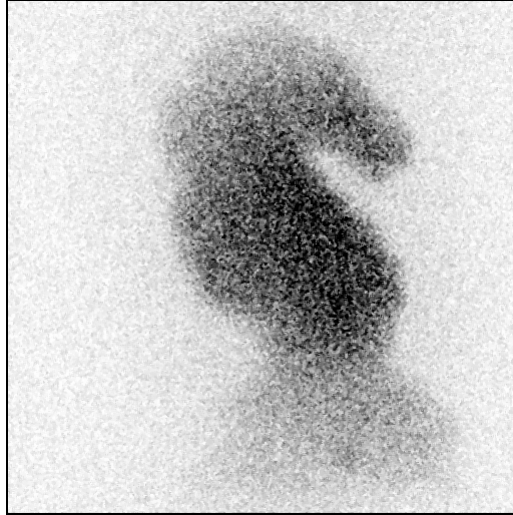
*Figure 4.5 Reconstructed image from the 4 bit/pixel quantized hologram phase given in Figure 3.7(b)*

In order to show the effectiveness of phase only reconstruction of the holograms, experiments are also performed on binary METU emblem given in Figure 3.9. As a result, it becomes possible to evaluate similarities between the original logo and the reconstructions from original hologram, its phase or quantized phase. Bit correct ratio (BCR) is used for this purpose and it is evaluated as given below:

$$BCR = 1 - \frac{\sum_m \sum_n A_{m,n} \oplus B_{m,n}}{M \times N} \qquad (4.1)$$

where $\oplus$ denotes the XOR operator. This metric gives 1 if $A$ and $B$ are same and gives 0 if $A$ is the inverse of $B$. BCR between the original METU emblem and the reconstruction from original hologram (see Figure 3.11) is 1; i.e. they are exactly same. In , the results are given for reconstructions from only the phase of the generated hologram and its 4 bits/pixel quantized version. These results show that the BCR between the original logo and the reconstruction from only the phase of the hologram is 0.9241. Besides, there is not a significant difference between the reconstructions from the phase of the hologram and its 4 bit/pixel quantized version (BCR = 0.9082).

*Figure 4.6 Reconstructions from (a) phase of the generated METU emblem hologram and (b) its 4 bit/pixel version*

A very recent approach [45], proposes to use nonuniform quantizers in order to divide the quantization space efficiently. In this technique the design of the quantizers is achieved iteratively for a set of holograms which ends up with some problems despite providing good compression ratios. The first problem is the computation complexity and the second one is that the quantizer does not necessarily work well for an unseen hologram.

There are also some proposed methods based on the compression of the recorded interference patterns to evaluate the hologram of the object [46, 47]. Mills and Yamaguchi, [46], investigated the effect of the quantization of the holograms on the reconstructed image where Darakis and Soraghan [47] proposed to use image compression techniques like JPEG and JPEG-2000 to compress the interference patterns.

# CHAPTER 5

# LITERATURE SURVEY

## 5.1   Introduction

Watermarking using holography is a very novel approach and only a few works presents. These methods are mainly divided into two groups as holographic domain, [48, 49], and space domain [50-53] methods in terms of the domain where the hologram is embedded into the host image. Another technique existing in the literature is to hide perceptually meaningful data, especially logos, in the images[54-56]. These methods are similar to the holographic methods in such a way that both methods embed perceptually meaningful patterns as the watermark. Hence, these proposed watermarking methods are explained in this chapter.

## 5.2   Holographic Domain Methods

The holographic domain methods are in fact used for watermarking the hologram of a 3-D object. However, since the hologram of an image can be evaluated by the method given in Chapter 4.4, an image can be watermarked with these methods.

This kind of method is first proposed by Kishk and Javidi [48]. According to that method, the hologram of an object is watermarked by another hologram. The hologram used as the watermark is encrypted by the double phase encoding scheme and added to the host hologram after scaling with a constant factor. Then the

obtained signal is also double phase encoded in order to get the encrypted and watermarked hologram of the 3-D object (see Figure 5.1).
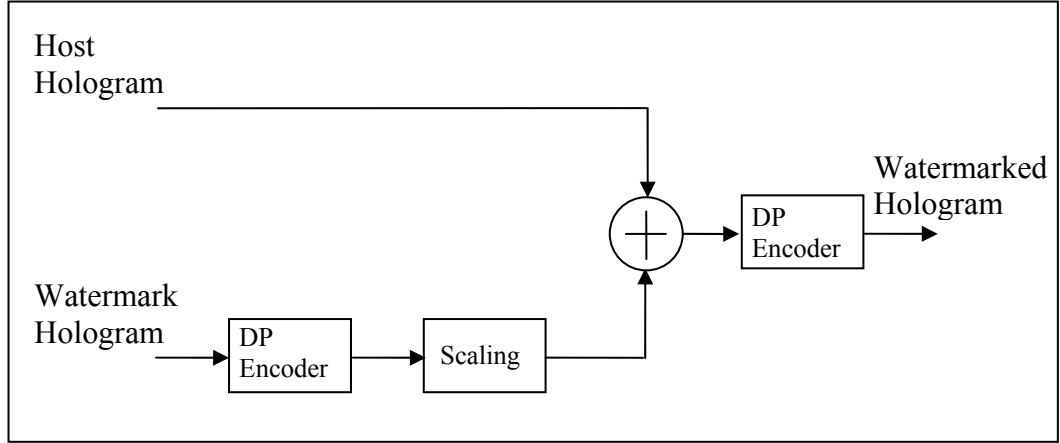


*Figure 5.1 Watermark embedding method proposed in [48]*

Note that the double phase encoding is evaluated by the equation below:

$$H_d(x,y) = \left\{ H(x,y)e^{jb_1(x,y)} \right\} \otimes IFT\left\{ e^{jb_2(\xi,\eta)} \right\} \tag{5.1}$$

where H(x,y) is the hologram to be encrypted, $b_1$ and $b_2$ are the random phase mask uniformly distributed in [0, 2π), IFT is the inverse Fourier Transform operator and $H_d(x,y)$ is the resultant encrypted hologram. The host 3-D and the watermark 3-D objects are obtained by the method given in Figure 5.2.
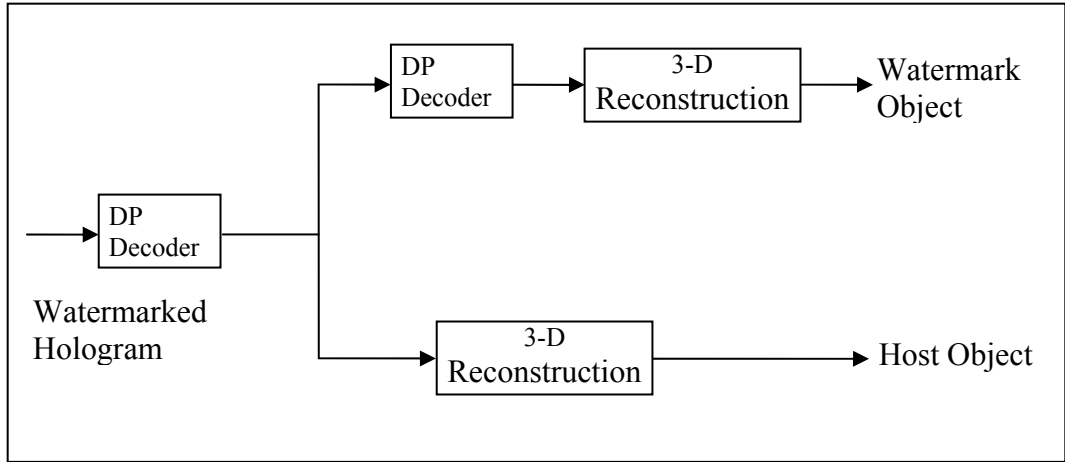
*Figure 5.2 Host and watermark objects extraction process proposed in [48]*

In [49], the proposed hologram watermarking approach proposed to use real one dimensional sequence as the watermark. Other processes are similar with the previous method and the authors try to evaluate the optimal scaling factors that minimize the error of the reconstructed host object and extracted watermark.

In these studies, it is reported that the proposed watermarking approaches are robust to cropping and occlusion. However, when they are used for image watermarking, the size of the resultant data doubles since holograms are complex signals. Moreover, you obtain encrypted data which requires a set of transformations to obtain the original image back. Hence, it can be inferred that for many applications this method is not applicable.

## 5.3    Space Domain Methods

These types of watermarking methods propose embedding a hologram into some components of an image. Takai and Mifune [50] proposed a method that embeds the hologram into the image in spatial domain. In this method, both the host image, $Q(\xi,\eta)$, and the hologram, $H(\xi,\eta)$, is normalized to have

$$0 \leq Q(\xi,\eta) \leq 1 \text{ and } 0 \leq H(\xi,\eta) \leq 1 \qquad (5.2)$$

Then the watermarked image is obtained by the formula given below:

$$Q_m(\xi,\eta) = Q(\xi,\eta) + \alpha(\xi,\eta)H(\xi,\eta) \qquad (5.3)$$

where $Q_m(\xi,\eta)$ is the watermarked image and $\alpha(\xi,\eta)$ is the scaling factor. In this study, $\alpha(\xi,\eta)$ is selected as a constant scale as $\alpha$ or an image dependent weighting factor as $\alpha.Q(\xi,\eta)$ and for both choices of $\alpha(\xi,\eta)$, the success of the watermarking scheme is examined. Fourier holograms are used in this study but since phase shifting digital holograms are used in the thesis, Takai and Mifune's method is implemented with Chess Knight hologram. In Figure 5.3, the original and watermarked Lena images with two type of weighting factors are given, respectively. Note that, for this method the resultant watermarked image is a complex signal and their absolute values are seen in Figure 5.3. As it can be inferred from the figure, the image dependent weighting gives better quality watermarked images since the energy of the added watermark signal is adjusted depending on the host's energy.

The reconstruction of the hidden hologram, which is in fact the watermark, is obtained by taking the inverse Fresnel Transform of the watermarked content. Then the reconstructed image becomes:

$$IFrT\{Q_m(\xi,\eta)\} = IFrT\{Q(\xi,\eta)\} + IFrT\{\alpha(\xi,\eta)H(\xi,\eta)\} \qquad (5.4)$$

*(a)*



*(b)*          *(c)*

*Figure 5.3 (a) Original and marked Lena images using (b) constant level weighting, (c) image dependent weighting respectively when α=0.2 using Takai and Mifune's method*

When $\alpha(\xi,\eta)$ is a constant, the resultant image becomes:

$$q_m(x, y) = q(x, y) + \alpha h(x, y) \tag{5.5}$$

Since the host image has low-pass characteristics in general and the inverse Fresnel Transform is expressed by inverse Fourier Transform (see Equation (4.15)) by

high-pass filtering q(x,y) can be omitted. When α(ξ,η) is host image dependent, the reconstruction watermark is evaluated by the same way assuming q(x,y) = δ(x,y). In Figure 5.4, the reconstruction of the extracted watermark can be seen. If the host image is known in receiver side, i.e. the method is non-blind; the effect caused by the host image can be removed perfectly.



<div align="center">(a)                                                                 (b)</div>
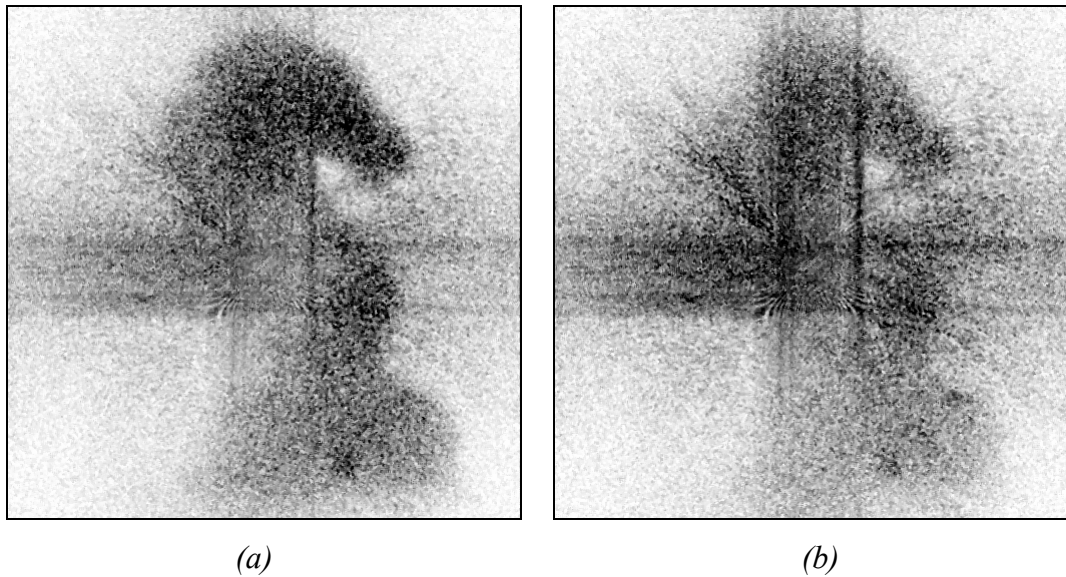
*Figure 5.4 Reconstructions of the extracted watermark from the marked images in (a) Figure 5.3(b) and (b) Figure 5.3(c)*

Another method is proposed by Cai et. al. [51]. In this method, the recorded interferograms are hidden in the host image. Again they are embedded into the image in spatial domain by multiplying a scale factor as given below:

$$I_i' = I_i + \alpha_i A_i \tag{5.6}$$

where $I_i$ is the $i^{th}$ interferogram, $I_i'$ is its modified version, $\alpha_i$ is the scaling factor and $A_i$ is the host image for the $i^{th}$ interferogram. When $\alpha_i$'s and $A_i$'s are same for all i's, Equation (4.8) still holds even if the modified interferograms are replaced

with the original ones. On the other hand, this method is more appropriate for steganographic cases, not for watermarking.

He et. al. [52] investigated the effect of the reduction in hologram to be embedded. They keep the data embedding strategy same with previous two methods but they examined the reconstructed watermark quality if only the real, imaginary or phase part of the hologram is embedded into the host image. They propose to send the host image and the scaling factor in order to get the reconstruction of the hidden hologram properly.

In Figure 5.5, the watermarked Lena images using real, imaginary and phase parts of the Chess Knight hologram, respectively. One can easily predict that the best reconstruction is obtained from the marked image that hides the phase of the hologram (see Figure 4.11).

Those methods provide optical reconstruction of the watermarks and robustness against some geometrical attacks (cropping, occlusion) at a level. However, these methods are impractical for many applications since they require the original image in order to obtain perfect reconstruction of the watermark. If they are desired to be designed as blind, the content image should be low-pass filtered before the superposition stage. Hence, the quality of the watermarked image degrades seriously. As a result, these studies cannot propose effective and practical watermarking methods but show the idea of using holograms as the watermark is applicable and very effective for some cases.

*(a)*　　　　　　　　　　　*(b)*



*(c)*

*Figure 5.5 Watermarked Lena images by He et. al.'s method using (a) real, (b) imaginary, (c) phase of the Chess Knight hologram*

On the other hand, Chang and Tsan [53] proposed to embed the watermark into the median-frequency components of the image in discrete cosine transform (DCT) domain. The region of the DCT coefficients to be modified is shown in Figure 5.6.
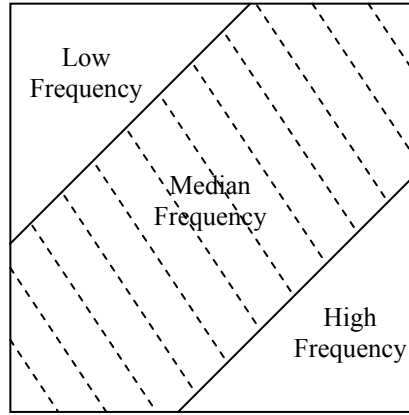
*Figure 5.6 Median frequency DCT coefficients for embedding the watermark*

In this method, Fourier holograms are used as the watermark. The size of the hologram is selected as half of the original image but it can be smaller if it is desired to obtain higher quality image. According to this, the modified DCT coefficients are given as follows:

$$Q'_{MED}(x, y) = Q_{MED}(x, y) + \alpha h(x, y) \tag{5.7}$$

Then, the watermark image is obtained by taking inverse DCT of the modified DCT coefficients. In Figure 5.7, the watermarked Lena image can be seen where the half of the Chess Knight hologram is used as the watermark and α=0.5.

*Figure 5.7 Watermarked Lena image using Chang and Tsan's method*

Obtaining the reconstructed watermark is easier since it only requires to taking the DCT of the watermarked image and taking the inverse Fresnel Transform of the modified coefficients. In this case, the noise caused by the DCT coefficients is much smaller than the noise in Takai and Mifune's method since the values of these coefficients are much smaller. The reconstruction of the extracted watermark can be seen in Figure 5.8. However, in this case the size of the watermark is half of the one used in other methods.

As a result, by embedding the hologram into these median frequencies, the quality of the image is degraded less since generally images have low-pass characteristics. Moreover, this method provides robustness against some additional attacks which degrade the high frequency components of the watermarked image. However, again the watermarked image has both real and imaginary components which double the size of the modified image.
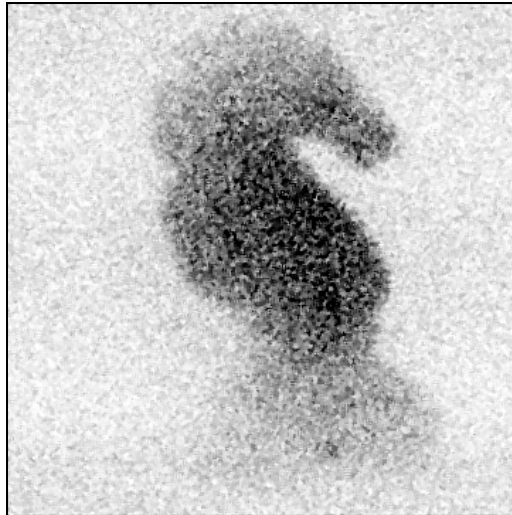
*Figure 5.8 Reconstruction of the extracted watermark from image in Figure 5.7*

## 5.4   Logo Watermarking

Logo watermarking approaches in the literature use very different type of methods to hide a gray scale or binary logo into the image.  For instance, in [54] a gray scale logo is embedded into an image using image fusion principles. Image fusion is a method that produces a single image from a group of input images. In this method, l level DWT of the image and first level DWT of the watermark is taken. Then, the obtained coefficients are fused according to some rules obtained by taking the HVS into account. The watermark embedding procedure is shown in Figure 5.9.

In this method, the watermark is usually much smaller than the host image and repeatedly embedded into different components of the image. Hence, the watermark is spread throughout the different frequency components of the image which provides robustness to the system.
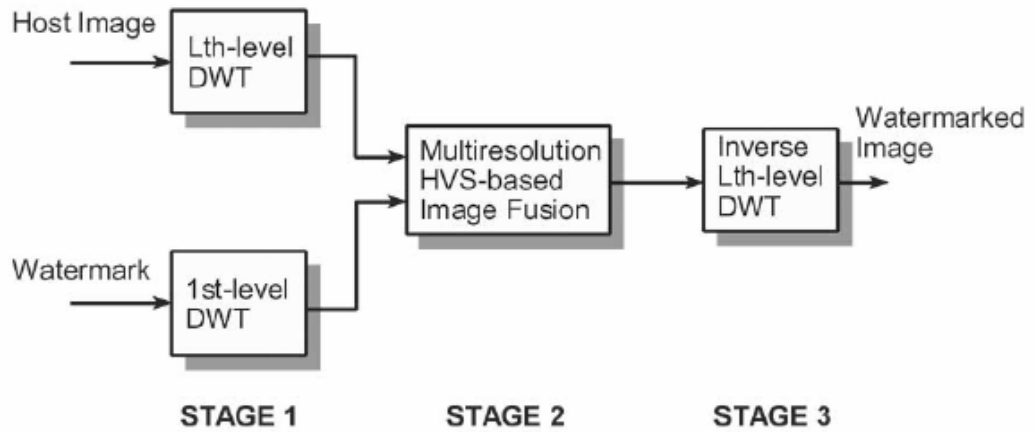
*Figure 5.9 3-stage watermark embedding strategy proposed by Kundur et. al. The figure is taken from [54]*

However, this method is not blind and requires the host image in the watermark extraction process. The watermark extraction process is as shown in Figure 5.10. This is basically comparing the DWT coefficients of the host and watermarked images and detecting the watermark using the rules for watermark embedding. The repeated parts are then combined to form the DWT coefficients of the watermark. Finally the hidden logo is estimated by taking the inverse DWT of these coefficients.
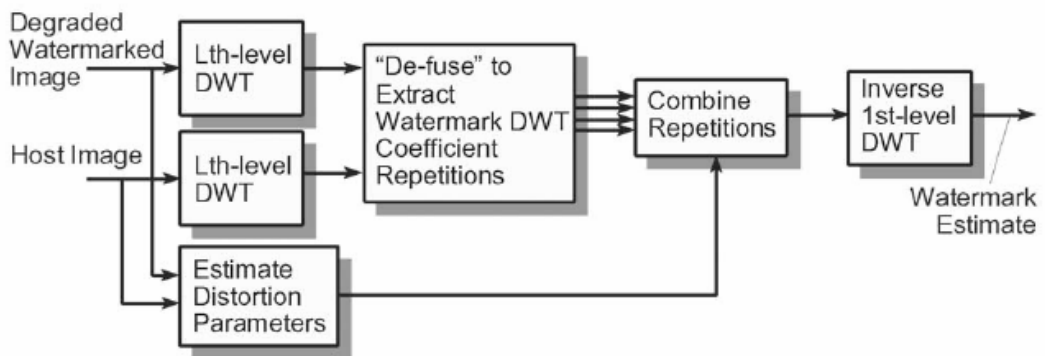


*Figure 5.10 Watermark extraction proposed by Kundur et. al. The figure is taken from [54]*

Another logo watermarking method is proposed by Zhang et. al. [55]. In this method, a binary logo is embedded into an image in the multi-wavelet domain. First of all, a binary logo is lexicographically ordered and reordered by a secret strategy in order to encrypt the watermark. In this work, the authors stated that, embedding the information into the mean of the corresponding coefficients in four subblocks is more stable than embedding it into a single coefficient. Hence, they quantize the mean of the four subblocks in the coarsest level as below where Q is the quantization function, q is the quantization interval and $\overline{x}(i, j)$ is the elements of the matrix, $\overline{X}$, obtained by the mean of the subblocks:

$$Q(\overline{x}(i, j), q) = \begin{cases} 0, \text{if } kq \leq \overline{x}(i, j) < (k+1)q \text{ for } k = 0, \pm 2, \pm 4, .. \\ 1, \text{if } kq \leq \overline{x}(i, j) < (k+1)q \text{ for } k = \pm 1, \pm 3, .. \end{cases} \tag{5.8}$$

Each 1-bit pixel value of the reordered logo into the each element of the corresponding subblock, $x_n(i,j)$ as follows where n=1,2,3,4.

$$\hat{x}_n(i, j) = \begin{cases} floor(\dfrac{x_n(i, j)}{q}) \cdot q + 0.5q, \text{if } Q(x_n(i, j), q) = w(i, j) \\ floor(\dfrac{x_n(i, j)}{q}) \cdot q + 1.5q, \text{if } Q(x_n(i, j), q) \neq w(i, j) \text{ and } r(i, j) > 0.5q \\ floor(\dfrac{x_n(i, j)}{q}) \cdot q - 0.5q, \text{if } Q(x_n(i, j), q) \neq w(i, j) \text{ and } r(i, j) \leq 0.5q \end{cases} \tag{5.9}$$

where r(i,j) is the error caused by quantization defined as:

$$r(i, j) = \overline{x}(i, j) - floor(\dfrac{\overline{x}(i, j)}{q}) \cdot q \tag{5.10}$$

As a result, the mean value of the coefficients is difficult to move away from the shifted interval. The watermarked image is finally obtained by taking the inverse multi-wavelet DWT of these modified coefficients.

The watermark is extraction process is very similar to watermark embedding but it does not require the host image. The forward multi-wavelet DWT of the watermarked image is evaluated and the mean values of the corresponding 4 coefficients in the subblocks of the coarsest level, $\overline{x}'(i,j)$'s ,are evaluated. Then the information in each mean value is decided as follows:

$$\hat{w}(i,j) = \begin{cases} 0, \text{if } Q(\overline{x}'(i,j),q) \text{ is odd} \\ 1, \text{if } Q(\overline{x}'(i,j),q) \text{ is even} \end{cases} \tag{5.11}$$

Finally the binary logo used as the watermark is estimated by reordering the obtained coefficients. This method is advantageous for some scenarios since it is a blind method but the hidden information is less since it is applicable for binary logos.

Reddy et. al. proposed to add the wavelet coefficients of a logo image onto the wavelet coefficients of the host image [56]. First of all, the l-level DWT coefficients of the host are found in order to find the weighting factors. These weighting factors are evaluated by taking the HVS into account and the DWT coefficients are sorted in descending order according to these weighting factors to form $S_l^{\theta}(i,j)$. In this case, $\theta$ represent the orientation of the DWT coefficients. Then the first p percentage of them is used to obtain wavelet coefficients of the watermarked image by the formula below:

$$\hat{S}_l^{\theta}(i,j) = S_l^{\theta}(i,j) + \alpha \cdot w_l^{\theta}(i,j) \cdot x_1^{\theta}(i,j) \tag{5.12}$$

Here, $\hat{S}_l^{\theta}(i,j)$ is the modified DWT coefficients, $x_1^{\theta}(i,j)$ is the 1$^{st}$ level DWT coefficients of the logo and $\alpha$ is the watermark strength. After reordering the coefficients and taking the inverse DWT of the modified coefficients, watermarked image is obtained.

This method also requires the original image at the decoder side of the system. The weighting factors are evaluated using the original image and the embedded watermark is obtained as:

$$\hat{x}_1^{\theta}(i,j) = \frac{\hat{S}_l^{\theta}(i,j) - S_l^{\theta}(i,j)}{w_l^{\theta}(i,j)}$$

(5.13)

Since the watermark is repeatedly embedded into the image, the extracted watermark values are combined and the obtained coefficients are reordered. Finally, the watermark logo is evaluated by taking the inverse DWT of the extracted coefficients.

# CHAPTER 6

# DIGITAL IMAGE WATERMARKING BY USE OF HOLOGRAPHY

## 6.1 Introduction

In this chapter, we will present a new image watermarking algorithm which embeds a hologram into the wavelet coefficients of an image. In the embedding process a technique called quantization index modulation (QIM) is used so we will first explain this technique in details and then present the watermarking approach.

## 6.2 Quantization Index Modulation (QIM)

QIM [16, 57] is a method proposed for embedding one signal into another host signal to create another composite signal which can be used for different applications. This technique is classified as a host-interference rejection technique, [1, 13], which does not require the host signal in the decoder. This method is also more robust than many other host-interference rejection techniques like low bit(s) modulation (LBM) [58, 59] against various classes of attacks.

In order to explain QIM technique, let x be the host signal, m be the message to be hidden. Then, s(x,m), which is the resultant composite signal, can be seen as the ensemble of functions of x, indexed by m. As a result, if the distortion induced by the information embedding is small, then:

$$s(x, m) \approx x \tag{6.1}$$

Naturally, in the design process, the ranges of the functions should be taken into account such that the range of one function should be far away from the range of another function. In other words, the ranges of the functions should be non-intersecting in order to determine the hidden message, m, uniquely. Therefore, the range of these functions should be discontinuous in order to hold the nonintersecting property. Since quantizers are discontinuous functions and designed to approximate the original content, they are useful for the explained data hiding scheme. Hence, QIM is defined as modulating an index with the embedded information and then quantizing the host signal with the associated quantizer.

For instance, if one desires to embed one bit information, m, into the host signal, x, the resultant composite signal can be expressed as follows:

$$s(x, m) = \begin{cases} q_0(x), & \text{if } m = 0 \\ q_1(x), & \text{if } m = 1 \end{cases} \tag{6.2}$$

where $q_0$ and $q_1$ are quantizers with nonintersecting range spaces. Hence, knowing the all reconstruction points of the quantizers, the embedded message can be extracted using a minimum distance decoder as:

$$\hat{m} = \arg\min_m \|y - s(y, m)\| \tag{6.3}$$

where $\hat{m}$ is the estimated message from the received signal, y.

QIM can be improved by a distortion compensation term and the embedding is achieved as follows:

$$s(x, m) = q(x; m, \frac{\Delta}{\alpha}) + (1 - \alpha) \cdot \left[ x - q(x; m, \frac{\Delta}{\alpha}) \right] \tag{6.4}$$

where $\alpha \leq 1$ is a scaling factor and $\Delta$ is the distance between the reconstruction points of the quantizers. This is so called distortion compensation QIM (DC-QIM). In this process, the first term represents a normal QIM process and the second term is the distortion compensation term which is achieved by adding a fraction $1-\alpha$ of the quantization error. In this case, the distortion compensation term should be added to the decoder in order to get the message back. However, the probability density functions of the quantization error for each quantizer in the QIM ensemble are similar and independent of m. Hence, the distortion compensation term can be seen as independent noise.

## 6.3  Digital Wavelet Transform (DWT)

The wavelet transform arise in the last decade [60, 61]. The applications areas vary from compression to other many signal processing operations but here, we introduce some basic and necessary concepts of DWT in terms of the purpose of this work.

The main idea behind this transform is to divide a signal into parts according to the frequency spectrum of the signal. For instance a 1-D DWT split a signal into two parts, generally the low frequency and high frequency components. The edges in the signal are generally confined in the high frequency part. The low frequency part is then split into two parts again and again until the signal is entirely decomposed or the desired level of decomposition is obtained. The original signal can be obtained by use of these decomposed parts (DWT coefficients) and this process is called inverse DWT (IDWT).

In order to describe this transform mathematically let define a low-pass filter, *H(w)* and a high-pass filter *G(w)* as:

$$H(w) = \sum_k h_k \cdot e^{-kw} \qquad (6.5)$$

$$G(w) = \sum_{k} g_k \cdot e^{-kw} \qquad (6.6)$$

Then a signal *F(n)* can be decomposed recursively as follows:

$$f_{j+1}^{low}(k) = \sum_{n} h_{n-2k} \cdot f_j(n) \qquad (6.7)$$

and

$$f_{j+1}^{high}(k) = \sum_{n} g_{n-2k} \cdot f_j(n) \qquad (6.8)$$

where j = 0,1,..J for $f_0(n) = F(n)$ and J is the highest level resolution index. The obtained coefficients $f_J^{low}$, $f_{J-1}^{high}$, $f_{J-2}^{high}$, …, $f_1^{high}$ are called the DWT of the signal *F(n)*. $f_J^{low}$ is the lowest resolution level which is in fact the approximation of the original signal and $f_k^{high}$ is the detail of the images in the $k^{th}$ level. Furthermore, the IDWT is obtained by recursively obtaining the low frequency components as follows:

$$f_{j-1}^{low}(n) = \sum_{k} h_{n-2k} \cdot f_j^{low}(k) + \sum_{k} g_{n-2k} \cdot f_j^{high}(k) \qquad (6.9)$$

Note that, in order to ensure the DWT and IDWT relation, the orthogonality condition on the filters *H(w)* and *G(w)* should be satisfied which can be expressed as follows:

$$\left| H(w) \right|^2 + \left| G(w) \right|^2 = 1 \qquad (6.10)$$

One of the examples of the wavelets is Haar wavelets where *H(w)* and *G(w)* are defined as follows:

$$H(w) = \frac{1}{2} + \frac{1}{2} e^{-jw} \qquad (6.11)$$

$$G(w) = \frac{1}{2} - \frac{1}{2}e^{-jw} \qquad\qquad (6.12)$$

The DWT or IDWT for a 2-D signal (image) is defined similarly by evaluating 1-D DWT or IDWT of each dimension separately which creates a pyramidal decomposition structure given in Figure 6.1. In this figure, 3-level DWT decomposition is illustrated where $I_3^0$ is the approximate low-resolution image, $I_k^1$ represents the vertical details, $I_k^2$ represents the horizontal details and $I_k^3$ represents the diagonal details at $k^{th}$ decomposition level.
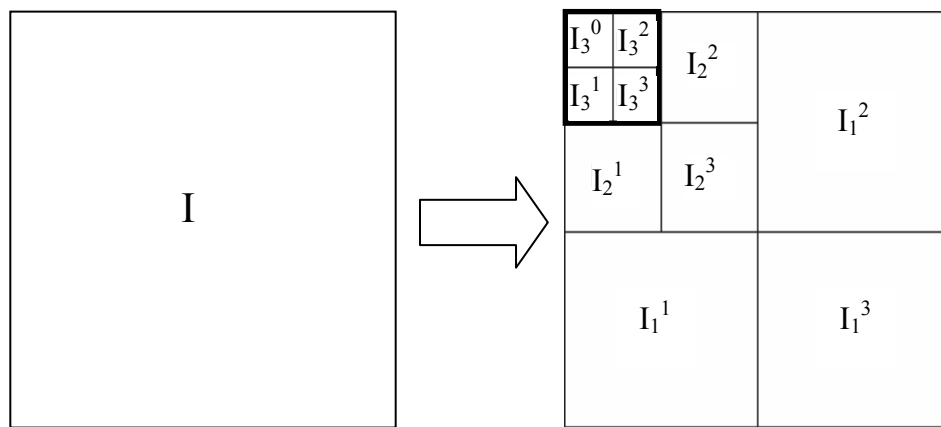


*Figure 6.1 Three level discrete wavelet transform (DWT) of an image*

## 6.4   Watermark Embedding

In this proposed watermark embedding method, 4-bit quantized hologram phase information is hidden into a digital image. The general block diagram of the watermark embedding scheme is given in Figure 6.2. In this method, the size of the hologram to be embedded is M/8xN/8 if the host image is MxN.

In the "WM Embedder" block of the figure above, first of all, 3-level discrete wavelet transform (DWT) of the host image is evaluated to form four levels: $I_l^\upsilon$ where $l \in \{1, 2, 3\}$ denotes the resolution level and $\upsilon \in \{0,1,2,3\}$ is the orientation

of the DWT coefficients (see Figure 6.1). $I_3{}^0$ has the lowest, $I_3{}^3$ has the highest and the other two have the mid-frequency coefficients of the image at $3^{rd}$ resolution level. Note that, these coefficients are obtained using Haar wavelets and each of them is M/8xN/8 sized.
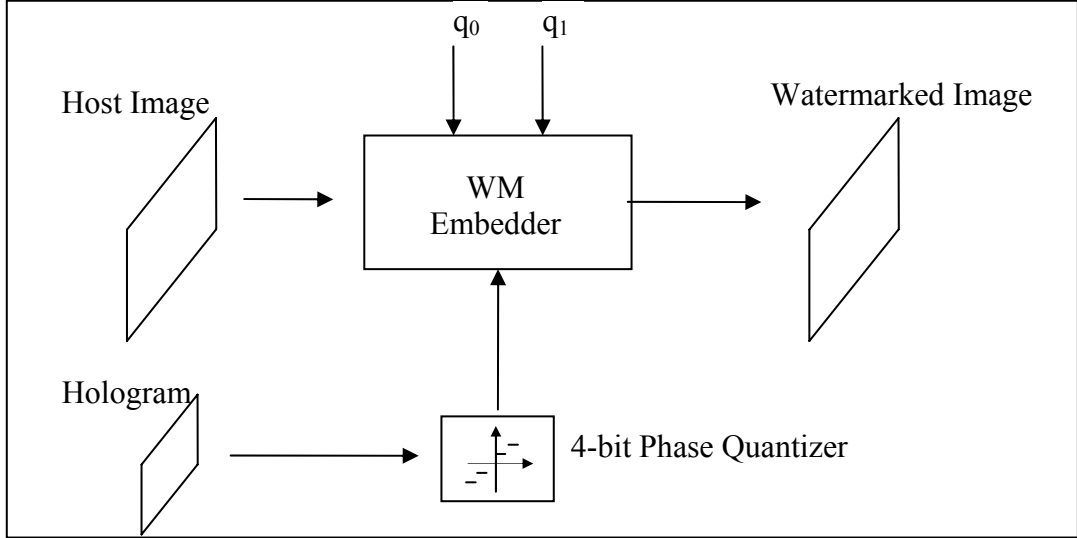


*Figure 6.2 Watermark embedding*

After that, 4 binary M/8xN/8 matrices, $B_i$'s where i $\in$ {0,1,2,3}, are obtained using each bitplane of the watermark signal, i.e. most significant bits of the pixels form $B_0$ and the least significant ones form $B_3$. Hence, each element in $B_i$ can be embedded into the corresponding element of $I_3{}^i$ and the modified wavelet coefficients, $\hat{I}_3{}^i$, are obtained as follows:

$$\hat{I}_3{}^i(k,l) = s\left(I_3{}^i(k,l), B_i(k,l)\right) \quad \text{where } i = 1,2,3,4;$$
$$k = 0,1,\dots,\frac{M}{8}-1 \text{ and } l = 0,1,\dots,\frac{N}{8}-1 \qquad (6.13)$$

As seen from the equation (6.13), the quality of the resultant watermarked image and the robustness of the proposed scheme depend on the design of s. In this thesis, we propose to use two uniform quantizers, $q_0$ and $q_1$, holding the equations (6.2) and (6.14).

70

$$q_1(x) = q_0(x) + \frac{\Delta}{2} \qquad\qquad (6.14)$$

where $\Delta$ is the step size of the quantizers. These quantizers are defined between the maximum and minimum values of the DWT coefficients. In Figure 6.3, an illustration of the proposed QIM technique is shown.
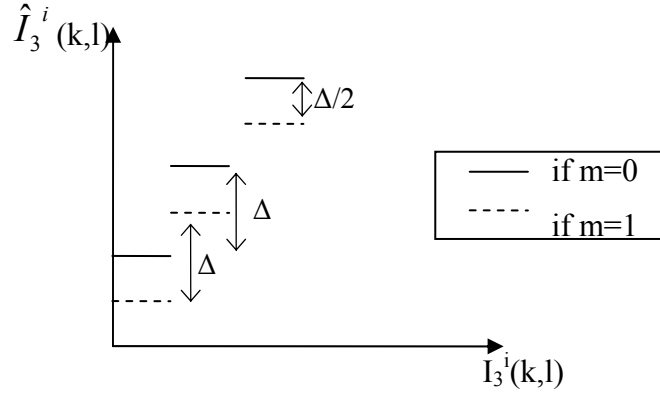


*Figure 6.3 Proposed QIM scheme for watermark embedding*

In the end, the watermarked image is obtained by taking the inverse DWT of these modified wavelet coefficients.

From Figure 6.4 to Figure 6.6, various watermarked images are obtained by both changing the host image and the step size of the quantizers. The bounds of the wavelet coefficients can be evaluated theoretically. Since we use Haar wavelets, the minimum and maximum coefficient values in the lower frequency band ($I_i^0$) are as follows:

$$\begin{aligned}
\min_i^0 &= 0 \\
\max_i^0 &= 510^{i-1}
\end{aligned} \qquad\qquad (6.15)$$

where i is the decomposition level. For the coefficient values in the other three bands are between the minimum and maximum values given below:

$$\min{}_i^k = -255 \cdot 2^{i-1}$$
$$\max{}_i^k = 255 \cdot 2^{i-1}$$

(6.16)

where i is the decomposition level and k={1,2,3} represents the subband of the coefficient. Note that, the quantizers $q_0$ and $q_1$ should be symmetric around the mid point of these minimum and maximum values in order to minimize the distortion induced by quantization process. This is because of the message (phase of the hologram) is uniformly distributed. In other words, if q is the best uniform quantizer in the specified range, $q_0$ and $q_1$ should be designed as follows:

$$q_0(x) = q(x - \frac{\Delta}{4}) + \frac{\Delta}{4}$$
$$q_1(x) = q(x + \frac{\Delta}{4}) - \frac{\Delta}{4}$$

(6.17)

From Figure 6.4 to Figure 6.6, various watermarked images are obtained by both changing the host image and the step size of the quantizers. Since the bounds of the coefficients are fixed, $\Delta$ is proportional to the number of steps (bins) of the quantizer. Thus, number of bins of the quantizers is considered as the parameter of the watermarking system in this thesis.

*(a)*                                   *(b)*

*(c)*                                   *(d)*

*Figure 6.4 (a) Original Lena image and its watermarked versions using (b) 16-bin (c) 64-bin (d) 256-bin quantizers when the hologram of the METU emblem is used as the watermark*
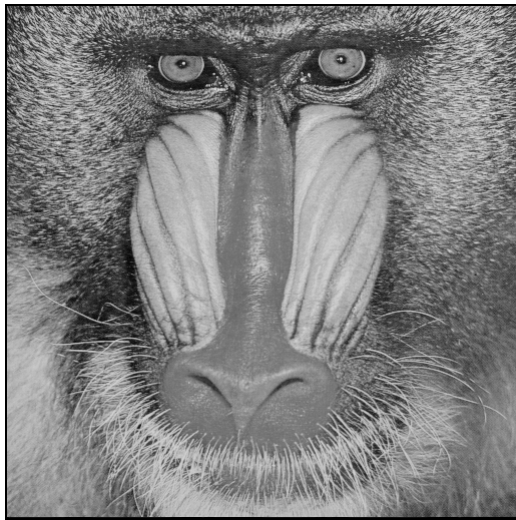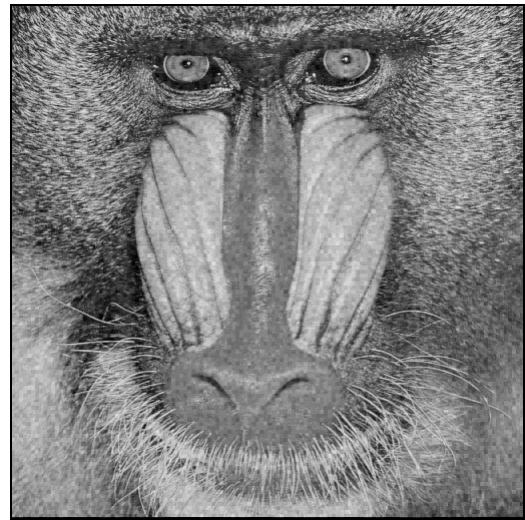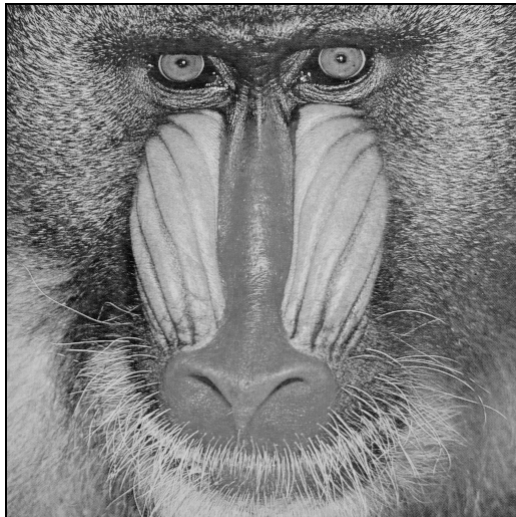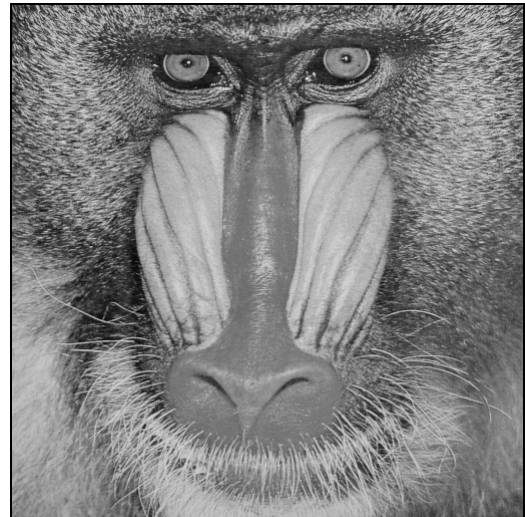
*Figure 6.5 (a) Original Baboon image and its watermarked versions using (b) 16-bin (c) 64-bin (d) 256-bin quantizers when the hologram of the METU emblem is used as the watermark*

*(a)*  *(b)*



*(c)*  *(d)*

*Figure 6.6 (a) Original Man image and its watermarked versions using (b) 16-bin (c) 64-bin (d) 256-bin quantizers when the Chess Knight hologram is used as the watermark*

For Lena image (Figure 6.4) PSNR values for the watermarked images are 28.6675 dB, 40.7436 dB, 51.9138 dB; for Baboon image (Figure 6.5) they are 28.3759 dB, 40.7182 dB, 51.9602 dB; and for Man image (Figure 6.6) these values are 28.7840 dB, 40.8104 dB, 51.9723 dB, respectively. As expected, when the step size of the quantizers gets bigger, the quality of the watermarked images decreases. However, for high frequency images like Baboon image, the decrease in quality is less

perceptible. In Figure 6.7, the effect of the quantizers on the quality of the images can be seen.
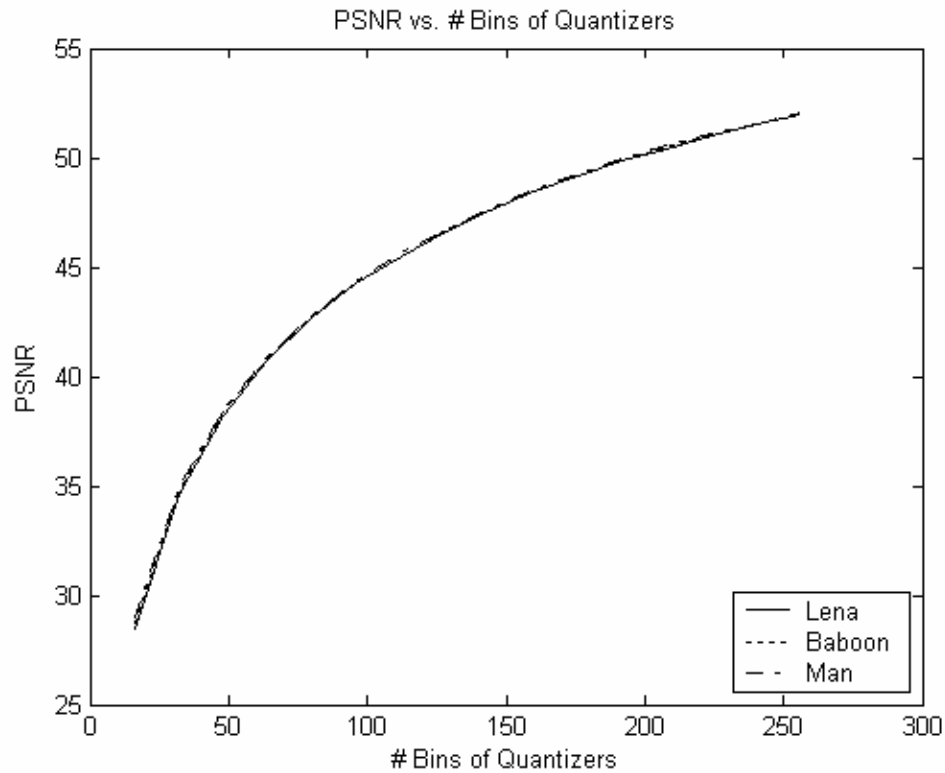


*Figure 6.7 Effect of the number of bins of the quantizers on the quality of the watermarked image, for Lena, Baboon and Man images*

## 6.5 Watermark Extraction

As explained in section 6.1, the extraction of the hidden message is easy if the quantizers used during the embedding process is known. The general scheme for watermark extraction is given in Figure 6.8.

In the "WM Extractor" block, first of all 3rd level DWT of the watermarked image is obtained by Haar wavelets. After that, each wavelet coefficient, $\hat{I}_3^{\,i}(k,l)$, is fed

to a minimum distance decoder which decides the hidden bit value in this coefficient.
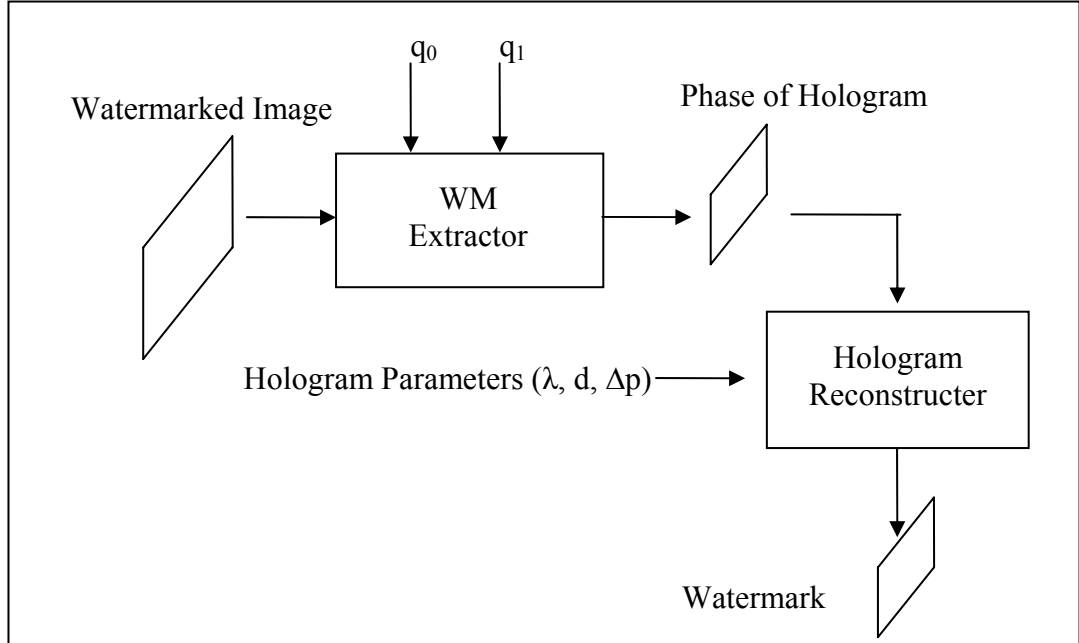


*Figure 6.8 Watermark extraction*

The minimum distance decoder decides the hidden message as follows:

$$\hat{B}_i(k,l) = \begin{cases} 0, \text{if } \left| \hat{I}_3^{\,i}(k,l) - q_0(x) \right| \leq \left| \hat{I}_3^{\,i}(k,l) - q_1(x) \right| \\ 1, \text{ if } \left| \hat{I}_3^{\,i}(k,l) - q_0(x) \right| > \left| \hat{I}_3^{\,i}(k,l) - q_1(x) \right| \end{cases} \tag{6.18}$$

where k, l, i values are same with the ones in equation (6.12). Hence, $\hat{B}_i$ 's represent the bitplanes of the extracted watermark. After reordering these values, the hologram phase, hidden into the image can be obtained. Hence, knowing the λ, d, Δp values the hidden object is reconstructed by equation (4.15).

In Figure 6.9 (a), the extracted hidden object in the watermarked Lena (Figure 6.4 (b)-(d)) and Baboon (Figure 6.5 (b)-(d)) images can be seen. Also, the extracted object from the watermarked Man image (Figure 6.6 (b)-(d)) is given in Figure 6.9 (b).
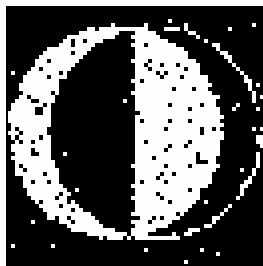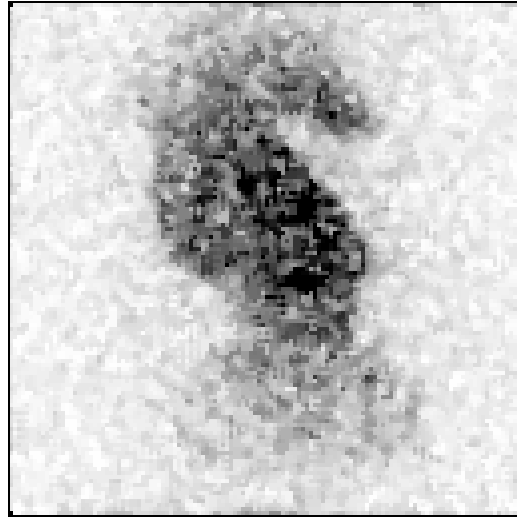


*(a)*                                                      *(b)*

*Figure 6.9 Extracted hidden marks from watermarked (a) Lena and Baboon, (b) Man images*

# CHAPTER 7

# EXPERIMENTAL RESULTS

## 7.1   Introduction

In this chapter, the performance of the proposed method will be studied and the results of the experiments performed will be presented. These experiments are mainly focused on the robustness of the system.

In order to test the robustness of the system, the extracted watermark is investigated after the watermarked images are attacked. These attacks are mainly divided into two groups as removal attacks and geometric attacks. The experiments are performed for each of the watermarked Lena, Baboon and Man images in order to provide fair experiments and assess the success of the proposed method. After the performance evaluation of the proposed system, this is compared with the performance of the existing methods given in Chapter 5.

The correctness of the extracted watermark is measured using two different metrics [55, 56]. One metric is the 2-D correlation coefficient given in equation (7.1) which is used for non-binary data:

$$cc = \frac{\sum_m \sum_n (A_{m,n} - \overline{A})(B_{m,n} - \overline{B})}{\sqrt{(\sum_m \sum_n (A_{m,n} - \overline{A})^2)(\sum_m \sum_n (B_{m,n} - \overline{B})^2)}} \qquad (7.1)$$

where $\bar{A}$ and $\bar{B}$ are the mean values of $A$ and $B$ images. The other is the bit correct ratio (BCR) which is given in equation (4.1). Another metric is used in Takai and Mifune's, [50], work which evaluates the difference between the reconstructions of the embedded and extracted holograms:

$$\sigma_I = \frac{\left\langle (I_{ext} - I_{emb})^2 \right\rangle^{1/2}}{\left\langle I_{emb} \right\rangle} \qquad (7.3)$$

where $\langle \ \rangle$ is the mean operator; $I_{emb}$ and $I_{ext}$ are the reconstructions of the embedded and extracted holograms, respectively. As a result, a low $\sigma_I$ provides better reconstructed watermark.

## 7.2    Experiments on Removal Attacks

### 7.2.1.  JPEG Compression

JPEG is one of the most prevalent image compression techniques. We therefore study the robustness of the watermarking scheme against the JPEG compression technique.

The watermarked images are compressed by Matlab's JPEG compression with different quality parameters from 100 (no compression) to 5 (50% compression). In Figure 7.1(a), the correlations between the embedded and extracted holograms from the watermarked Lena images for different JPEG quality factors and quantizers are given. In Figure 7.1(b), for the same parameters, the BCR's between the reconstructions of the embedded and extracted holograms can be seen. The same graphs are also obtained for the watermarked Baboon image (see Figure 7.2). Note that, the hologram of the METU emblem is used as the watermark for these two images. For each case, the reconstructions are recognizable if BCR ≥ 0.7. This value is also valid for the following experiments and this value is showed with a dashed line in the figures.

*(a)*                 *(b)*
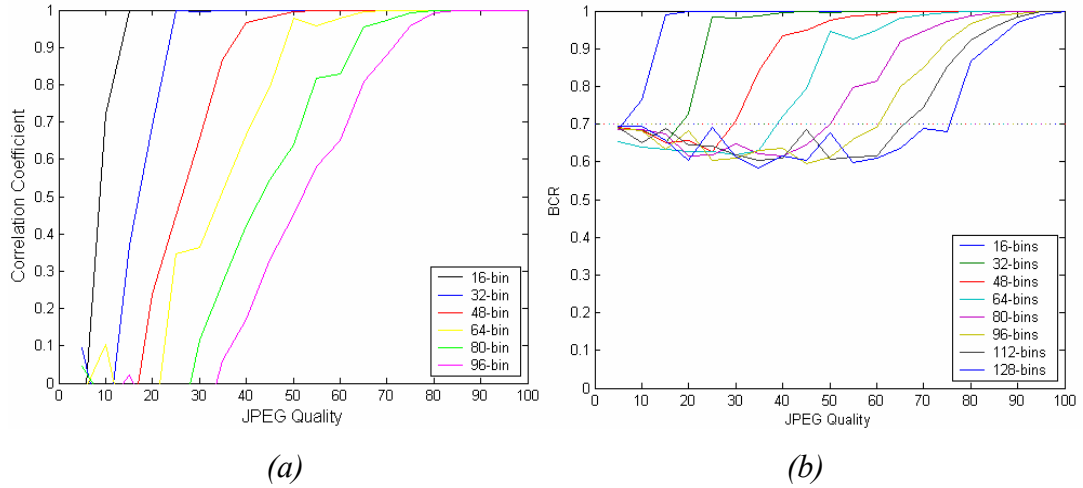
*Figure 7.1 (a) Correlation between the embedded and extracted hologram and (b) BCR between their reconstructions for different JPEG quality factors for watermarked Lena image*



*(a)*                 *(b)*
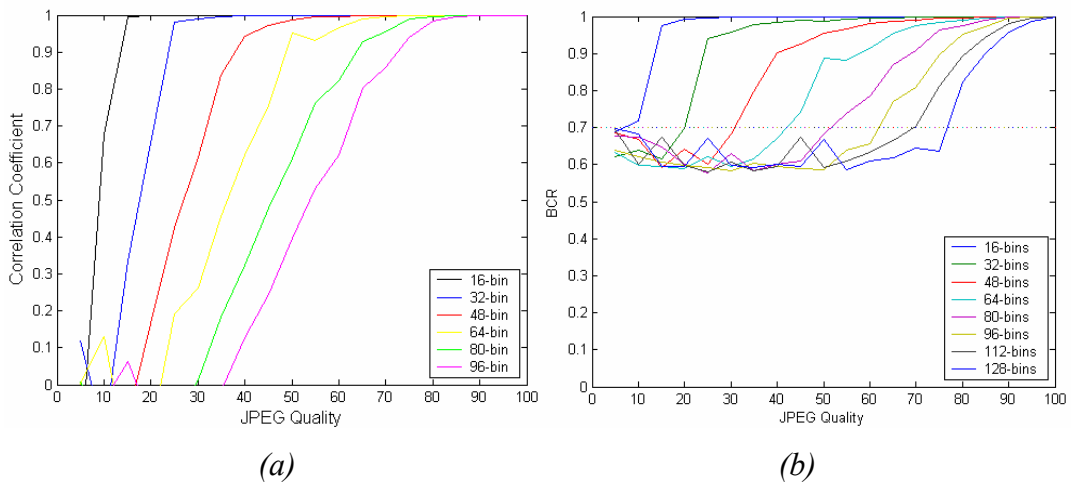
*Figure 7.2 (a) Correlation between the embedded and extracted hologram and (b) BCR between their reconstructions for different JPEG quality factors for watermarked Baboon image*

In Figure 7.3, the effect of JPEG compression is illustrated on Man image watermarked using a 128x128 part of the Chess Knight hologram. For this case, the watermark is a real 3-D object rather than a binary image. Hence, the correlation coefficients between the reconstructions of the embedded and extracted holograms are taken into account in this figure. If the correlation coefficient between the

81

reconstructions from the embedded and extracted holograms is above 0.75, the watermark is recognizable. Note that, this value is also valid for the following experiments and it is showed by a straight line in the following figures.
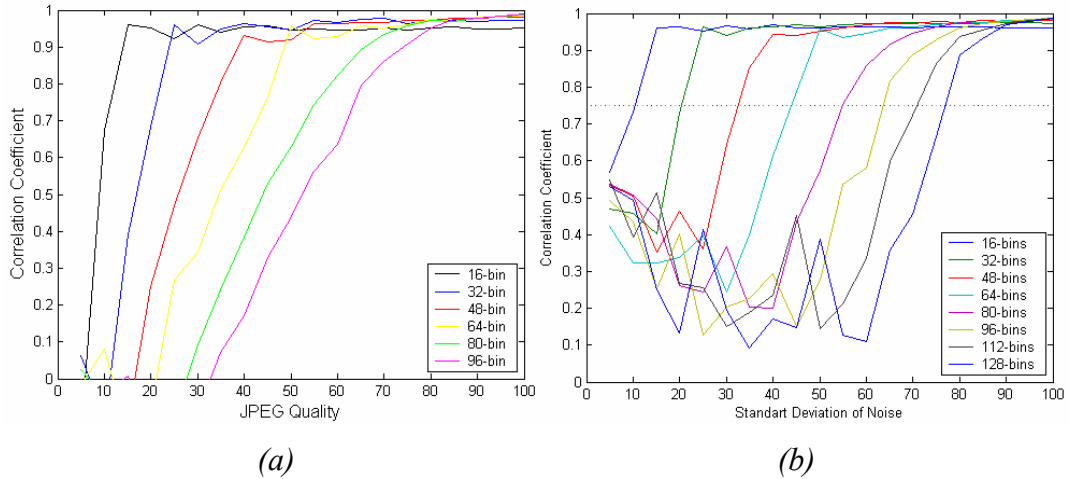


*Figure 7.3  Correlations between (a) the embedded and extracted hologram and (b) their reconstructions for different JPEG quality factors for watermarked Man image*

For the uniform quantizers which have more than 96 bins, the proposed method becomes very vulnerable to JPEG compression. Even with quality factor more than 90, it becomes impossible to recover the watermark properly. On the other hand, the figures above show that the robustness against JPEG compression can be adjusted by changing the step size of the quantizer. However, while increasing the step size, the quality of the watermark image decreases. So, the optimum parameters should be found depending on the application.

It is observed that for the given quantizers the method cannot resist to JPEG compression with quality factor less than 10. The step size of the quantizers should be raised which makes the quality of the watermarked image being unacceptable. As a result, it can be said that the method is robust against JPEG compression unless having too low quality factors. From Figure 7.4 to Figure 7.6, the

compressed watermarked images and the reconstructed watermarks from those attacked images are illustrated for different JPEG quality factors.



*(a)*          *(b)*
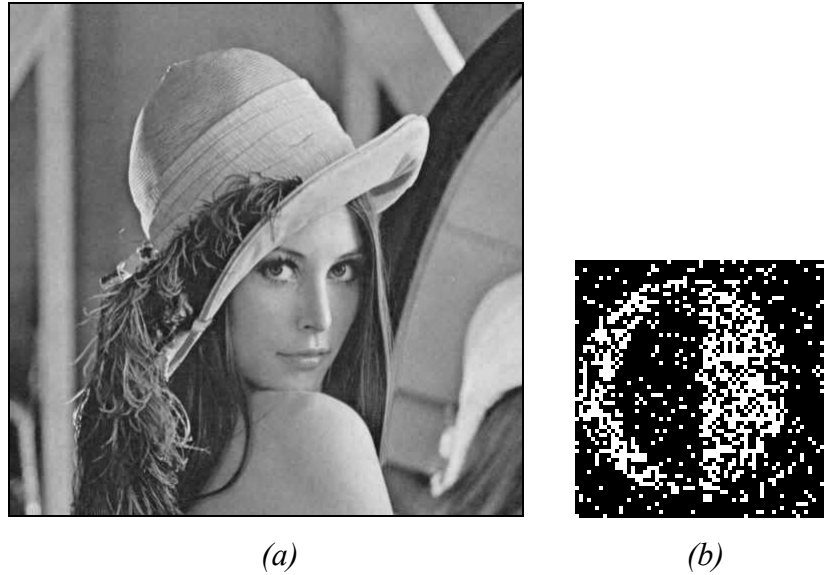
*Figure 7.4 (a) Compressed watermarked Lena image with quality factor 45 and (b) reconstructed watermark from that. 64-bin quantizers are used*



*(a)*          *(b)*
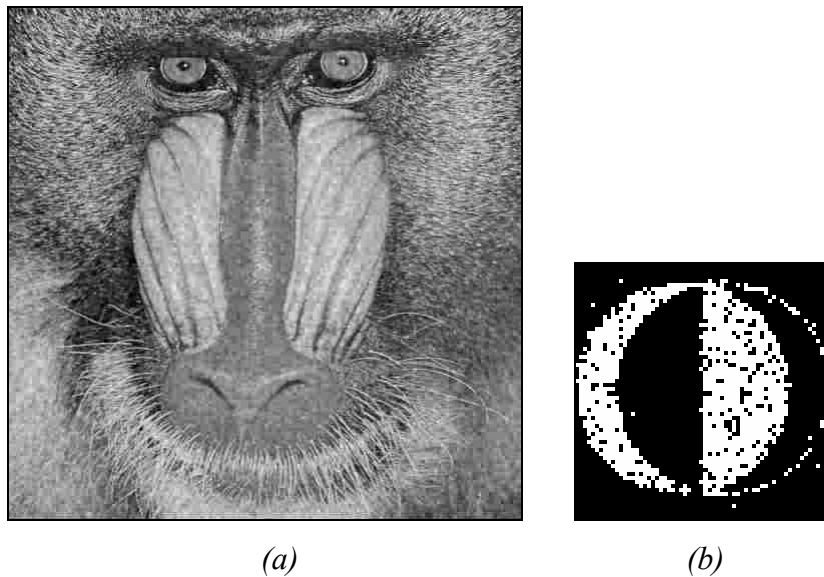
*Figure 7.5 (a) Compressed watermarked Baboon image with quality factor 15 and (b) reconstructed watermark from that. 16-bin quantizers are used*

<center>*(a)*                 *(b)*</center>
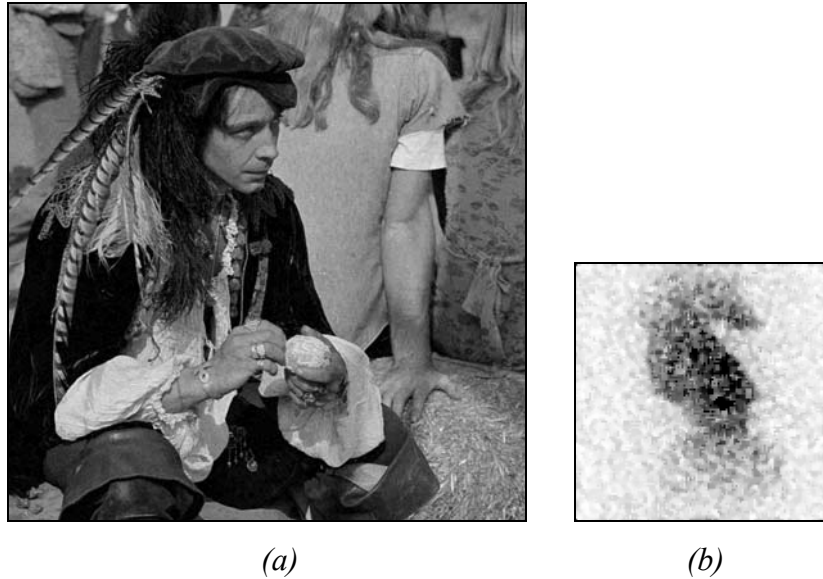
*Figure 7.6 (a) Compressed watermarked Man image with quality factor 25 and (b) reconstructed watermark from that. 32-bin quantizers are used*

### 7.2.2. Noise Addition

Another widely addressed attack in the literature is noise addition. In order to test the robustness of the proposed watermarking scheme against this type of attacks, random Gaussian white noise with different variances are added to the marked image. Then the similarities between the extracted watermarks from those noisy images and the embedded one are investigated. Again, the experiments performed in three different images in order to see if the robustness of the attack differs depending on the host image. The hologram of the METU emblem is used to watermark Lena and Baboon image and Chess knight hologram is used for watermarking the Man image. The results for those images are given from Figure 7.7 to Figure 7.9, respectively.

These results show that, all the images degraded similarly with the additional noise since the noise is spread over all frequency components equally. If the used quantizers in QIM are designed to have large step size, the robustness of the system increases against the noise. For instance, the watermarked Baboon image after

<center>84</center>

noise addition with variance 400, when 16-bin quantizers are used in watermarking, is presented in Figure 7.10 (a) and the reconstruction of the watermark from that image is still recognizable (Figure 7.10 (b)). However, if 128-bin quantizers are used, the watermark cannot be properly reconstructed after adding of noise with variance of 5.25 (Figure 7.11).



*(a)*              *(b)*
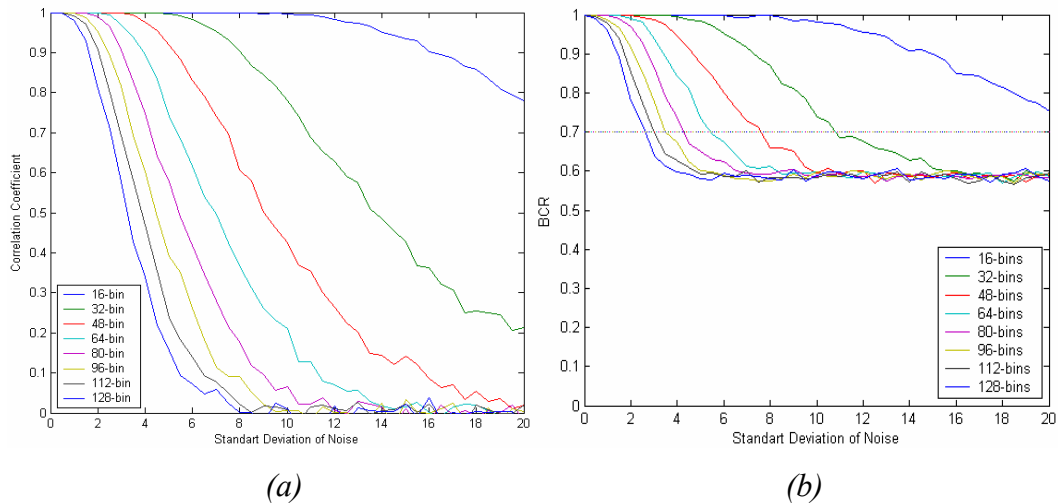
*Figure 7.7 (a) Correlation coefficient between the embedded and extracted hologram and (b) BCR between their reconstructions for varied noise power for Lena image*



*(a)*              *(b)*
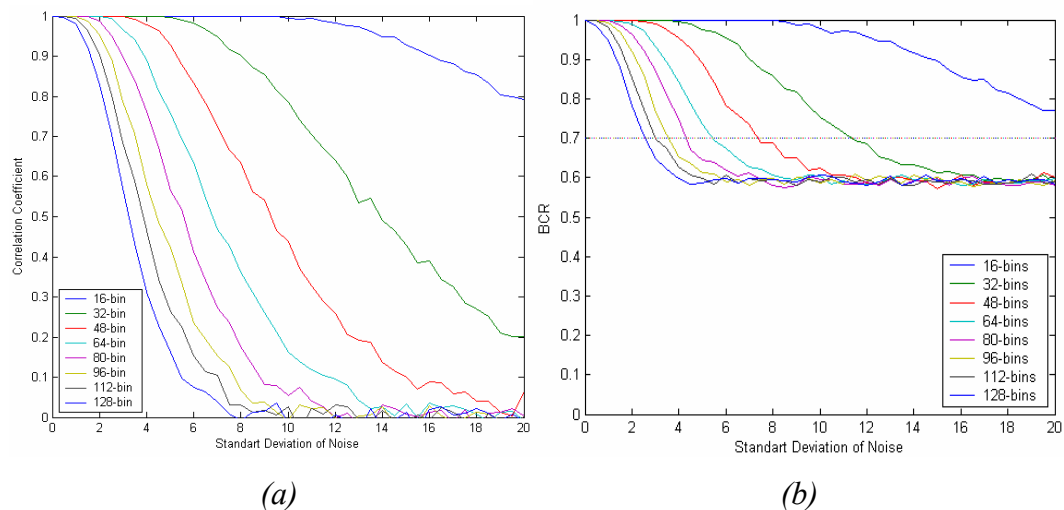
*Figure 7.8 (a) Correlation coefficient between the embedded and extracted hologram and (b) BCR between their reconstructions for varied noise power for Baboon image*
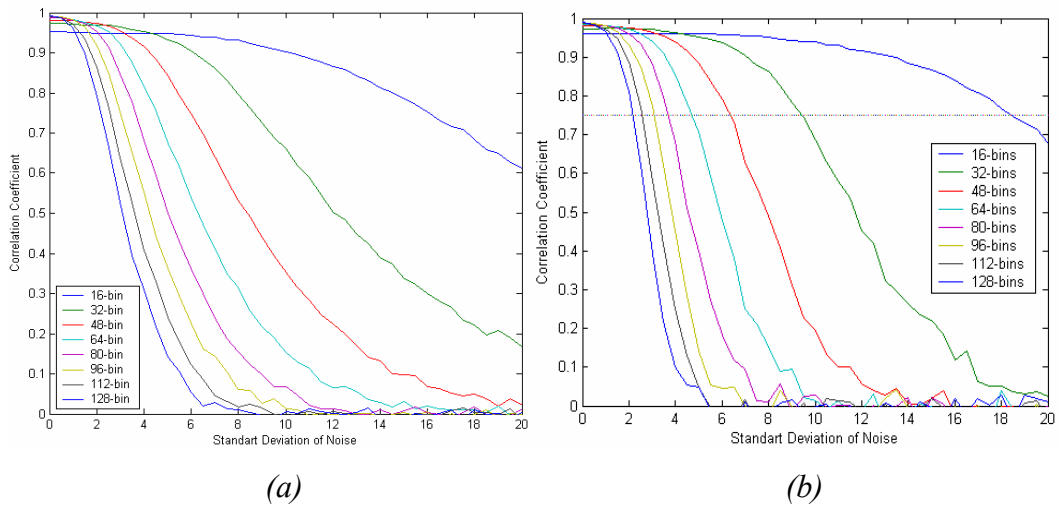
*Figure 7.9 (a) Correlation coefficient between the embedded and extracted hologram and (b) their reconstructions for varied noise power Man image*
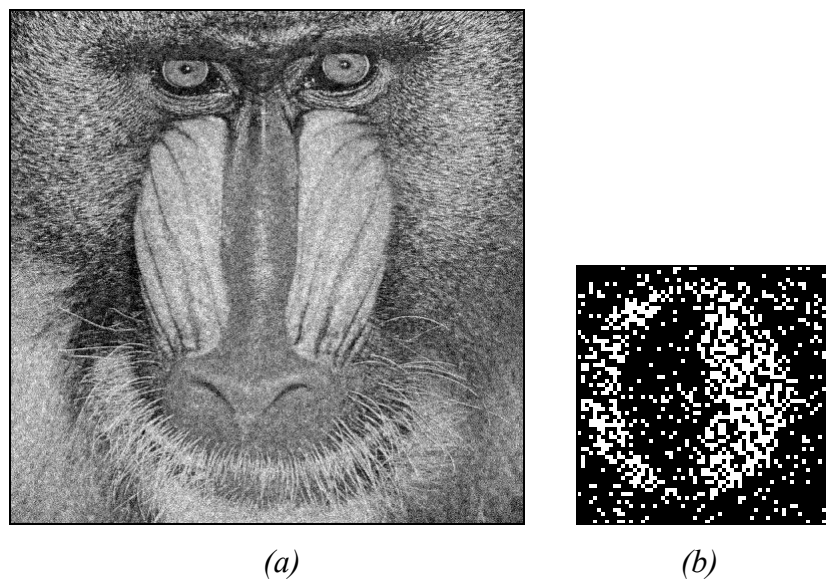


*Figure 7.10  (a) White Gaussian noise with variance of 400 added watermarked Baboon image (PSNR=22.12 dB) and (b) the reconstruction of the watermark extracted from this image. 16-bin quantizers are used in QIM*

86

*(a)*          *(b)*
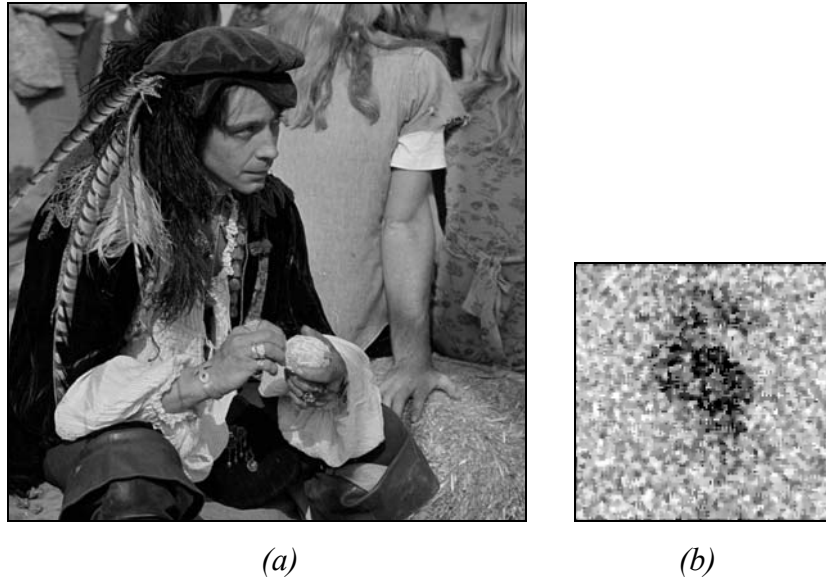
*Figure 7.11 (a) White Gaussian noise with variance of 5.25 added watermarked Man image (PSNR=40.25 dB) and (b) the reconstruction of the watermark extracted from this image. 128-bin quantizers are used in QIM*

### 7.2.3. Low Pass Filtering

The hackers can try to remove or corrupt the watermark hidden in an image by different filtering approaches. However, all these filters are mainly low-pass filters since most of the watermarking approaches preserve the low frequency parts and embed the watermark into mid or high frequency components.

The low-pass filters used to test the proposed method are Gaussian, circular averaging, horizontal motion, mean and median filters. The characteristics of the filters in frequency domain are given in Figure 7.12. Note that, the frequency spectrum of the median filter cannot be illustrated since it is a non-linear filter.

The experiments are performed for all watermarked Lena, Baboon and Man images for different quantizer parameters. The results are demonstrated from Table 7.1 to Table 7.4, for 16, 32, 48 and 64-bin quantizers since for quantizers having more than 64, the method becomes unrobust to these filtering operations. These results

show that the low-pass filtering effects the Baboon image more than the other images since it has high-pass characteristics. However, for the given parameters and filters, the extracted watermarks are still recognizable. Note that, the PSNR values in these tables are evaluated between the watermarked images and their attacked versions. Some examples of the attacked images and extracted watermarks from those images are also given from Figure 7.13 to Figure 7.17.



*(a)*

*(b)*

*(c)*

*(d)*
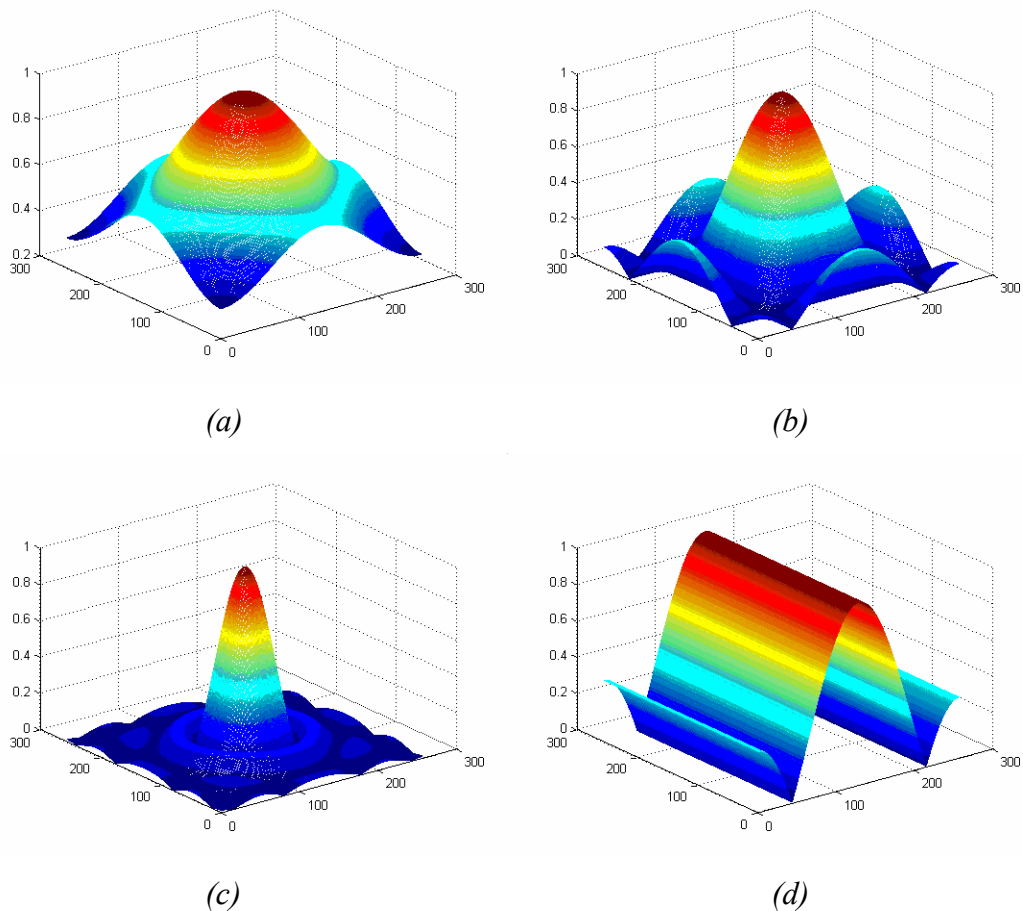
*Figure 7.12 The frequency spectrum for (a) 3x3 Gaussian low-pass, (b) 3x3 mean, (c) circular average with radius of 3 pixels and (d) 3 pixels horizontal motion filters*

*Table 7.1 Effect of low-pass filtering on watermarked Lena, Baboon and Man images using 16-bin quantizer*

| | | Gaussian LP | Circ. Avrg. | Horz. Mot. | Mean | Median |
|---|---|---|---|---|---|---|
| | | *4x4, σ=0.4* | *r = 2 pixels* | *6 pixels* | *3x3* | *3x3* |
| **Lena** | *PSNR* | 28.57 | 29.04 | 27.58 | 30.19 | 32.98 |
| | *CC(Holo)* | 0.78 | 0.87 | 0.84 | 0.92 | 1 |
| | *BCR(Rec)* | 0.79 | 0.85 | 0.81 | 0.91 | 0.98 |
| | $\sigma_I$ | 0.63 | 0.51 | 0.59 | 0.37 | 0.12 |
| **Baboon** | *PSNR* | 23.18 | 22.23 | 23.08 | 23.01 | 23.5 |
| | *CC(Holo)* | 0.74 | 0.81 | 0.84 | 0.88 | 0.83 |
| | *BCR(Rec)* | 0.76 | 0.78 | 0.8 | 0.85 | 0.83 |
| | $\sigma_I$ | 0.7 | 0.65 | 0.62 | 0.51 | 0.55 |
| **Man** | *PSNR* | 28.79 | 28.71 | 27.5 | 29.95 | 31.45 |
| | *CC(Holo)* | 0.78 | 0.86 | 0.82 | 0.91 | 0.96 |
| | *CC(Rec)* | 0.85 | 0.9 | 0.86 | 0.94 | 0.96 |
| | $\sigma_I$ | 0.17 | 0.13 | 0.16 | 0.1 | 0.08 |

*Table 7.2 Effect of low-pass filtering on watermarked Lena, Baboon and Man images using 32-bin quantizer*

| | | Gaussian LP | Circ. Avrg. | Horz. Mot. | Mean | Median |
|---|---|---|---|---|---|---|
| | | *3x3, σ=6* | *r = 1.5 pixel* | *3 pixels* | *3x3* | *3x3* |
| **Lena** | *PSNR* | 31.48 | 32.34 | 29.65 | 31.45 | 34.63 |
| | *CC(Holo)* | 0.88 | 0.89 | 0.79 | 0.88 | 0.95 |
| | *BCR(Rec)* | 0.86 | 0.87 | 0.81 | 0.86 | 0.92 |
| | $\sigma_I$ | 0.49 | 0.46 | 0.64 | 0.49 | 0.31 |
| **Baboon** | *PSNR* | 23.23 | 23.93 | 24.14 | 23.2 | 23.68 |
| | *CC(Holo)* | 0.7 | 0.76 | 0.72 | 0.7 | 0.52 |
| | *BCR(Rec)* | 0.73 | 0.76 | 0.74 | 0.73 | 0.7 |
| | $\sigma_I$ | 0.74 | 0.69 | 0.72 | 0.74 | 0.8 |
| **Man** | *PSNR* | 30.96 | 31.69 | 29.36 | 30.94 | 32.45 |
| | *CC(Holo)* | 0.87 | 0.88 | 0.8 | 0.87 | 0.91 |
| | *CC(Rec)* | 0.9 | 0.92 | 0.85 | 0.9 | 0.93 |
| | $\sigma_I$ | 0.13 | 0.12 | 0.17 | 0.13 | 0.11 |

*Table 7.3 Effect of low-pass filtering on watermarked Lena, Baboon and Man images using 48-bin quantizer*

|  |  | **Gaussian LP** *3x3, σ=3* | **Circ. Avrg.** *r = 1.5 pixel* | **Horz. Mot.** *3 pixels* | **Mean** *3x3* | **Median** *3x3* |
|---|---|---|---|---|---|---|
| **Lena** | *PSNR* | 31.85 | 32.6 | 33.81 | 31.71 | 35.03 |
|  | *CC(Holo)* | 0.83 | 0.85 | 0.91 | 0.82 | 0.9 |
|  | *BCR(Rec)* | 0.83 | 0.85 | 0.89 | 0.83 | 0.87 |
|  | $\sigma_I$ | 0.57 | 0.54 | 0.42 | 0.57 | 0.46 |
| **Baboon** | *PSNR* | 23.36 | 23.95 | 27.61 | 23.23 | 23.71 |
|  | *CC(Holo)* | 0.55 | 0.6 | 0.88 | 0.54 | 0.38 |
|  | *BCR(Rec)* | 0.68 | 0.7 | 0.85 | 0.67 | 0.66 |
|  | $\sigma_I$ | 0.84 | 0.81 | 0.52 | 0.85 | 0.87 |
| **Man** | *PSNR* | 31.27 | 31.88 | 33.4 | 31.14 | 32.69 |
|  | *CC(Holo)* | 0.81 | 0.84 | 0.92 | 0.8 | 0.83 |
|  | *CC(Rec)* | 0.86 | 0.88 | 0.93 | 0.86 | 0.88 |
|  | $\sigma_I$ | 0.16 | 0.15 | 0.11 | 0.16 | 0.15 |

*Table 7.4 Effect of low-pass filtering on watermarked Lena, Baboon and Man images using 64-bin quantizer*

|  |  | **Gaussian LP** *3x3, σ=0.8* | **Circ. Avrg.** *r = 1 pixels* | **Horz. Mot.** *3 pixels* | **Mean** *3x3* | **Median** *3x3* |
|---|---|---|---|---|---|---|
| **Lena** | *PSNR* | 34.33 | 35.6 | 33.89 | 31.82 | 35.2 |
|  | *CC(Holo)* | 0.85 | 0.88 | 0.88 | 0.76 | 0.84 |
|  | *BCR(Rec)* | 0.84 | 0.86 | 0.86 | 0.78 | 0.83 |
|  | $\sigma_I$ | 0.65 | 0.5 | 0.5 | 0.55 | 0.54 |
| **Baboon** | *PSNR* | 25.54 | 26.57 | 27.63 | 23.24 | 23.72 |
|  | *CC(Holo)* | 0.56 | 0.66 | 0.79 | 0.4 | 0.3 |
|  | *BCR(Rec)* | 0.69 | 0.72 | 0.79 | 0.64 | 0.64 |
|  | $\sigma_I$ | 0.82 | 0.77 | 0.64 | 0.89 | 0.91 |
| **Man** | *PSNR* | 33.52 | 34.56 | 33.47 | 31.21 | 32.78 |
|  | *CC(Holo)* | 0.83 | 0.86 | 0.87 | 0.71 | 0.73 |
|  | *CC(Rec)* | 0.88 | 0.91 | 0.91 | 0.79 | 0.81 |
|  | $\sigma_I$ | 0.15 | 0.13 | 0.13 | 0.21 | 0.19 |

|     |     |
| --- | --- |
| *(a)* | *(b)* |
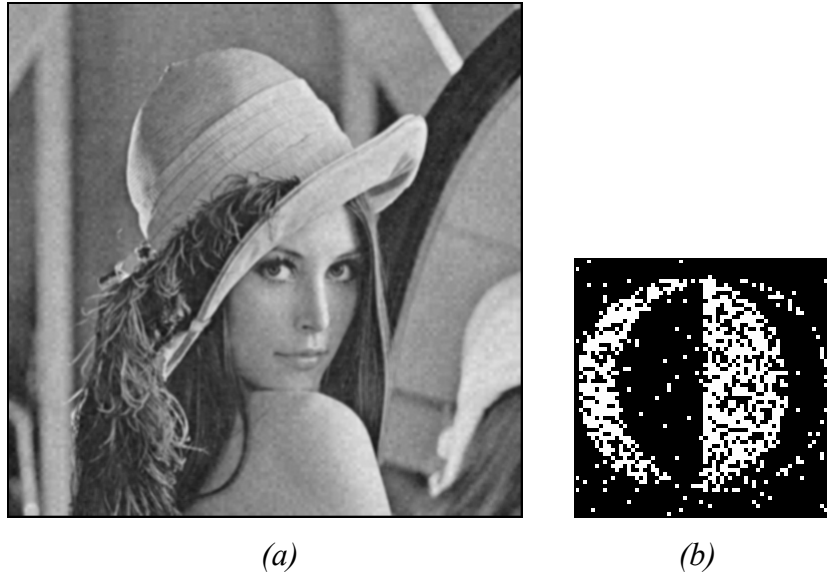
*Figure 7.13 (a) Watermarked Lena image after Gaussian low-pass (3x3, σ=6)*
*filtering and (b) the reconstruction of the extracted hologram (32-bin quantizers*
*are used in watermarking process)*



|     |     |
| --- | --- |
| *(a)* | *(b)* |
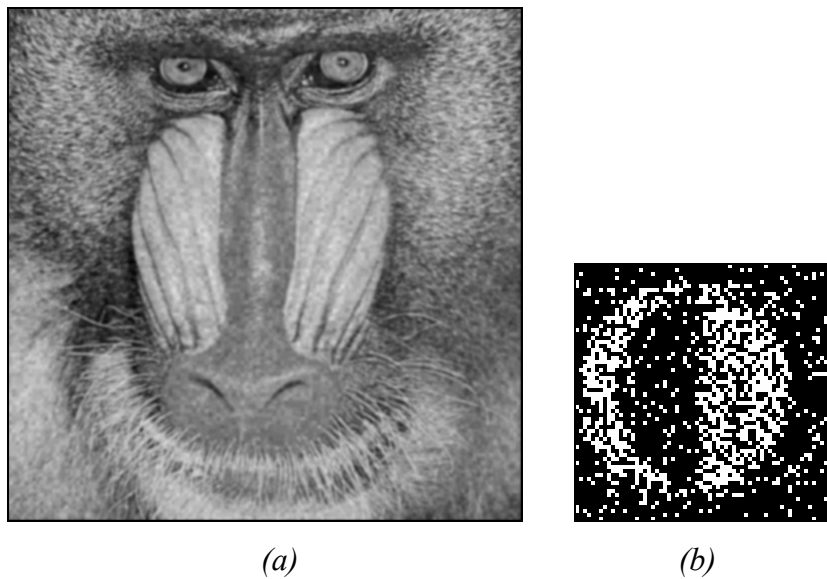
*Figure 7.14 (a) Watermarked Baboon image after circular motion (r=2 pixels)*
*filtering and (b) the reconstruction of the extracted hologram (16-bin quantizers*
*are used in watermarking process)*

<div align="center">

*(a)*            *(b)*
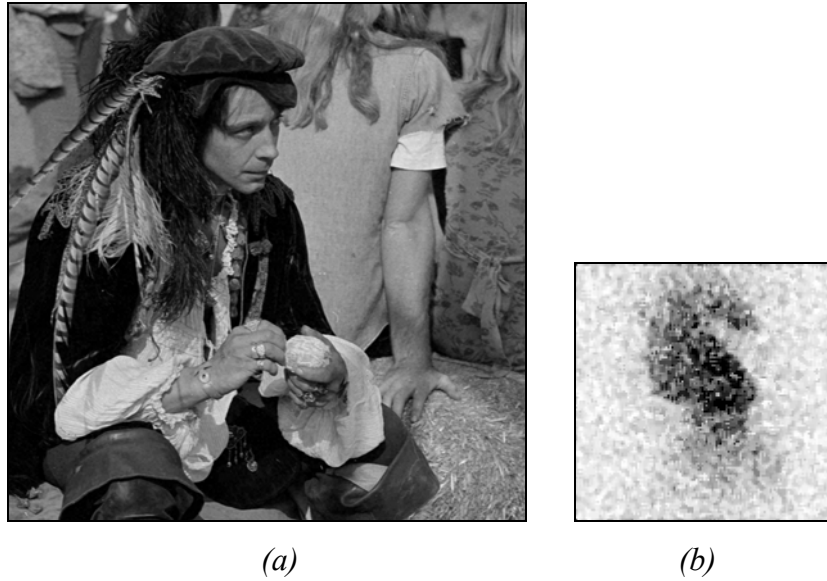
*Figure 7.15 (a) Watermarked Man image after horizontal motion (2 pixels)*
*filtering and (b) the reconstruction of the extracted hologram (48-bin quantizers*
*are used in watermarking process)*

</div>



<div align="center">

*(a)*            *(b)*
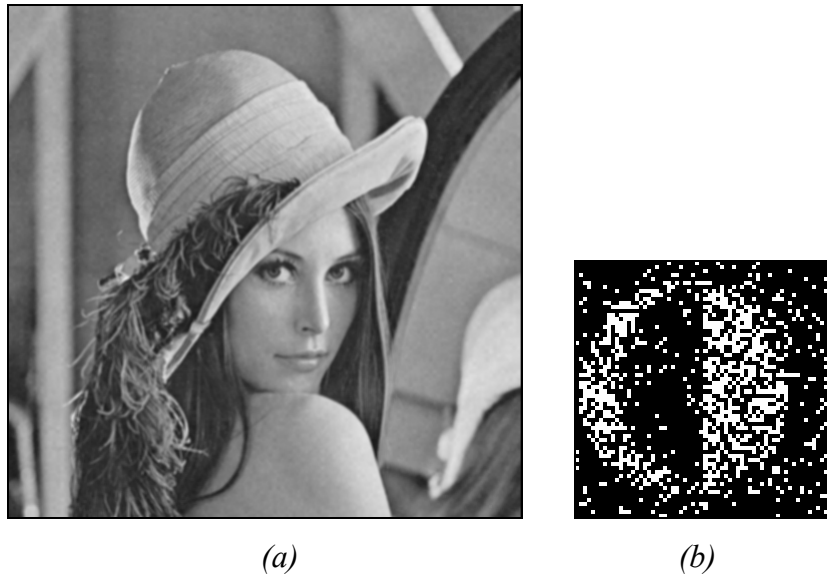
*Figure 7.16 (a) Watermarked Lena image after 3x3 mean filtering and (b) the*
*reconstruction of the extracted hologram (64-bin quantizers are used in*
*watermarking process)*

</div>

*(a)*             *(b)*
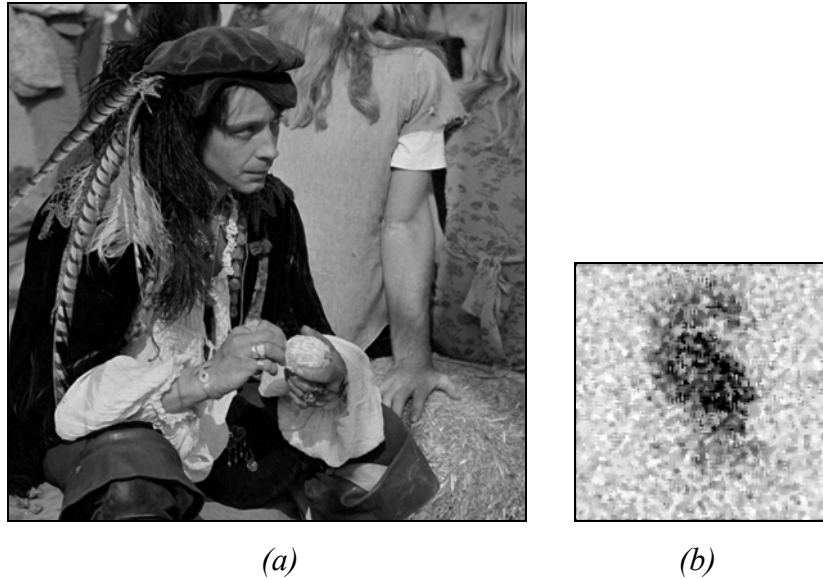
*Figure 7.17 (a) Watermarked Man image after 3x3 median filtering and (b) the reconstruction of the extracted hologram (64-bin quantizers are used in watermarking process)*

### 7.2.4. Sharpening

These filters can be used as an effective attack on some watermarking schemes because they are very effective at detecting high frequency noise introduced by some digital watermarking software. More subtle attacks are based on the Laplacian operator. In its simplest version, the attacked image is $I' = I - \alpha \cdot \nabla^2 (\nabla^2 I - I)$ where α is the strength of the attack. The frequency spectrum of the 3x3 unsharp contrast enhancement filter in Matlab is as in Figure 7.18.

The experiments performed show that the proposed method is very vulnerable to this type of attack and the embedded watermark cannot be extracted properly after unsharp contrast enhancement (see Figure 7.19). This is because the watermark is only embedded into low frequency components. After these components are suppressed, the watermark is also suppressed and it becomes unable to detect it. In order to overcome this problem, the watermark should be repeatedly embedded into

93

both low and high frequency components. However, this causes the watermarked image to degrade more.
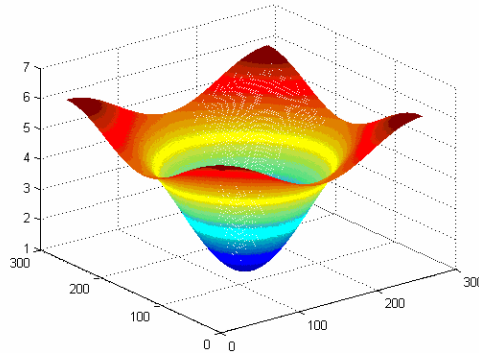


*Figure 7.18 Frequency spectrum of 3x3 unsharp masking filter in Matlab*



*(a)*                      *(b)*

*Figure 7.19 (a) Watermarked Lena image after 3x3 unsharp contrast enhancement filtering and (b) the reconstruction of the extracted hologram (64-bin quantizers are used in watermarking process)*

Histogram equalization is also used for sharpening of the brightness. The experiments also show that, the watermark cannot be extracted properly after histogram equalization. This is illustrated in Figure 7.20.



(a)　　　　　　　　　　　　　　(b)

*Figure 7.20 (a) Watermarked Man image after histogram equalization and (b) the reconstruction of the extracted hologram (64-bin quantizers are used in watermarking process)*

The experiments performed about the robustness of the proposed method against removal attacks show that the most important part of the design is the quantizers. When their step size gets larger the robustness of the system increases and vice versa. On the other hand, the large step sized quantizers reduce the quality of the resultant watermarked image.

Moreover, the watermark should be embedded into low frequencies to withstand the removal attacks. Thus, the embedding strategy becomes important but the holographic properties do not affect the robustness of the proposed method against removal attacks.

## 7.3 Experiments on Geometric Attacks

### 7.3.1. Occlusion

The occlusion is mainly caused of transmission errors or inadequate bandwidth of the network rather than the attacks of the hackers. Since the watermark is embedded in wavelet domain and the property of the hologram explained in Chapter 4.4, the watermark can be extracted properly after occlusion. 85% occluded watermarked Lena image illustrated in Figure 7.21 with the reconstruction of extracted hologram.



*(a)*        *(b)*
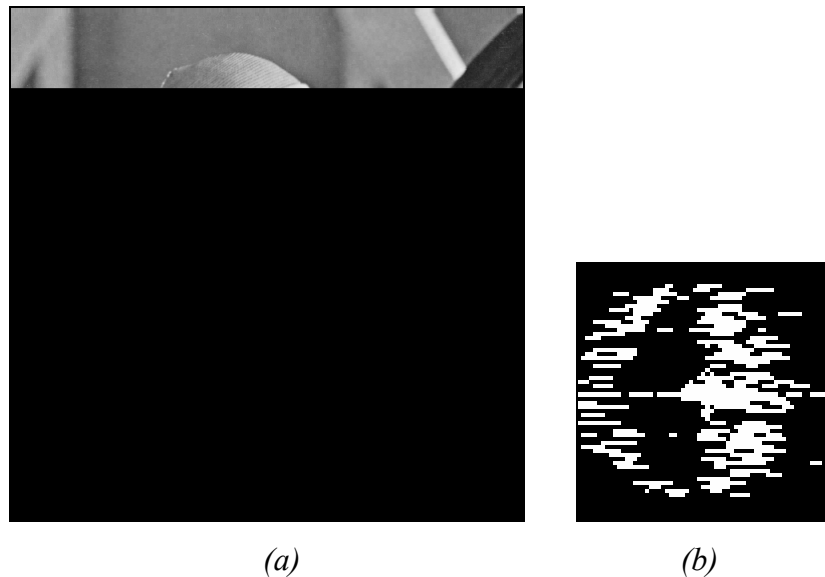
*Figure 7.21 (a) 85% occluded watermarked Lena image and (b) reconstruction of the extracted hologram from this image*

### 7.3.2. Cropping

In some cases, only some regions of the copyrighted content may be important and enough for the pirates. For instance, if there is a human in the scene, one desire to use only his/her face. As a result, the watermark should be extracted from a small portion of the watermarked content.

This watermarking scheme is also robust against cropping since a hologram can be reconstructed from a small part of itself. Moreover each wavelet coefficient is obtained from 8x8 pixels in its neighborhood. Therefore, if the image is cropped by 8mx8n in size starting from the first pixel, it is possible to reconstruct the watermark. If it is not appropriately cropped, it is still possible to detect the watermark by searching 8mx8n parts in that image. In Figure 7.22, the cropped watermarked Man image and the extracted watermark are presented.



(a)                                    (b)
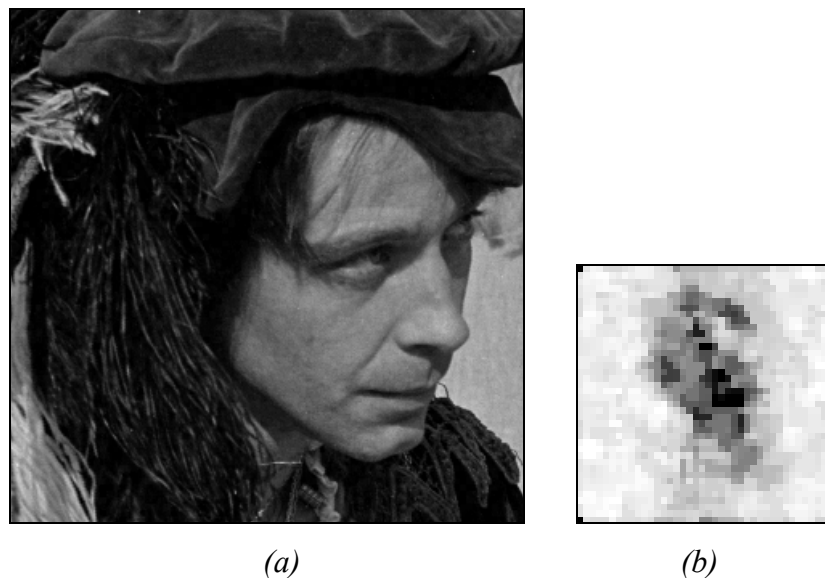
*Figure 7.22 (a) 10% cropped watermarked Man image (320x320) and (b) reconstruction of the extracted watermark (40x40)*

Note that, the size of the extracted watermark is reduced with the same ratio of between the original content and the cropped part. Hence, if the size of the host image is very large, the extracted hologram can be reconstructed even after a higher percentage of the content is cropped. For instance, if the host image is 4096x4096 whole Chess Knight hologram (512x512) can be hidden. Thus, when 320x320 (0.61%) part of that image is cropped, 40x40 part of the Chess Knight hologram is extracted and the image in Figure 7.22 (b) can be reconstructed.

### 7.3.3. Translation

Translation can occur in filtering operations where the original size is not preserved. If a *MxM* sized image is filtered with a *NxN* sized filter, the resulting filtered image size becomes (M+N+1)x(M+N+1). The translated of the watermarked Baboon image is shown in Figure 7.23 (a). We preserve the entire image by padding the outer region into the translated region to prevent data loss. This will allow us to see the effect of translation individually. In Figure 7.23 (b), the reconstruction of the extracted hologram from this image is given.



*(a)*          *(b)*
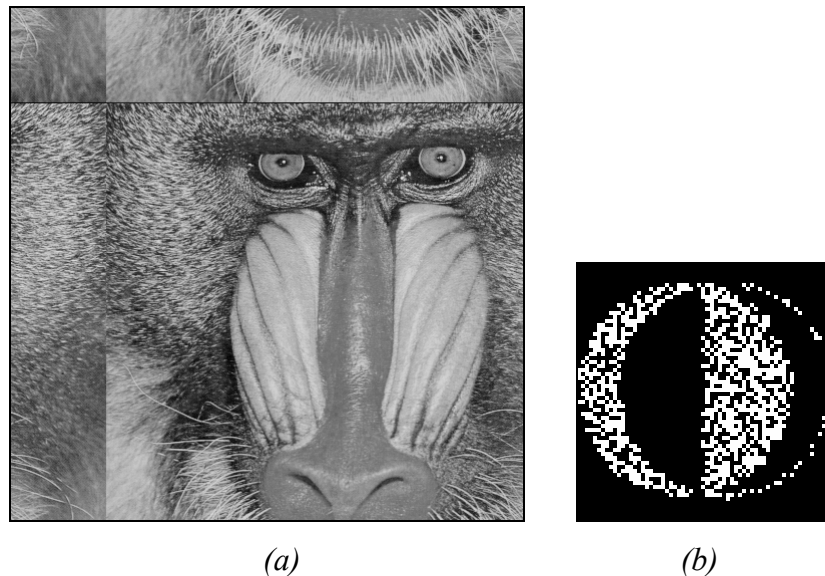
*Figure 7.23 (a) Watermarked Baboon image translated by 96 pixels in both vertical and horizontal direction and (b) reconstruction of the extracted hologram*

### 7.3.4. Rotation & Cropping

Small angle rotation, often in combination with cropping, does not usually change the commercial value of the image but can make the watermark undetectable. The proposed watermarking method does not provide robustness against rotation since all pixel values, so all DWT coefficients, circularly shift. In Figure 7.24, 1° rotated watermarked Lena image and the extracted watermark are presented.

On the other hand, the watermark can be reconstructed if the attacked image is rotated to the initial position back. This operation becomes adding noise to the image and cropping the parts exceeding the size of the original image. In order to find the rotation angle, template insertion [62] is the most common method. According to this approach, 4 peaks are located into two diagonals of the image symmetrically either in spatial or transform domain. Hence, the rotation angle can be predicted using these peaks.



*(a)*            *(b)*
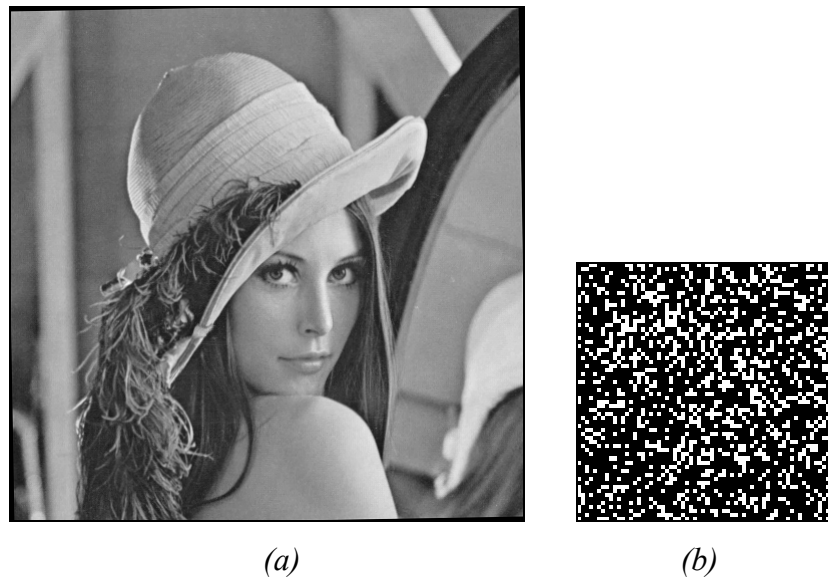
*Figure 7.24 (a) 1° degree rotated watermarked Lena and (b) extracted watermark from this image*

These experiments show that the robustness of the proposed method against the geometrical attacks is independent of the spectral characteristics of the host image or step size of the quantizers. This is because only the amount of the hologram data or its orientation is changed after these types of attack. Moreover, the hologram data is intrinsically robust against these types of geometric modifications as explained in Chapter 4. As a result, if the hidden hologram can be extracted

correctly, even it is cropped, occluded or translated; the watermark (reconstruction of the hologram) can be obtained properly.

## 7.4    Comparisons of the Proposed Method with the Existing Methods

As explained in Chapter 5, the watermarking using digital holography is a new approach so that in the literature there have not been proposed a mature method, yet. On the other hand, the existing studies try to emphasize the intrinsic robustness of the hologram data against some geometric attacks. In many of these methods many criteria like size and quality of the watermarked image or robustness against removal attacks are not taken into account.

In [50-52], the hologram is embedded into the image in spatial domain by a simple superposition. As a result, the quality of the image is reduced much in order the watermark to have enough power to detect. Besides, to have high PSNR, the watermarked image becomes very sensitive to any kind of removal attack since the watermark spreads over the high frequency components. Nevertheless, these approaches are robust against many of the geometrical attacks because of the holograms' properties given in Chapter 4. The advantage of the method we proposed over these methods is providing high PSNR and more robustness. For instance, for Takai et. al. method, the PSNR of the watermarked image is about 23 dB, where it is not least than 28 dB by the proposed method for the most robust case.

On the other hand, Chang et. al. [53] took the quality and robustness criteria into account in order to improve the Takai et. al.'s method. Good quality watermarked images ($\approx$38 dB) were obtained by superposing the hologram into the DCT coefficients of the image. This method is also robust against occlusion, low pass filtering and tampering. However, for none of the attacks, Chang et. al.'s method provides better results than the ones obtained by the proposed method in this thesis. Moreover, it is very sensitive to data compression where our method provides robustness against JPEG compression. Furthermore, all these methods double the

size of the image after watermarking since the complex amplitude is directly superposed to the image. The only exception is valid for He et. al's method [52] since they proposed to embed phase information only.

It is also possible to compare the proposed method with the existing logo watermarking methods since for both approaches the aim is hiding perceptually meaningful data. In Table 7.5, the attacks, against which these logo and proposed schemes are robust, are given in order to compare the performance of the algorithms. Note that, for all these images the PSNR values are about 40-42 db, hence the performance for the proposed method is given for the one obtained by using 64-bin quantizers.

*Table 7.5 Comparisons of the methods in terms of their robustness*

|  | **Reddy** | **Kundur** | **Zhang** | **Proposed** |
|---|---|---|---|---|
| **JPEG Comp.** | CR = 50 | CR = 30 | CR = 18.5 | CR = 14 |
| **AWGN** | STD = 30 | STD = 26 | STD = 5.5 | STD = 5.5 |
| **Median Filt.** | 9x9 | 5x5 | 3x3 | 3x3 |
| **Mean Filt.** | 7x7 | 5x5 | 3x3 | 3x3 |
| **Occlusion** | 15% remained | 15% remained | 25% remained | 25% remained |
| **Cropping** | N\A | N\A | N\A | 25% remained |

Kundur et. al.'s, [54] and Reddy et. al.'s, [56], methods are more robust especially against removal attacks. The method in [56] is the most robust method among these methods. The watermark can be extracted after the image is compressed to its 1/50 in size or degraded with AWGN with variance 30. Kundur et. al.'s method also provides similar results but resistant to less amount of compression and noise. It is also less robust against low pass filtering but gives same results against occlusion.

On the other hand, these methods are non-blind methods and it is possible to obtain more robust watermarked images. Zhang et. al's proposed a blind watermarking scheme. The robustness of the method we proposed is comparable with this method. Zhang et. al.'s method is more resistive to sharpening (unsharp contras enhancement and histogram equalization) and rescaling. The behavior of the systems against JPEG compression is almost same but Zhang et. al.'s method is more resistant to the compression. However, by reducing the quality of the watermarked image a bit, more robust watermarked images can be obtained by the proposed method in this thesis. Moreover, the performance of our method is better than Zhang et. al.'s one against other geometric distortions. Besides, the Zhang et al.'s method uses binary logos to hide where we hide 4 bit/pixel phase information of the hologram of an object. Hence, the size of the hidden information in our scheme is 4 times of the other one's and by the reconstruction of that data a grayscale image (the watermark) is obtained.

# CHAPTER 8

# CONCLUSIONS AND FUTURE WORK

The aim of this study is to embed a visually meaningful pattern into a digital image in order to watermark this content. For this purpose, the hologram of a real 3-D object or a binary image is used as the secret mark. The proposed scheme is blind and it requires neither the original image nor the embedded hologram during the watermark extraction process. Therefore, we believe that the proposed method is applicable for several practical scenarios.

Before establishing a method for the watermarking approach, the characteristics of the holograms are investigated especially for reducing its size. Since the hologram is a complex data, a compact way to represent the information should have been found. For that purpose, the nature of the hologram that enables to reconstruct the object from only its phase part makes it easier. Besides, the experiments show that the quantization of this data is also possible and for 4 bit/pixel representation of phase map of the hologram is appropriate to use.

Some other experiments are also made in order to see the response of the holograms against possible kinds of attacks. These experiments are concentrated on their robustness against geometrical attacks like cropping and occlusion. It is seen that, the reconstruction of the object is possible even after these manipulations of the hologram.

The hologram is embedded into the image in wavelet domain since it is desired to embed the data into low enough frequencies to make the system robust while keeping spatial orientation of the hologram to make it robust against the geometrical attacks. Furthermore, QIM is utilized for watermarking process in order to extract the hidden mark using only the watermarked image, i.e. make it blind. Uniform quantizers are used in QIM and the effect of the different step size of the quantizers is examined upon the quality of the watermarked images.

In this thesis, the robustness of the system against possible kinds of attacks is also investigated. It is seen that the proposed method provides robustness against JPEG compression, noise addition and various kinds of filtering. Moreover, it is robust against cropping and occlusion as expected because of the nature of the holograms. The experiments show that step size of the quantizers used in QIM affect the robustness of the method directly, especially against the removal attacks. The large step size (less number of bins) makes the watermarked image more robust but in lower quality. As a result, depending on the application and the spectral characteristics of the host image this factor can be adjusted.

The obtained results by the experiments are compared with the results of some methods existing in the literature. These methods are also aimed to hide visually meaningful patterns into the host image but classified in two groups.

In the first approach, the holograms are used to hide. Our method also belongs to this type of watermarking approach. However, these approaches in the literature had not proposed a complete scheme which degrades the host image less and robust against different types of attacks. They are mainly focused on the applicability of hologram usage and emphasize their robustness against geometrical attacks. Consequently, in this thesis, a holographic watermarking scheme is proposed by taking the invisibility and the robustness criteria into account. To the best of our knowledge there has not been proposed a similar approach in the literature, yet.

The performance of the proposed method is also compared with some logo embedding approaches. The performance of our method is worse than some of these approaches but it is expected since they are non-blind. On the other hand, the obtained results are very similar to the ones obtained by the method which is blind. Moreover, our approach has some advantages over that one in robustness against the geometrical attacks.

Despite the trade-off between the watermarked image quality and the robustness can be improved by DC-QIM, it is better to investigate another data embedding approach taking the hologram properties into account. Hence, it becomes possible to embed the hologram into the image optimally.

As a future work, it is planning to compare the results of the proposed system with the results of such a system that achieves robustness against geometrical attacks by some error protection operations. It can also be studied for approaches to make the watermarking scheme robust against geometric distortions like rotation. Besides, another type of hologram (i.e. phase only holograms) may be used. We are also planning to extend the algorithm for stereo image or mesh watermarking.

# REFERENCES

[1]     F. Hartung and M. Kutter, "Multimedia watermarking techniques," *Proceedings of the IEEE*, vol. 87, pp. 1079-1107, 1999.

[2]     I. J. Cox, M. Miller, and J. Bloom, *Digital watermarking*. San Francisco, Calif.: Morgan Kaufmann, 2002.

[3]     S. E. Balcı, "Robust watermarking of images," in *Department of Electrical and Electronics Engineering*. Ankara: Middle East Technical University, 2003, pp. 117.

[4]     T. Gökozan, "Template based image watermarking in the fractional fourier domain," in *Department of Electrical and Electronics Engineering*. Ankara: Middle East Technical University, 2005, pp. 111.

[5]     S. Katzenbeisser and F. A. P. Petitcolas, *Information hiding techniques for steganography and digital watermarking*. Boston: Artech House, 2000.

[6]     I. J. Cox, M. L. Miller, and J. A. Bloom, "Watermarking applications and their properties," presented at Int. Conf. on Information Theory, Las Vegas, 2000.

[7]     I. J. Cox, J. Kilian, F. T. Leighton, and T. Shamoon, "Secure spread spectrum watermarking for multimedia," *IEEE Transactions on Image Processing*, vol. 6, pp. 1673-1687, 1997.

[8]     K. Tanaka, Y. Nakamura, and K. Matsui, "Embedding secret information into a dithered multilevel image," presented at IEEE Military Commun. Conf., 1990.

[9]     G. C. Langelaar, I. Setyawan, and R. L. Lagendijk, "Watermarking digital image and video data - A state-of-the-art overview," *IEEE Signal Processing Magazine*, vol. 17, pp. 20-46, 2000.

[10]    C. Y. Lin and S. F. Chang, "A robust image authentication method distinguishing JPEG compression from malicious manipulation," *IEEE Transactions on Circuits and Systems for Video Technology*, vol. 11, pp. 153-168, 2001.

[11]    J. Wang and L. Ji, "A region and data hiding based error concealment scheme for images," *IEEE Transactions on Consumer Electronics*, vol. 47, pp. 257-262, 2001.

[12]    M. H. Chen, Y. He, and R. L. Lagendijk, "A fragile watermark error detection scheme for wireless video communications," *IEEE Transactions on Multimedia*, vol. 7, pp. 201-211, 2005.

[13]    M. D. Swanson, M. Kobayashi, and A. H. Tewfik, "Multimedia data-embedding and watermarking technologies," *Proceedings of the IEEE*, vol. 86, pp. 1064-1087, 1998.

[14]    R. B. Wolfgang, C. I. Podilchuk, and E. J. Delp, "Perceptual watermarks for digital images and video," *Proceedings of the IEEE*, vol. 87, pp. 1108-1126, 1999.

[15]    C. I. Podilchuk and W. J. Zeng, "Image-adaptive watermarking using visual models," *IEEE Journal on Selected Areas in Communications*, vol. 16, pp. 525-539, 1998.

[16]    B. Chen and G. W. Wornell, "Quantization index modulation: A class of provably good methods for digital watermarking and information embedding," *IEEE Transactions on Information Theory*, vol. 47, pp. 1423-1443, 2001.

[17]    C. I. Podilchuk and E. J. Delp, "Digital watermarking: Algorithms and applications," *IEEE Signal Processing Magazine*, vol. 18, pp. 33-46, 2001.

[18]    M. Barni, F. Bartolini, V. Cappellini, and A. Piva, "A DCT-domain system for robust image watermarking," *Signal Processing*, vol. 66, pp. 357-372, 1998.

[19]    J. J. K. O. Ruanaidh and T. Pun, "Rotation, scale and translation invariant spread spectrum digital image watermarking," *Signal Processing*, vol. 66, pp. 303-317, 1998.

[20]    V. Solachidis and I. Pitas, "Circularly symmetric watermark embedding in 2-D DFT domain," *Ieee Transactions on Image Processing*, vol. 10, pp. 1741-1753, 2001.

[21]    R. Dugad, K. Ratakonda, and N. Ahuja, "A new wavelet-based scheme for watermarking images," presented at ICIP, 1998.

[22]    G. Saxby, *Practical holography*, 3rd ed. Bristol, UK ; Philadelphia: Institute of Physics Pub., 2004.

[23]    D. Gabor, "Holography, 1948-1971," *Proceedings of the Institute of Electrical and Electronics Engineers*, vol. 60, pp. 655-668, 1972.

[24]    T. Kreis, *Holographic interferometry : principles and methods*, 1st ed. Berlin: Akademie Verlag, 1996.

[25]    I. Yamaguchi and T. Zhang, "Phase-shifting digital holography," *Optics Letters*, vol. 22, pp. 1268-1270, 1997.

[26]    D. Gabor, "A New Microscopic Principle," *Nature*, vol. 161, pp. 777-778, 1948.

[27]    D. Gabor, "Microscopy by Reconstructed Wave-Fronts," *Proceedings of the Royal Society of London Series a-Mathematical and Physical Sciences*, vol. 197, pp. 454-487, 1949.

[28]    D. Gabor, "Microscopy by Reconstructed Wave Fronts .2.," *Proceedings of the Physical Society of London Section B*, vol. 64, pp. 449-469, 1951.

[29]    P. Hariharan, *Optical holography : principles, techniques, and applications*. Cambridge ; New York: Cambridge University Press, 1984.

[30]    E. N. Leith and Upatniek.J, "Wavefront Reconstruction with Continuous-Tone Objects," *Journal of the Optical Society of America*, vol. 53, pp. 1377-&, 1963.

[31]     M. Lucente, "Diffraction-specific fringe computation for electro-holography," 1994, pp. 175.

[32]     R. S. Pappu, "Minimum information holograms," 1995, pp. 76 p.

[33]     J. W. Goodman and R. W. Lawrence, "Digital Image Formation from Electronically Detected Holograms," *Applied Physics Letters*, vol. 11, pp. 77-&, 1967.

[34]     U. Schnars and W. P. O. Jüptner, "Review Article: Digital recording and numerical reconstruction of holograms," *Measurement Science and Technology*, vol. 13, pp. R85-R101, 2002.

[35]     U. Schnars, "Direct Phase Determination in Hologram Interferometry with Use of Digitally Recorded Holograms," *Journal of the Optical Society of America a-Optics Image Science and Vision*, vol. 11, pp. 2011-2015, 1994.

[36]     J. Pomarico, U. Schnars, H. J. Hartmann, and W. Juptner, "Digital Recording and Numerical Reconstruction of Holograms - a New Method for Displaying Light in-Flight," *Applied Optics*, vol. 34, pp. 8095-8099, 1995.

[37]     I. Yamaguchi, J. Kato, S. Ohta, and J. Mizuno, "Image formation in phase-shifting digital holography and applications to microscopy," *Applied Optics*, vol. 40, pp. 6177-6186, 2001.

[38]     H. J. Caulfield, *Handbook of optical holography*. New York: Academic Press, 1979.

[39]     O. Matoba, T. J. Naughton, Y. Frauel, N. Bertaux, and B. Javidi, "Real-time three-dimensional object reconstruction by use of a phase-encoded digital hologram," *Applied Optics*, vol. 41, pp. 6187-6192, 2002.

[40]     T. J. Naughton, Y. Frauel, B. Javidi, and E. Tajahuerce, "Compression of digital holograms for three-dimensional object reconstruction and recognition," *Applied Optics*, vol. 41, pp. 4124-4132, 2002.

[41]     T. J. Naughton, J. B. McDonald, and B. Javidi, "Efficient compression of Fresnel fields for internet transmission of three-dimensional images," *Applied Optics*, vol. 42, pp. 4758-4764, 2003.

[42]    T. J. Naughton and B. Javidi, "Compression of encrypted three-dimensional objects using digital holography," *Applied Optics*, vol. 43, pp. 2233-2238, 2004.

[43]    N. C. Gallagher, "Optimum quantization in digital holography," *Applied Optics*, vol. 17, pp. 109-115, 1978.

[44]    I. Yamaguchi, K. Yamamoto, G. A. Mills, and M. Yokota, "Image reconstruction only by phase data in phase-shifting digital holography," *Applied Optics*, vol. 45, pp. 975-983, 2006.

[45]    A. E. Shortt, T. J. Naughton, and B. Javidi, "A companding approach for nonuniform quantization of digital holograms of three-dimensional objects," *Optics Express*, vol. 14, pp. 5129-5134, 2006.

[46]    G. A. Mills and I. Yamaguchi, "Effects of quantization in phase-shifting digital holography," *Applied Optics*, vol. 44, pp. 1216-1225, 2005.

[47]    E. Darakis and J. J. Soraghan, "Compression of interference patterns with application to phase-shifting digital holography," *Applied Optics*, vol. 45, pp. 2437-2443, 2006.

[48]    S. Kishk and B. Javidi, "3D Object Watermarking by a 3D Hidden Object," *Optics Express*, vol. 11, pp. 874-888, 2003.

[49]    H. Kim and Y. H. Lee, "Optimal Watermarking of Digital Hologram of 3D Object," *Optics Express*, vol. 13, pp. 2881-2886, 2005.

[50]    N. Takai and Y. Mifune, "Digital watermarking by a holographic technique," *Applied Optics*, vol. 41, pp. 865-873, 2002.

[51]    L. Z. Cai, M. Z. He, Q. Liu, and X. L. Yang, "Digital image encryption and watermarking by phase-shifting interferometry," *Applied Optics*, vol. 43, pp. 3078-3084, 2004.

[52]    M. Z. He, L. Z. Cai, Q. Liu, and X. L. Yang, "Phase-only encryption and watermarking based on phase-shifting interferometry," *Applied Optics*, vol. 44, pp. 2600-2606, 2005.

[53] H. T. Chang and C. L. Tsan, "Image watermarking by use of digital holography embedded in the discrete-cosine-transform domain," *Applied Optics*, vol. 44, pp. 6211-6219, 2005.

[54] D. Kundur and D. Hatzinakos, "Toward robust logo watermarking using multiresolution image fusion principles," *IEEE Transactions on Multimedia*, vol. 6, pp. 185-198, 2004.

[55] J. Zhang and F. Xiong, "A novel watermarking for image security," *Computer and Information Sciences - Iscis 2004, Proceedings*, vol. 3280, pp. 420-429, 2004.

[56] A. A. Reddy and B. N. Chatterji, "A new wavelet based logo-watermarking scheme," *Pattern Recognition Letters*, vol. 26, pp. 1019-1027, 2005.

[57] B. Chen and G. W. Wornell, "Quantization index modulation methods for digital watermarking and information embedding of multimedia," *Journal of Vlsi Signal Processing Systems for Signal Image and Video Technology*, vol. 27, pp. 7-33, 2001.

[58] M. Wu and B. Liu, "Data hiding in image and video: Part I - Fundamental issues and solutions," *IEEE Transactions on Image Processing*, vol. 12, pp. 685-695, 2003.

[59] M. Wu, H. Yu, and B. Liu, "Data hiding in image and video: Part II - Designs and applications," *IEEE Transactions on Image Processing*, vol. 12, pp. 696-705, 2003.

[60] I. Daubechies, "Orthonormal Bases of Compactly Supported Wavelets," *Communications on Pure and Applied Mathematics*, vol. 41, pp. 909-996, 1988.

[61] I. Daubechies, *Ten lectures on wavelets*. Philadelphia, Pa.: Society for Industrial and Applied Mathematics, 1992.

[62] S. Pereira and T. Pun, "Robust template matching for affine resistant image watermarks," *IEEE Transactions on Image Processing*, vol. 9, pp. 1123-1129, 2000.